Golgi cell mediated inhibition in the cerebellar granule cell layer

Daniel Robin Ward

Department of Neuroscience, Physiology and Pharmacology

University College London

2012

Thesis submitted to University College London for the degree of Doctor of Philosophy. The work presented is my own; where information has been derived from other sources it has been indicated.

Abstract

The cerebellar cortex integrates multimodal information from mossy fibre (MF) and climbing fibre inputs to perform a variety of computations relating to movement, motor learning and balance. Before MF information can be combined with climbing fibre input in Purkinje cells (PCs) it must pass through the granule cell (GrC) layer wherein it is transformed by the anatomical connectivity and local inhibitory circuit. GrCs receive both tonic and phasic inhibition, the latter arising from the release of gamma aminobutyric acid (GABA) from Golgi cell (GoC) axons. However, the properties of GoC mediated inhibition and its computational significance are not well understood.

I have characterised the GoC–GrC synaptic connection using paired whole-cell patch-clamp recordings. My results show that unitary GoC inputs are smaller than previously realised and are frequently mediated purely by spillover from synapses onto adjacent GrCs. I have used the dynamic clamp method to investigate how changes in the frequency and synchrony of spiking in the GoC network can affect GrC computation. I found that changes in GoC firing rate strongly modulate the gain of the GrC input–output (I–O) function, while GoC synchrony can create permissive and non-permissive windows resulting in a patternation of GrC firing that may convey a temporal signal to downstream PCs.

GoCs are subject to regulation through the activation of metabotropic glutamate receptors (mGluRs) and nicotinic acetylcholine receptors (nAChRs). I have investigated how these modulatory inputs to GoCs might affect their inhibitory output and show that mGluR activation dramatically reduces GABA release while nAChR activation dramatically increases GABA release from GoCs.

My results show that GoCs can exert potent inhibitory control over GrCs that could be relevant to the processing of both temporally coded and rate coded information.

Acknowledgements

"Research is the process of going up alleys to see if they are blind." *Marston Bates*

I would like to dedicate this thesis to the rats, without them none of this would have been possible.

I offer my severe thanks to my supervisor; Prof. Angus Silver, for his guidance, support, patience, and for helpfully pointing out when I utilise adjectives inappropriately. Angus is not only an extremely gifted scientist but also an exceptionally nice and generous person. His good nature and patience has been a tremendous blessing for which I am very grateful.

I am indebted to several members of the Silver lab who inspired, taught, helped or entertained me in some regard. In particular Jason Rothman, whose expertise with Igor Pro saved me countless hours of tedious analysis. I thank Matteo Farrinella for his friendship and artistic support, Koen Verveake and Roby Kanichay who were both great sources of scientific advice, support and motivation, Laszlo Bicskei for having my back in the past few months and Florencia Iacaruso for services rendered.

I would like to thank my examiners Christopher Yeo and Nick Hartell for taking the time and effort to read and scrutinise my thesis, I know it will have been a chore in places, for this I apologise.....

I'm grateful to my many friends. A special mention should go to my best friends; Lisa Beeren, Bob Aldus, Kevin Jones, Mark Sheffield and Ben Judkewitz (Lisa's name is first because she cares about that kind of thing, Ben's name is last because he doesn't)

and my ex-girlfriends Laura Cornelissen and Zara Richardson (both put up with a great deal) who helped me through some tough times. I also wish to mention Marisol Sampedro Castaneda and Caroline Mestrallet who have shown me particular kindness. I can scarcely believe how lucky I am to have such good friends.

Finally I thank my family for their love, support and where appropriate, their genetic material.

Table of contents

List of figures

List of tables

List of abbreviations

5-HT	5-Hydroxytryptophan
ACh	Acetylcholine
ACPD	(1*S*,3*R*)-1-Aminocyclopentane-1,3-dicarboxylic acid
ACSF	Artificial cerebrospinal fluid
AMPA	α-amino-3-hydroxy-5-methyl-4-isoxazolepropionic acid
ANOVA	Analysis of variance
AP5	(2R)-amino-5-phosphonovaleric acid
BAPTA	1,2-bis(o-aminophenoxy)ethane-N,N,N',N'-tetraacetic acid
Best1	Bestrophin 1
C_m	Membrane capacitance
CV	Coefficient of variation
DβE	Dihydro-β-erythroidine
DCN	Deep cerebellar nuclei
DIC	Differential interference contrast
EGTA	Ethylene glycol tetraacetic acid
eIPSC	Evoked inhibitory post synaptic current
EPSC	Excitatory post synaptic current
FFT	Fast Fourier transformation
GABA	γ-Aminobutyric acid
$GABA_AR$	GABA type A receptor
$GABA_BR$	GABA type B receptor
GBZ	Gabazine (SR-95531)
GrC	Granule cell
GoC	Golgi cell
HEPES	4-(2-hydroxyethyl)-1-piperazineethanesulfonic acid
IF	Integrate and fire

I_{hold}	Holding current
I_m	Membrane current
I–O	Input–output
I_{pip}	Pipette current
ISI	Interspike interval
IPSC	Inhibitory post synaptic current
LTD	Long term depression
LTP	Long term potentiation
MF	Mossy fibre
mGluR	Metabotropic glutamate receptor
NA	Noradrenaline
nAChR	Nicotinic acetylcholine receptor
NBQX	2,3-dihydroxy-6-nitro-7-sulfamoyl-benzo[f]quinoxaline-2,3-dione
NMDA	N-methyl D-aspartate
PC	Purkinje cell
R_m	Membrane resistance
R_{pip}	Pipette resistance
R_s	Series resistance
RT	Rise time
SD	Standard deviation
SEM	Standard error of the mean
sIPSC	Spontaneous inhibitory post synaptic current
STD	Short term depression
TTX	Tetrodotoxin
V_c	Command potential
V_m	Membrane potential
VOR	Vestibulo–ocular reflex

Chapter One

1. General introduction

1.1 The cerebellum

A cerebellum can be found in all vertebrates and despite undergoing considerable evolutionary expansion possesses a basic anatomy and circuitry that is well conserved (Bell 2002). In the early 18th century a collection of lesion studies implicated the cerebellum in the control of fine movement, motor learning, posture and equilibrium (Fine *et al*. 2002). Recent studies have shown, more specifically, that the cerebellum regulates the timing of movement and that it can make use of implicit memory to perform sensory prediction (Spencer & Ivry 2009). It has also been linked to a range of cognitive processes (Katz & Steinmetz 2002; Ito 2008; Strick *et al*. 2009; Moulton *et al*. 2010; Rochefort *et al*. 2011). The efforts of many anatomists perhaps most notably Santiago Ramón y Cajal (1894) and Camillo Golgi (1883) helped elucidate the cellular elements of the cerebellar circuit (**Fig. 1.1**), laying the foundation for physiologists of the following century, most notably John Eccles (1967), to delineate how the cerebellum's uniform structure and microcircuity might function to process sensorimotor and indeed other types of information (Ito 2006; Ito 2008).

1.1.1 Anatomical overview of the cerebellum

The cerebellum is a hindbrain structure located dorsocaudal to the brainstem, isolated from the cerebrum by the tentorium cerebelli. It consists of 4 pairs of nuclei (from lateral to medial); the dentate, the emboliform and globose (which are fused in some animals and termed the interposed) and the fastigial nuclei which are collectively known as the deep cerebellar nuclei (DCN). The DCN are surrounded by an area of white matter, which is in turn surrounded by a region of grey matter termed the cerebellar cortex (**Fig. 1.2**; Apps & Hawkes 2009).

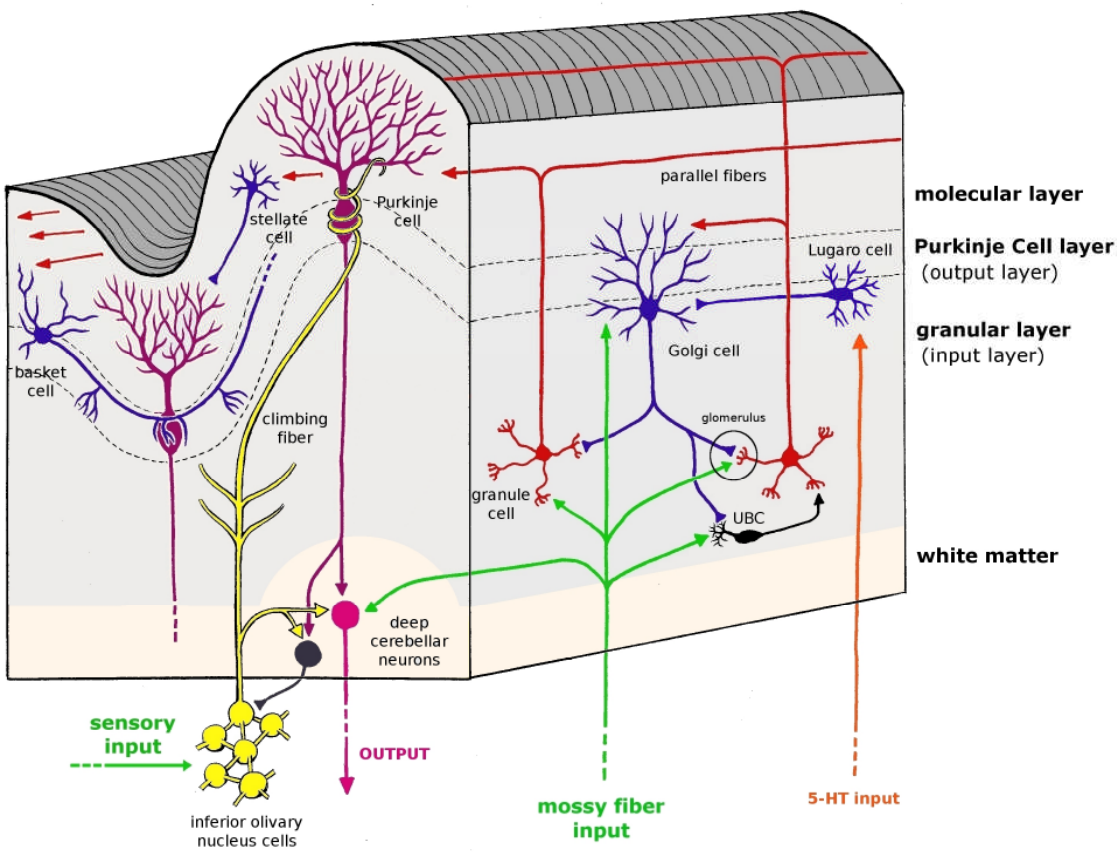

Fig. 1.1: Schematic of cerebellar circuitry. The cerebellar cortex is comprised of just three layers with seven major cell types and two principal inputs. The first layer, the granular layer constitutes the input layer of the cerebellar cortex. It is principally comprised of granule cells (GrCs). GrCs receive excitatory input from mossy fibres (MFs) which arise from multiple sources. MFs also excite unipolar brush cells (UBCs) and Golgi cells (GoCs) which provide feedforward excitatory and inhibitory input to GrCs respectively. GoCs are also regulated by inhibitory input from Lugaro cells which are thought to be controlled predominantly by serotonergic (5-HT) fibres. GrCs send axons into the molecular layer which bifurcate giving rise to parallel fibres that travel in the coronal plane to provide excitatory input to Purkinje cells (PCs), GoCs, basket cells and stellate cells. Excitatory input from the GrCs is integrated in the PCs with inhibitory input from the basket and stellate cells as well as an excitatory climbing fibre input from the inferior olive. PCs provide inhibitory input to neurons in the deep cerebellar nuclei (DCN) and vestibular nuclei which integrate the input with other signals including collateral MF and climbing fibre input to produce the cerebellum's ultimate output. Figure by M. Farinella.

The cerebellum can be divided longitudinaly into the vermis (medial cerebellum), the paravermis (intermediate cerebellum or pars intermedia) and the hemispheres (lateral cerebellum; Apps & Garwicz 2005). And along the anteroposterior axis into the anterior, posterior and flocculonodular lobes or in finer detail into 10 individual lobules each with a species-dependent number of folia (**Fig. 1.2**; for a more detialed anatomical description see Apps & Garwicz 2005 and Apps & Hawkes 2009).

The cerebellar cortex has a remarkably simple and uniform architecture comprising three layers, 7 cell types (though others have been identified), two major types of input and one type of output (**Fig. 1.1**).

The three layers are: The granular, or granule cell (GrC) layer, named for the predominant cell type within the layer, which is also home to two types of inhibitory interneuron; Golgi cells (GoCs) which inhibit the GrCs, and the Lugaro cells which inhibit the GoCs, and one type of excitatory interneuron; the unipolar brush cell. The Purkinje cell (PC) layer; comprised of a row of PC bodies. And the molecular layer, comprised of GrC axons (which provide excitatory drive to the layer), dendrites of PCs and GoCs as well as two further types of interneuron; stellate cells and basket cells both of which inhibit PCs (Eccles 1967).

The two types of input arriving at the cerebellar cortex are mossy fibres (MFs; which arise from a range of precerebellar nuclei) and climbing fibres (which arise from the inferior olive). Both MFs and climbing fibres are excitatory (though there have been reports of inhibitory MFs; Hámori & Takács 1989; Hamori *et al*. 1990) and target the GrC layer and PCs respectively. Both fibre types send collaterals to the DCN (FitzGerald & Folan-Curan 2002). The cerebellar cortex also receives aminergic (Schweighofer *et al*. 2004) and peptidergic (Ito 2008) input though to a much less significant extent.

PCs represent the sole output of the cerebellar cortex. PC axons exclusively target the DCN with the exception of those arising from the flocculonodular lobe some of which target the vestibular nuclei of the brainstem (FitzGerald & Folan-Curan 2002).

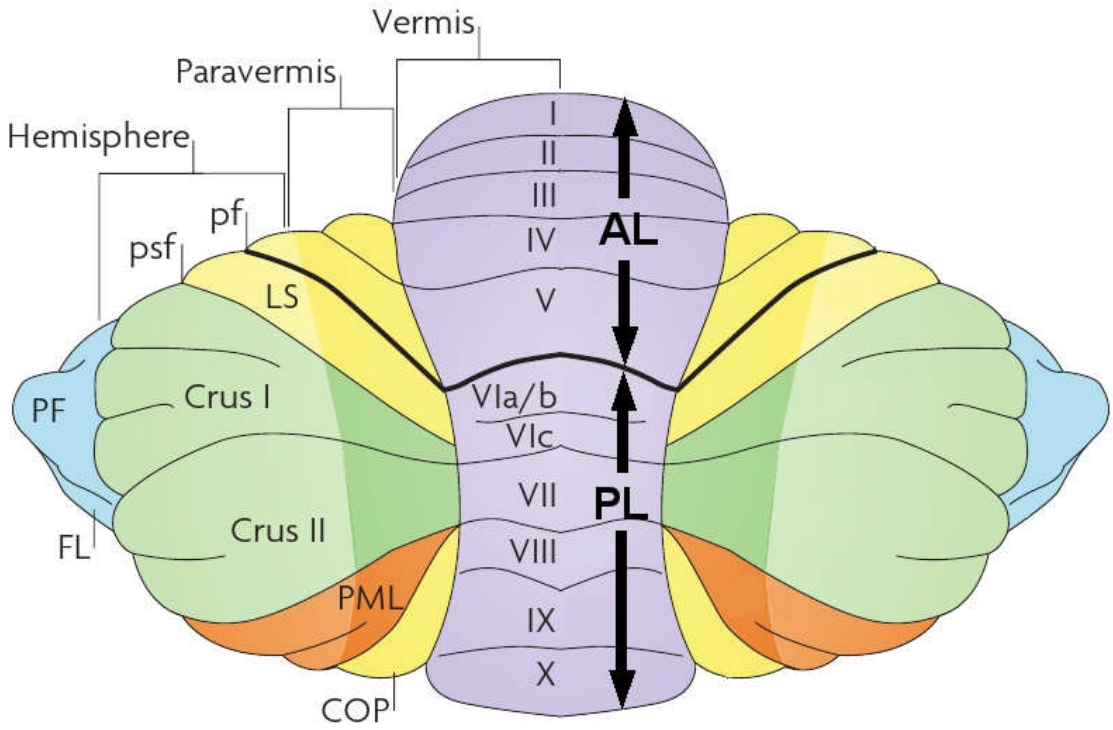

Fig 1.2: Gross morphology of the cerebellum. Dorsal view of the rat cerebellum. Three longitudinal compartments are indicated (the vermis, the paravermis and the hemisphere). Lobules in the vermis are numbered according to Larsell's schema. The primary fissure (pf) dividing the anterior and posterior lobes is highlighted in bold. AL, anterior lobe; COP, copula pyramidis; Crus I and Crus II, ansiform lobule; FL, flocculus; LS, lobulus simplex; PF, paraflocculus; PL, posterior lobe; PML, paramedian lobule; psf, posterior superior fissure. Figure is modified from Apps & Hawkes 2009.

It is thought that PCs can be divided into functional blocks known as microzones; sagittal strips containing 1,000 or so cell bodies with common receptive fields, climbing fibre, aminergic, peptidergic and interneuronal input (Oscarsson 1979; Apps & Garwicz 2005; Schweighofer *et al*. 2004; Ito 2008). PCs within a microzone also tend to target common circuits within the DCN which in turn send inhibitory input to regions of the inferior olive providing the PCs with climbing fibres (Apps & Garwicz 2005; Uusisaari & De Schutter 2011).

The basic wiring of the cerebellar cortex is schematised in **Fig. 1.1**, each of the constituents are discussed in greater detail below.

1.1.2 The deep cerebellar nuclei

With the exception of the vestibular nuclei (which are responsible for much of the output of the flocculonodular lobe; Barmack 2003), the DCN represent the sole output of the cerebellum. In addition to PC input the DCN receive MF and climbing fibre collaterals. Broadly speaking the DCN are comprised of at least 6 cell types (**Fig. 1.3**; Uusisaari & De Schutter 2011) and send inhibitory input to the inferior olive (Fredette & Mugnaini 1991) and predominantly excitatory input to the cortex via various brainstem nuclei and the thalamus, with different cerebellar nuclei targeting different cortical regions/systems (Kelly & Strick 2003).

Inhibitory projection neurons in the DCN have been shown to target areas in the inferior olive that provide climbing fibre input to PCs that in turn inhibit the same DCN projection neurons creating an olivo–cortico–nucleo–olivary loop. However, while evidence for this arrangement between the flocculus and associated regions of the cerebellum and inferior olive is strong, it is not clear how well it can be generalised to other areas (Uusisaari & De Schutter 2011).

The fastigial nuclei receive input from the vermal cerebellar cortex and project to the ipsi- and contralateral vestibular nuclei as well as the reticular formation. Outputs to the medial and superior vestibular nuclei have been related to eye movement while outputs to the lateral vestibular nuclei (including those arising directly from the flocculonodular cortex) are involved in balance and eye movement (FitzGerald & Folan-Curan 2002).

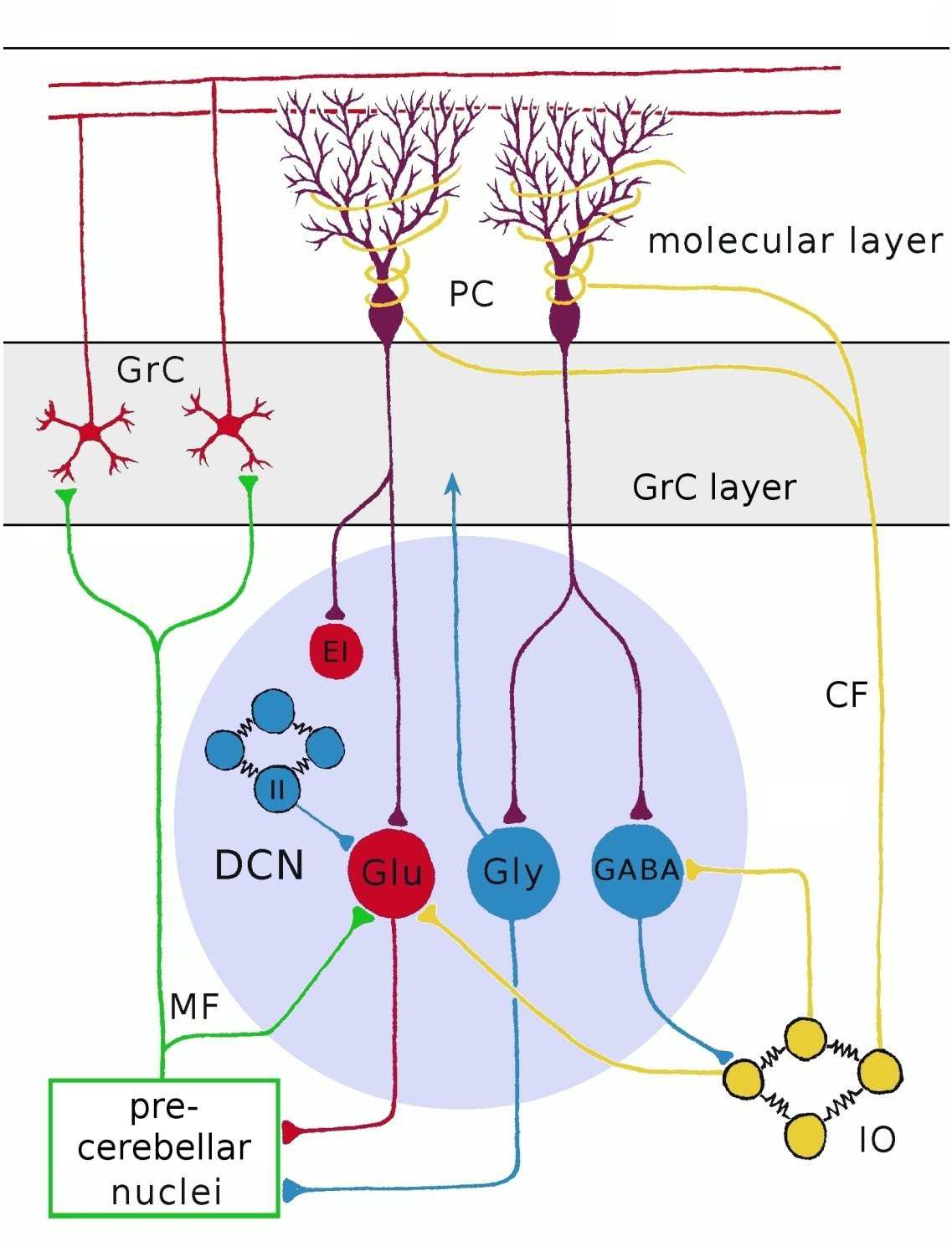
molecular layer
PC
GrC
GrC layer
EI
II
DCN
Glu
Gly
GABA
CF
MF
pre-
cerebellar
nuclei
IO

Fig. 1.3: Known circuitry of the deep cerebellar nuclei (DCN). Unlike the cerebellar cortex, the basic functional anatomy of the DCN is still poorly understood. Both the DCN and the cerebellar cortex receive excitatory input in the form of mossy fibres (MF) arising from various vestibular and sensorimotor (and perhaps other) nuclei and climbing fibres (CFs) arising from the inferior olive (IO). In the cerebellar cortex MFs target GrCs while CFs target Purkinje cells (PCs). Purkinje cells integrate the CF and MF-derived inputs and send inhibitory output to the DCN (several types of interneuron have been omitted from the cerebellar cortex for clarity (see **Fig. 1.1**). PCs target many neuronal types in the DCN including excitatory interneurons (EI; the targets of which are unknown), GABAergic projection neurons (GABA) which target the IO, glycinergic projection neurons (Gly) which target the cerebellar cortex and vestibular/motor nuclei and glutamatergic projection neurons (Glu) which also target vestibular/motor nuclei. The glutamatergic projection neurons are also regulated by local inhibitory interneurons. These interneurons are connected via gap junctions (Van der Giessen *et al*. 2006) but it is unknown what synaptic input they receive. Figure by M. Farinella.

The interposed nuclei receive major input from the anterior and medial cerebellar cortex and predominantly project to the contralateral reticular formation and red nucleus. Projections to the former are thought to regulate the activity of the reticulospinal tract in relation to posture and locomotion while projections to the latter are believed to play a role in motor learning (FitzGerald & Folan-Curan 2002).

The dentate nucleus predominantly receives input from the lateral cerebellar cortex and outputs primarily to the contralateral motor cortex (via the thalamus), though it sends significant collateral input to the red nucleus and superior colliculus, and is involved in the control of eye movements (Glickstein & Doron 2008; Middleton & Strick 1997).

1.1.3 The cerebellar cortex

Mossy fibres

MFs convey multimodal information from a range of sources including the cortex (via the pontocerebellar pathway), vestibular nerve and nuclei, spinal cord and reticular formation. MFs target the GrC layer wherein they branch extensively before forming specialised presynaptic structures known as rosettes (on average ~ 14–25 rosettes/MF; Wu *et al*. 1999). These rosettes provide glutamatergic (though putative cholinergic and GABAergic MFs have been identified; Hámori & Takacs 1989; Hamori *et al*. 1990; Jaarsma *et al.* 1996) synaptic input to GrCs, unipolar brush cells, GoCs and Lugaro cells (Palay & Chan-Palay 1974), each rosette is thought to contact 20–50 GrCs (Eccles *et al*. 1967; Jakab & Hamori 1988). Each MF–GrC synaptic contact has on average 5 functional release sites (Sargent *et al*. 2005). These contacts are densely packed (0.46–0.6 µM separation distance; Xu-Friedman & Regehr 2003; Nielsen *et al*. 2004) and surrounded by an astrocytic sheath, promoting spillover of glutamate from adjacent release sites (Xu-Friedman & Regehr 2003; DiGregorio *et al*. 2002).

Granule cells

GrCs are the most abundant cell type in the vertebrate brain (there are ~10^{11} in human; Braitenberg & Atwood 1958). They have small spherical cell bodies (5–6 µm in diameter in the rat; Palay & Chan-Palay 1974) with (on average) four short dendrites each of which receives synaptic input from a single MF (Eccles *et al*. 1967) and GoCs

(on average 0.6/dendrite; Jakab & Hamori 1988). Despite their dendrites GrCs are electrically compact and as such can be treated as a single electrical compartment (Silver *et al*. 1992; Silver *et al*. 1996).

GrC axons ascend into the molecular layer before bifurcating to give rise to parallel fibres that extend in the coronal plane (parallel fibre length is ~ 3 mm in adult rats; Haung & Huang 1998) where they provide excitatory input to PCs (94 % of parallel fibre synapses) as well as GoCs, stellate cells and basket cells (Palay & Chan-Palay 1974). Parallel fibres are thought to contact almost half of the PC arborisations they pass through forming on average only one or two synapses, it is estimated that they contact between 45 (Palay & Chan-Palay 1974) and 300 PCs (Eccles *et al*. 1967) along their length.

Unipolar brush cells

Unipolar brush cells are excitatory interneurons intermediate in size between GrCs and GoCs found predominantly in the vestibulocerebellum (Diño *et al*. 1999). They receive a unitary giant MF input to their single brush shaped dendrites (Diño *et al*. 2000). The giant nature of the MF–unipolar brush cell synapse promotes the build up of glutamate spillover (Rossi *et al*. 1995). *In vitro* activation of these synapses typically triggers a burst of action potentials; however *in vivo* unipolar brush cells are thought to exhibit a regular spiking pattern (Ruigrok *et al*. 2011; Simpson *et al*. 2005; Barmack & Yakhnitsa 2008). Unipolar brush cells give rise to axons which extend within the GrC layer forming presynaptic densities similar in nature to the rosettes arising from MFs (Rossi *et al*. 1995). Like typical MFs they target GrCs, GoCs and other unipolar brush cells (Diño *et al*. 2000). Unipolar brush cells receive mixed glycinergic/GABAergic inhibitory input from GoCs (Dugue *et al*. 2005; Galliano *et al*. 2010).

Golgi cells

GoCs are inhibitory GABAergic and/or glycinergic interneurons (Simat *et al*. 2007). They have a rounded or polygonal soma (10–30 µm in diameter) and possess an ascending dendritic tree that reaches into the molecular layer as well as basolateral dendrites and a large axonal plexus that are restricted to the GrC layer (Golgi 1874; Ramon y Cajal 1911). GoCs receive excitatory drive via MF input to their basolateral

dendrites (providing feedforward, or perhaps lateral, inhibiton; Kanichay & Silver 2008) and parallel fibre input to their ascending dendrites (traditionally thought to generate a feedback inhibitory loop; Dieudonné 1998; Palay & Chan- Palay 1974). There is also evidence to suggest that they receive input from climbing fibres (Xu & Edgley 2008) and cholinergic fibres (Jaarsma *et al.* 1997). GoCs receive inhibitory input from Lugaro cells (Dieudonné & Dumoulin 2000) and perhaps from molecular layer interneurons and PC collaterals (Dumoulin *et al*. 2001; Palay & Chan-Palay 1974; Larramendi & Lemkey- Johnston 1970).

In the absence of excitatory drive GoCs are spontaneously active in the rat and fire at ~ 8 Hz in slice at near physiological temperature (34ºC; Dieudonné, 1998; Forti *et al*. 2006) and from ~2 to 30 Hz *in vivo* under anaesthesia (Vos *et al*. 1999a; Vos *et al*. 1999b; Maex *et al*. 2000; Simpson *et al*. 2005; Holtzman *et al*. 2006a; Dugue *et al*. 2009; Ruigrok *et al*. 2011).

GoCs are connected to one another via connexin36-containing gap junctions (Dugue *et al*. 2009; Vervaeke *et al*. 2010) which promote synchrony of the GoC network under low input conditions but can trigger rapid network desynchronization in response to sparse, coincident mossy fibre input (Vervaeke *et al*. 2010).

GoCs are the only source of inhibitory synaptic input to GrCs and unipolar brush cells. A single GoC axon occupies an area of 29 μm^3, innervates ~ 145 glomeruli, has been estimated to make direct synaptic contacts with ~ 1500 GrCs (Kanichay 2008) and likely also gives rise to many indirect spillover inputs (Rossi & Hamann 1998).

Lugaro cells

The intermediate cell of Lugaro (Lugaro, 1894) is a fusiform neuron (cell body 9–10 µm in thickness 25–30 µm in length) with long horizontal dendrites (300–600 µm) laying just beneath the PC layer (Palay & Chan -Palay 1974). Lugaro cells are mixed GABAergic/glycinergic inhibitory interneurons. They are sensitive to 5-HT, and are thought to be driven predominantly by a diffuse network of serotonergic fibres which innervate the cerebellar cortex (Dieudonné & Dumoulin 2000), however they may also be sensitive to MF input and limited anatomical evidence implies that they receive input from climbing fibres and PCs (Palay & Chan-Palay 1974). They have parasagittally

and transversely oriented thin varicose axons which traverse the GrC layer, where they typically contact > 100 GoCs (Dieudonné & Dumoulin 2000; Dumoulin *et al*. 2001), and the molecular layer where they are thought to target PCs (Dean *et al*. 2003) and molecular layer interneurons (Lainé and Axelrad 1998).

Purkinje cells

PCs are large (soma diameter ~ 25 µm in rat; Braitenberg & Atwood 1958) GABAergic neurons. Their dendritic trees fan out in the sagittal plane for 300–400 µm and only 15–20 µm in the longitudinal axis (Cajal 1911). PCs receives excitatory glutametergic input to their arbour from vast numbers of parallel fibres (~150,000; Harvey & Napper 1991) and a single climbing fibre. PCs also receive inhibitory input from basket cells (to the cell body) and stellate cells (to the dendrites).

Like GoCs PCs are autorythmic and fire regularly at between 10 and 150 Hz in the absence of defined excitatory drive (Latham & Paul 1971; De Zeeuw *et al*. 2011). GrC–parallel fibre inputs, which are individually weak (Bower 2002) and in many cases silent (Isope & Barbour 2002), serve to modulate the overall rate and pattern of PC firing. The GrCs with the largest impact on PC firing are those situated directly beneath which make functional contacts with the ascending part of their axon (these contacts have higher connection probabilities, synaptic weights and lower susceptibility to certain forms of long term depression; LTD; Isope & Barbour 2002; Sims & Hartell 2005; Sims & Hartell 2006). By contrast, climbing fibres, which traverse the PC arborisation making ~ 1,000 active contacts, are extremely potent and, upon activation, depolarise the bulk of the dendritic tree giving rise to a characteristic complex spike (De Zeeuw *et al*. 2011). Complex spikes are typically triggered at around 1 Hz (Latham & Paul 1971) reaching a maximum of 12 Hz (De Zeeuw *et al*. 2011). The association of a parallel fibre input with a complex spike has been suggested to alter its synaptic weight (Ito *et al*. 1982; Hartell 2002; Le Guen & De Zeeuw 2010). Basket and stellate cells provide inhibitory input to the PCs that serves primarily to regulate simple spike output (De Zeeuw *et al*. 2011).

PCs represent the sole output of the cerebellar cortex. They make inhibitory synapses onto neurons of the DCN (**Fig. 1.3**; and vestibular nuclei) which in turn represent the sole output of the cerebellum. PCs have a high convergence rate, with each DCN

neuron receiving 10s to 100s of PC inputs from a single microzone (Uusisaari & De Schutter 2011). PC axons also give rise to collaterals which are thought to innervate GoCs, basket cells and (at least in juvenile animals) other PCs (Hámori and Szentagothai 1968; Larramendi and Lemkey-Johnston 1970; De Camilli *et al*. 1984; Watt *et al*. 2009).

Climbing fibres

Climbing fibres arise from the inferior olive. The mammalian inferior olive is composed of the principal olive, the dorsal and medial accessory olives, and several smaller subnuclei which project to and receive input from the DCN in a reciprocally and topographically organized fashion (Ruigrok 1997; Uusisaari & De Schutter 2011). The DCN input to the inferior olive is inhibitory; however, the inferior olive receives excitatory input from several precerebellar nuclei, including the parvocellular red nucleus, the nucleus of Darkschewitsch, and the nucleus of Bechterew, all of which receive input from the DCN (Onodera 1984).

The projection neurons of the inferior olive are connected via gap junctions promoting synchrony of subthreshold oscillations, complex spike synchrony among the PCs within given microzones and coherence among PCs across larger parts of the cerebellar cortex (De Zeeuw *et al*. 2011).

The molecular layer interneurons

Basket and stellate cells are similar in terms of morphology; both are spiny stellate GABAergic interneurons (Jörntell *et al*. 2010). They have similar firing behaviour; both are autorythmic in slice and fire irregularly *in vivo* (Ruigrok *et al*. 2011). They share common inputs; excitatory drive from parallel fibres as well as spillover input from climbing fibres (Jörntell & Ekerot 2002; Szapiro & Barbour 2007) and inhibitory input from neighbouring interneurons (Kondo & Marty 1998) and perhaps from Lugaro cells (Lainé and Axelrad 1998). Both cells also share common targets; PCs, other molecular layer interneurons (Kondo & Marty 1998) and potentially GoCs (Dumoulin *et al*. 2001). However, basket cells and stellate cells can be differentiated by their axons; basket cell axons form dense pericellular nets around PC somas while stellate cells target PC dendrites (Eccles *et al*. 1967). Further, basket cells tend to lie deeper in

the molecular layer than stellate cells (Sultan & Bower 1998). Like GoCs, molecular layer interneurons are connected via gap junctions and as such fire in synchrony under certain conditions (Sotelo & Llinas 1972; Middleton *et al*. 2008).

Aminergic and peptidergic inputs to the cerebellar cortex

In addition to MFs and climbing fibres the cerebellum receives input from a number of aminergic and peptidergic fibres. Of these the most abundant are the serotonergic fibres which arise primarily from nuclei in the medullary and pontine reticular formation, and the various raphe nuclei (Schweighofer *et al*. 2004). In the cerebellar cortex they are known to excite Lugaro cells and may represent the principal input for these cells (Dieudonné & Dumoulin 2000). They have been shown to increase release at MFs but reports regarding their effect on GrCs have been mixed. They have also been suggested to inhibit PCs via an increase in inhibitory tone and a decrease in parallel fibre efficacy (Schweighofer *et al*. 2004). Their effect on the inferior olive and DCN appears to be predominantly excitatory (Saitow *et al*. 2009; Schweighofer *et al*. 2004).

Noradrenergic fibres represent the second most abundant aminergic input to the cerebellum and project to all parts of the cerebellar cortex originating from the dorsal and ventral parts of the locus coeruleus. They primarily target GrCs and PCs, however no direct effect of noradrenaline (NA) on GrCs has been reported. NA has a net inhibitory effect on PCs, but increases their sensitivity to parallel fibre inputs (Schweighofer *et al*. 2004). The inhibitory effect may be mediated via basket cells in which NA is shown to increase firing and release (via activation of β and α1 receptors, conversely however, NA suppresses release via α2 receptors; Hirono & Obata 2006; Herold *et al*. 2005; Saitow *et al*. 2005). In the DCN and inferior olive NA application has a net inhibitory effect and blocks oscillations (Schweighofer *et al*. 2004).

Cholinergic inputs to the cerebellum are sparse but potentially significant. They arrive in two forms; cholinergic MFs targeting the flocculonodular lobe that arise primarily from the caudal medial vestibular nucleus, and a diffuse plexus of beaded fibres targeting the cerebellar cortex and DCN that arise from the pedunculopontine tegmental nucleus, the lateral paragigantocellular nucleus, and to a lesser extent, the various raphe nuclei (Jaarsma *et al*. 1997). Acetylcholine (ACh) application to cerebellar slices has

been shown to evoke large action potential independent GABAergic currents in GrCs via a nicotinic receptor dependent mechanism (Rossi *et al*. 2003). ACh excites and triggers gamma band and very fast oscillations in molecular layer interneurons (de la Garza *et al*. 1987; Middleton *et al*. 2008) and reduces PC simple spike output (de la Garza *et al*. 1987).

Sparse dopaminergic inputs to the cerebellar cortex arising from the ventral tegmental area are thought to regulate PC activity. Dopamine is required for the PC depolarization-induced slow current (Kim *et al*. 2009) and regulates rebound potentiation and possibly parallel fibre LTD (Schweighofer *et al*. 2004).

Histaminergic inputs can also be found in the cerebellum and are thought to play a role in arousal having a net excitatory effect on PCs and GrCs (Schweighofer *et al*. 2004).

The cerebellum also contains 22 types of neuropeptide, however their expression is generally weak and diffuse, of these corticotrophin releasing factor may be of particular import as it is thought to be required for parallel fibre–PC LTD (Miyata *et al*. 1999; Ito 2009).

Aminergic and peptidergic inputs may serve to alter the functional state of microzones within the cerebellum (Schweighofer *et al*. 2004; Ito 2009).

1.2 Popular theories of cerebellar function

Several theories of cerebellar function have been proposed. Most early theories accounted for aspects of ongoing behavior on the basis of cerebellar signal processing (e.g. Braitenberg & Atwood 1958). With the delineation of the basic functional architecture of the cerebellum in the late 1960s (Eccles *et al*. 1967) the door was opened for theoreticians to develop more physiologically accurate models of cerebellar function. Many of the resulting theories can be termed "learning theories", which suppose that the cerebellum can modify its behavior through synaptic plasticity according to task demands. Almost all learning theories of cerebellar function are at least loosely derived from theoretical work by David Marr (Marr 1969). Indeed, a direct derivative of Marr's original theory, the Marr–Albus theory, which incorporates

the theoretical insights of James Albus (Albus 1971), remains a popular theory of cerebellar function to date on account of the strong empirical support it has received (Ito 2001). In spite of its popularity, the Marr–Albus theory is still viewed as an incomplete description of cerebellar function, various adaptations and replacements have been proposed including the adaptive filter model (Fujita 1982) and models that propose the cerebellum relies on a temporal coding strategy (e.g. the temporal pattern generator model; Jacobson *et al*. 2008). The Marr–Albus, adaptive filter and possible alternative models of cerebellar function relying on temporal coding regimes are discussed in brief below.

1.2.1 The Marr–Albus theory

Marr proposed that the cerebellar cortex performs the task of learning motor skills for movement and posture. The central tenet of Marr's theory is that the cerebellum acts as an associative learning machine. MFs carry sensory information to PCs (via parallel fibres) which is integrated with a climbing fibre input. The climbing fibre input is thought to serve as a learning signal; the association of this learning signal with the MF derived input is expected to alter the weight of the parallel fibre inputs. In this way PCs can be trained to respond to a very specific set of sensory inputs. Specific patterns of PC activity are expected to elicit/modify motor responses. As such sensory inputs and motor outputs can be matched. If the appropriateness of a motor output to a given sensory pattern changes, then the PCs can be retrained.

According to Marr's model, the principal role of the GrC layer is to maximise the number of input patterns a given PC can learn. Thus the GrC layer performs "expansion recoding" of MF inputs in order to make them sparser and more orthogonal. GoC are proposed to modulate the GrC responses to produce 'better" activity patterns, serving to further sparsify MF signals (and thereby increase the number of patterns that can be learned) and keep the GrC output range relatively stable in response to widely variable levels of MF input. The molecular layer interneurons were expected to perform a similar function at the PC level (Marr 1969).

Albus's principal contribution was to suggest that the learning mechanism applied at the parallel fibre–PC synapse was LTD (Marr had assumed long-term potentiation; LTP). He also proposed that synaptic weights onto the cerebellar interneurons might be

subject to modification (Albus 1971) an idea that has received recent experimental confirmation (Jörntell & Ekerot 2002; Szapiro & Barbour 2007).

The Marr–Albus theory has received a wealth of evidential support (Ito 2001) but equally data has come to light which casts doubt on its validity (for example there is an ongoing controversy over the importance of LTD at parallel fibre–PC synapses for cerebellar learning; Welsh *et al*. 2005; Schonewille 2011). Resultantly theorists have suggested adaptations of or alternatives to the Marr–Albus theory.

1.2.2 The adaptive filter theory

Adaptive filter is a term used in electronics to describe a filter that self-adjusts its transfer function according to an optimization algorithm driven by an error signal. Fujita (1982) was the first to suggest that the cerebellum might work in this way. His ideas have been popularised recently by the argument that Marr–Albus models are in effect adaptive filters (**Fig. 1.4**), the receipt of strong evidential backing for key theoretical predictions (symmetrical LTP and LTD at parallel fibre synapses, interneuron plasticity, silent parallel fibre synapses and recurrent mossy fibre connectivity; Dean *et al*. 2010), and demonstrations that adaptive filters could at least theoretically be utilised to implement several cerebellar functions including eye blink conditioning (Yeo & Hesslow 1998; Lepora *et al*. 2010), the vestibular–ocular reflex (VOR; De Zeeuw & Yeo 2005; Dean & Porrill 2011), saccadic accuracy (Schweighofer *et al*. 1996; Gad & Anastasio 2010), and noise cancellation (Dean & Porrill 2011).

Aspects of the adaptive filter theory are still controversial. For example, an important feature of the adaptive filter theory is that the GrC layer must decompose MF signals into different components. However, some studies have suggested that GrCs may serve as mere coincidence detectors or noise filters (Rancz *et al*. 2007; Jörntell & Ekerot 2006; Jörntell & Ekerot 2008; Bengtsson & Jörntell 2009). If GrCs do not perform complex signal decomposition then the diversity of parallel fibre signals required might be supplied by the MFs themselves (Yamamoto *et al*. 2002) or through the feedback activity of GoCs (Medina *et al*. 2000). However, it is not clear whether the GoC is well suited to perform such a task. Adaptive filter models of the cerebellum are also not easily compatible with evidence that PCs utilise a complex temporal coding strategy (De Zeeuw *et al*. 2011; De Schutter & Steuber 2009).

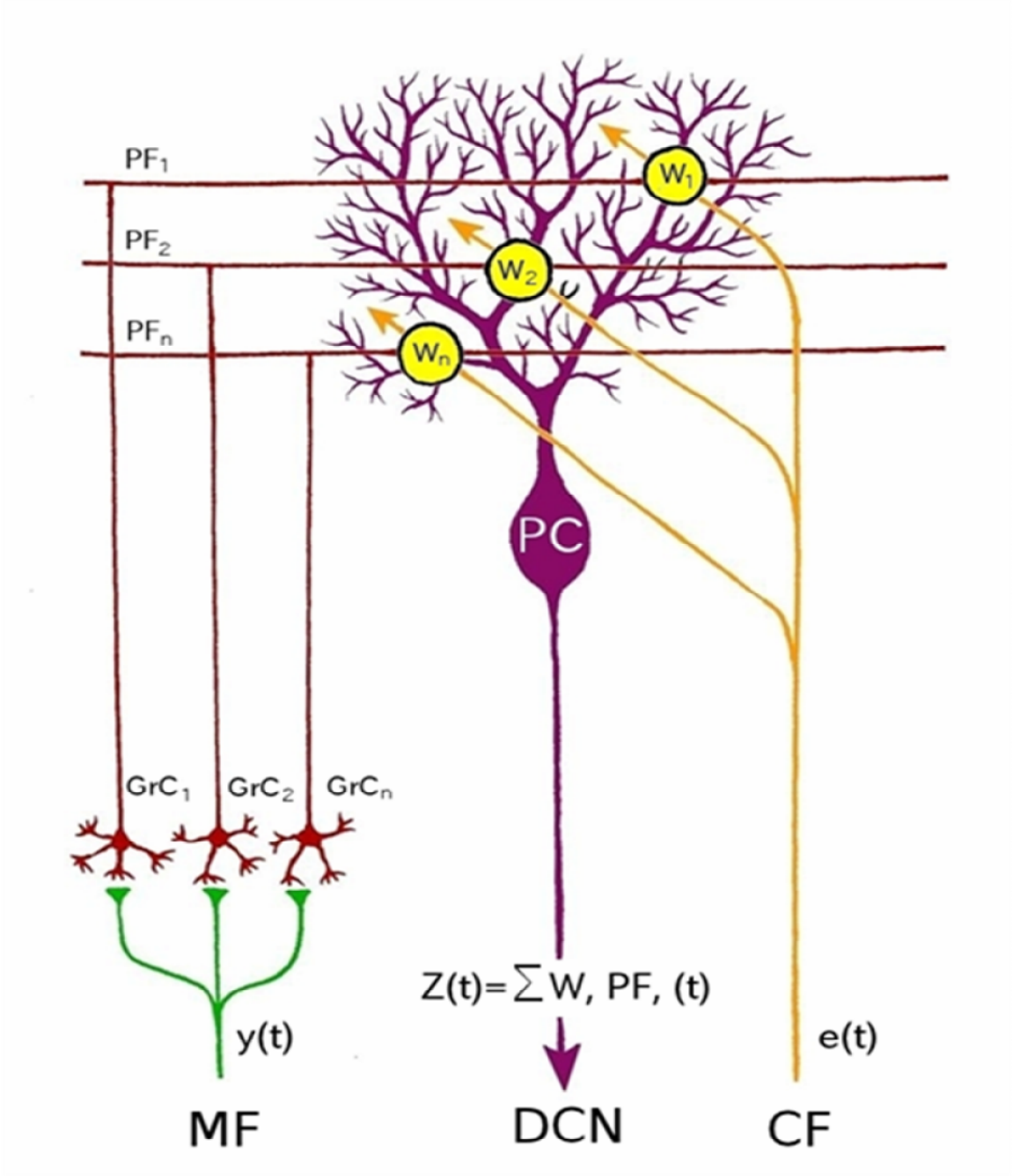
PF1
PF2
PFn
W1
W2
Wn
PC
GrC1
GrC2
GrCn
y(t)
Z(t)=∑W, PF, (t)
e(t)
MF
DCN
CF

Fig. 1.4: The cerebellar cortex as an adaptive filter. A mossy fibre (MF) input signal is distributed over many granule cells (GrCs), the axons of which form parallel fibres (PFs) that synapse onto Purkinje cells (PCs). Correlated firing of a PF and the climbing fibre (CF) alters the strength of the PF–PC synapse. Note that this figure omits a number of the microcircuit features shown in **Fig. 1.1**. The structure of this microcircuit can be identified with that of an adaptive filter as follows: the processing of a sensory input or motor signal by the GrC layer is interpreted as analysis by a bank of filters. PC output is modelled as a weighted sum of these PF inputs, with the weights corresponding to synaptic efficacies. The CF input is interpreted as a teaching signal that adapts synaptic weights using the covariance learning rule (Sejnowski 1977). Formally, the filter weights W_n are adjusted by $\delta W_n = -\beta(ePF_n)$, where δW_n is the change in weight, β is the learning rate, e is the teaching signal, PF_n is the signal to the weight and (ePF_n) denotes the covariance of e and PF_n. The teaching signal e is often performance error. The learning rule can then be shown theoretically to minimize mean square performance error (e^2). Most adaptive filter models rely on weights that can switch between positive and negative values. This is not true of individual synapses, however the problem can be overcome if the molecular layer interneurons are introduced to the model and conferred with similar plasticity/learning rules (but with opposite sign). Figure adapted from Dean *et al*. 2010 by M. Farinella.

1.2.3 Temporal theories of cerebellar function

The Marr–Albus and the adaptive filter theories provide useful but problematic descriptions of cerebellar function. A potential caveat for these theories is that PCs fire intrinsically (arguably lacking the pattern selective responsiveness required by the Marr–Albus framework) and have highly convergent outputs such that subtle changes in the rate of individual PC firing may not have much effect on cells within the DCN and therefore motor output. Additionally, PC simple spike firing has been shown to exhibit patterns and pauses (Shin & De Schutter 2006; De Schutter & Steuber 2009) which might denote a complex non-linear coding strategy that would be inconsistent with the simple linear code assumed to be employed by the Marr–Albus and the adaptive filter theories (indeed, both gain of function and loss of function mutations that affect the PC firing pattern but not rate can result in ataxia; Hoebeek *et al*. 2005). Further, inhibiting LTD (the mechanism presumed to underlie much of the learning in Marr–Albus and adaptive filter frameworks) does not necessarily seem to affect motor learning (Welsh *et al*. 2005; Schonewille *et al*. 2011).

Increasing evidence suggests that under certain conditions the cerebellum may utilise a temporal coding regime. Oscillations of various frequencies have been detected in the cerebellum: the inferior olive and resultant complex spike activity can oscillate from 1 to 9 Hz (Lang *et al*., 2006; Van Der Giessen *et al*., 2008), oscillations in the GrC layer have been detected in the Theta (4–9 Hz; Hartmann & Bower 1998; O'Connor *et al*. 2002; D'Angelo *et al*. 2001) and Beta bands (10–30 Hz; Courtemanche *et al*. 2002; O'Connor *et al*. 2002; Courtemanche & Lamarre 2005; Courtemanche *et al*. 2009), while oscillations in the molecular layer are known to occur in the Gamma range (30–80 Hz) and above (Middleton *et al*, 2008). Oscillations in the inferior olive have been associated with learning dependent timing (Lang *et al*., 2006; Van Der Giessen *et al*., 2008), while Theta and Beta oscillations in the GrC layer may be linked to the assessment of sensory state and/or communication with other brain regions during sensorimotor processing (Discussed in further detail in **1.4.2**; Hartmann & Bower 1998; D'Angelo *et al*. 2001; Courtemanche & Lamarre 2005; Soteropoulos & Baker 2006).

That many neurons in the DCN respond to breaks in PC-mediated inhibition with strong rebound spikes and groups of PCs often exhibit synchronous pauses implies that the timing of activity and pauses in PC output may convey a timing signal (De Schutter &

Steuber 2009; Tadayonnejad *et al*. 2010). It has also been suggested that olivary signals, rather than acting as a learning signal, directly control cerebellar output and may convey quick reaction commands (directly to the DCN and via the cerebellar cortex), while MF inputs can dictate improved conditioned reaction movements that occur with a short delay (DeZeeuw *et al*. 2011). Alternatively, it has been suggested that the inferior olive generates temporal patterns for use in motor, sensory and cognitive tasks and that MF input to the cerebellum can serve to reconfigure these temporal patterns according to task demand (Jacobson *et al*. 2008).

The idea that the cerebellum utlilises temporal coding is not necessarily at odds with the idea that the cerebellum uses a rate coding strategy. It is possible that rate coding and temporal coding strategies are employed according to task demand; control of slow compensatory eye and head movements, such as is performed by the vestibulocerebellum have been argued to require rate coding while the processing of rapid whisker movements by the neocerebellum has been argued to depend upon temporal coding. Further, some tasks are argued to rely upon a combination of the two, for example adaptation of the VOR (DeZeeuw *et al*. 2011). Whether the cerebellum utilises a rate or temporal code may depend to a large extent on the nature of information entering the GrC layer and how it is decomposed therein.

1.3 Information processing in the GrC

1.3.1 The mossy fibre–GrC synapse

Synaptic input from MFs onto GrCs is mediated via fast α-amino-3-hydroxy-5-methyl-4-isoxazolepropionic acid (AMPA) receptor and slower N-methyl D-aspartate (NMDA) receptor conductances (Silver *et al*. 1992; D'Angelo *et al*. 1995; Cathala *et al*. 2003) though the contribution of the latter to the excitatory post synaptic current (EPSC) diminishes with maturation due to the replacement of NR2B subunits with NR2A and C (Cathala *et al*. 2000; Cathala *et al*. 2003).

MF EPSCs result from both direct synaptic connections, and spillover following release from adjacent active zones which give rise to the fast and slow rising components of the EPSC respectively (DiGregorio *et al*. 2002). Spillover inputs are visible in isolation when the direct release sites fail (Sargent *et al*. 2005). Their slower rise time results

from the diffusional distance between release site and target coupled with slow channel activation resulting from low glutamate concentration. Diffusion of glutamate from increasingly distant release sites prolongs the decay phase of the EPSC (DiGregorio *et al*. 2002; Nielsen *et al*. 2004). Spillover is thought to account for roughly half the charge of the AMPA receptor-mediated EPSC. In the event of a failure in direct transmission a spillover current is likely to remain, thus increasing the reliability of the synapse. The slow timecourse of spillover extends the window for integration but may reduce the temporal precision of the GrC spike output (Sargent *et al*. 2005).

MFs can sustain rapid transmission as they have large vesicles pools and fast vesicle reloading. However, short term depression (STD) occurs at the MF–GrC synapse at frequencies ranging from > 20–300 Hz due to rapid AMPAR desensitisation (Saviane *et al*. 2006). LTP can be evoked at the MF–GrC synapse with theta burst stimulation via an NMDA- and metabotropic glutamate receptor- (mGluR) dependent mechanism (D'Angelo *et al*. 1999), increasing MF release (via retrograde nitric oxide signalling; Sola *et al*. 2004) and intrinsic GrC excitability (Armano *et al*. 2000). Conversely, LTD can be elicited with weak, low-frequency MF stimulation (D'Errico *et al*. 2009). Synaptic plasticity may serve to fine tune the precise spiking of GrCs (Arenz *et al*. 2009)

1.3.2 Sensory-evoked inputs to GrCs

In vivo whole cell recordings from GrCs in anaesthetised (Chadderton *et al*. 2004; Rancz *et al*. 2007; Arenz *et al*. 2008) and decerebrate (Jörntell & Ekerot 2006; Bengtsson & Jörntell 2009) animals have allowed the investigation of the types of input to which GrCs are subjected. These studies indicate that synaptic input varies widely between cerebellar regions. In Crus I and IIa of the rat spontaneous EPSCs occur at around 4 Hz (Rancz *et al*. 2007). However, in lobules IV and V of the C3 region of the decerebrate cat EPSCs occur at between 10 and 50 Hz (Jorntell & Ekerot 2006). Similarly in the flocculus of the mouse EPSCs occur at between <1 and 40 Hz (Mean 13 Hz; Arenz *et al*. 2008).

Broadly speaking sensory inputs to the GrC layer can be divided into two loose classes: Discrete sensory stimuli are encoded by bursts of activity which reliably report stimulus onset, as found for example in Crus I and IIa upon whisker deflection which elicits

instantaneous firing frequencies of up to 700 Hz (Rancz *et al*. 2007). While continuous sensory variables (such as joint angle) are typically encoded by a modulation of EPSC frequency (i.e. rate coded) as found for example in the flocculus in response to head movement relative to a preferred direction (Arenz *et al*. 2008). In the lateral paravermis of the decerebrate cat cutaneous stimulation of the forelimb evokes a phasic burst of synaptic responses, while joint angle manipulation of the digits of the forepaw evokes sustained synaptic activity (Jorntell & Ekerot 2006).

It is interesting to note that the spontaneous EPSC rates in Crus I and IIa (which seem to deal preferentially with discrete sensory inputs) are extremely low, most likely in order to provide an optimal signal to noise ratio (Rancz *et al*. 2007). While regions dealing with continuous sensory variables have high background synaptic activity, presumably conveying some form of rate coded input (Arenz *et al*. 2008).

1.3.3 GrC computation

The type of information GrCs relay to PCs will depend on the functional properties of the GrC and the types of input that they receive. Given that GrCs are electrically compact (Silver *et al*. 1992) and have not been shown to contain many complex conductances, individual GrCs are unlikely to perform complicated manipulations of the input they receive. However, at very least GrCs perform some form of filtering/thresholding operation.

MF inputs undergo STD, conferring the additional property of a low pass filter (Abbott & Regehr 2004); however MF EPSCs contain a large spillover component (DiGregorio *et al*. 2002) which might be expected to confer the synapse with the properties of a high pass filter. These two phenomena largely compensate one another at low and intermediate MF firing rates ensuring that the charge generated by a MF input remains fairly constant, at high rates however the build up of spillover outweighs the STD conferring high pass filtering characteristics on the synapse (Saviane & Silver 2006).

The extent to which GrCs are acting are acting as coincidence detectors or noise filters depends on their threshold. If GrCs require multiple MF inputs to fire they can be considered coincidence detectors while if they respond to single inputs they may serve predominantly to filter out noise. This is a controversial issue in the field; activation of

putative single MFs using a stimulating electrode *in vitro* has been reported to elicit GrC firing (Rancz *et al*. 2007), however several other studies have found that summation from multiple MFs is required to elicit GrC firing (D'Angelo *et al*. 1995; Jorntell & Ekerot 2006; Chadderton *et al*. 2004).

A related issue is whether individual GrCs receive input from MFs that is varied or similar in nature. If incoming information is functionally similar, all MF inputs to the GrC would be activated in relative synchrony, as such GrCs would serve to maximise transmission of the weakest MF input making them reliable relays of discrete and frequency-modulated signals, effective at filtering out non-synchronous noise (Dean *et al*. 2010). It is known that MFs from the same functional systems (Sugihara & Shinoda 1999) or carrying the same input type (Garwicz *et al*. 1998) colocalize to terminate in the same parts of the granular layer, and some studies have suggested that GrCs receive functionally similar inputs to multiple dendrites (at least in the anterior paravermis; Jörntell & Ekerot 2006; Bengtsson & Jörntell 2009).

Conversely there is indirect evidence to suggest that MFs with different modalities or receptive fields converge on single GrCs. Notably, whisker responses in Crus I and IIa are conveyed by a single input (Rancz *et al*. 2007), as is velocity information during horizontal rotation in the flocculus (Arenz *et al*. 2008), so it is possible that the remaining MFs carry information of different modalities or submodalities. This scheme of operation was elegantly shown to be employed in a cerebellum-like sensory structure in mormyrid fish (Sawtell 2010). The advantage of such a coding strategy is that it would give rise to a GrC output that is more selective and sparser than the MF input. While PCs could still pick out a signal conveyed by a single modality across a population of GrCs if desirable, through plasticity they could also learn to respond only to very specific activity patterns generated in the GrC layer, for example they could select for GrC inputs signalling leftward rotation during rightward eye movement rather than responding to GrC inputs conveying leftward rotation and GrC inputs conveying rightward eye movement which would give rise to a noisier, less specific signal.

The computations performed by GrCs are further complicated by inhibitory input.

1.4 Inhibitory regulation of GrCs

Broadly speaking GrCs are subject to two distinct flavours of inhibitory input: A tonic inhibitory input, arising from the persistent release of GABA from glial cells via the Bestrophin 1 (Best1) anion channel (Lee *et al*. 2010) which causes constitiutive activation of high affinity $GABA_A$Rs (which contain the α_6 & δ subunit; Farrant & Nusser 2005) at extrasynaptic sites on GrCs resulting in a persistent inhibitory Cl^- current (Kaneda *et al*. 1995; Tia *et al*. 1996; Wall & Usowicz 1997; Brickley *et al*. 1996; Farrant & Nusser 2005); and phasic inhibitory input; the synaptic release of GABA from GoCs (Eccles *et al*. 1964).

To date there is little evidence to suggest that the level of tonic inhibition can be directly modulated on a short time scale by physiological inputs (though tonic inhibition has been shown to be sensitive to nitric oxide and neurosteroids; Wall 2003; Stell *et al*. 2003), indeed it is possible that tonic inhibition exists at a fixed level to optimise the signal to noise ratio within the GrC layer (though this would seem an energetically costly solution to a relatively simple problem; Rossi *et al*. 2003) while GoCs serve to regulate inhibition in a stimulus dependent fashion.

1.4.1 GoC responses to sensory-evoked inputs

GoCs receive synaptic input to their basolateral dendrites from MFs providing feedforward (or lateral) inhibition to GrCs and from parallel fibres to their ascending dendrites providing feedback inhibition to GrCs. MF inputs to GoCs give rise to large, rapid EPSCs that are predominantly AMPA-mediated, and undergo little short term plasticity (Kanichay & Silver 2008). By contrast, parallel fibre inputs to GoCs have slower kinetics, smaller amplitudes, are mediated by AMPA, NMDA (Dieudonne 1998; Misra *et al*. 2000) and kainate receptors and undergo significant short-term facilitation (Bureau *et al*. 2000). Parallel fibre activity also activates mGluRs which can silence GoCs through the recruitment of G protein-coupled, inwardly rectifying K^+ channels (Watanabe & Nakanishi 2003; Holtzman *et al*. 2011).

Single unit recordings *in vivo* suggest that in the absence of defined sensory input GoCs fire spontaneously at variable rates (mean rate of ~6–15 Hz in rat and cat; Edgley & Lidierth 1987; Vos *et al*. 1999a; Vos *et al*. 1999b; Maex *et al*. 2000; Simpson *et al*.

2005; Holtzman *et al*. 2006a; Dugue *et al*. 2009; Ruigrok *et al*. 2011; lower in mouse (~3 Hz); Barmack & Yakhnitsa 2008; higher in monkey; Miles *et al*. 1980; van Kan *et al*. 1993; Heine *et al*. 2010).

In anaesthetised rats GoCs in Crus I and II of the posterior lobe of the cerebellum most commonly respond to sustained tactile stimulation over a large (even bilateral) receptive field with pauses in firing typically lasting hundreds of milliseconds (Tahon *et al*. 2005; Holtzman *et al*. 2006a; Holtzman *et al*. 2006b). The pause in firing is thought to rely on Lugaro cell activity and the activation of mGluRs via parallel fibres (Holtzman *et al*. 2011), though a contribution of gap junction mediated GoC network desynchronisation may also play a role (Vervaeke *et al*. 2009). In some cases this pause was preceded with a rapid increase in firing rate (Vos *et al*. 1999b; Holtzman *et al*. 2006a; Holtzman *et al*. 2006b). Excitatory responses to tactile stimuli showed an early (5–10 ms) and a late (13–26 ms) component the former of which is presumed to convey a direct spinocerebellar MF signal while the latter may arise from parallel fibre input or cerebrocerebellar MF input (Vos *et al*. 1999b). GoCs sometimes also show rebound firing upon the cessation of tactile input (Tahon *et al*. 2005).

In the cat GoC activity is slightly increased during locomotion with maximal firing rate tuned to a preferred phase of the swing cycle (Edgeley & Lidieth 1987). In the rat uvula-nodulus GoC firing rate is modulated relative to roll tilt in a preferred direction; interestingly GoC tuning was shown to be almost inverse to that of most surrounding GrCs (Barmack & Yakhnitsa 2008). In the intermediate cerebellar cortex of monkeys, tracking tasks involving the operation of specific devices and requiring a single joint movement elicited phasic GoC activity, with most cells responding to the manipulation of multiple joints, though not equally, and showing bidirectional discharge patterns relative to a preferred direction during both active and passive movement. GoC activity in these tasks did not closely reflect recorded activity from surrounding MFs (Van Kan *et al*. 1993). Recordings from the monkey oculomotor vermis found that GoC responses were broadly tuned and failed to correlate strongly with the metrics or timing of eye saccades (Prsa *et al*. 2009), by contrast GoCs in the ventral paraflocculus show bidirectional modulation with narrow tuning in response to eye movement (Heine *et al*. 2010) again GoC activity in this study did not closely reflect the activity of nearby MFs, in many cases having inverse directional tuning.

1.4.2 GoC synchrony

Local field potential oscillations in the Theta and Beta bands have been recorded in the GrC layer of the cerebellar cortex (Hartmann & Bower 1998; D'Angelo *et al*. 2001; O'Connor *et al*. 2002; Courtemanche & Lamarre 2005; Courtemanche *et al*. 2009). GoCs have been shown to discharge synchronously in phase with these oscillations (Dugue *et al*. 2009).

Oscillations in the GrC layer are likely to be mediated at least in part by GoC synchrony arising from connexin36-containing gap junctions between neighbouring GoCs which act as low pass filters preferentially allowing the transmission of the spike afterhyperpolarisation (Dugue *et al*. 2009; Vervaeke *et al*. 2010). However oscillations in synaptic input and the feedback loop between GoCs and GrCs may also contribute to oscillations and synchrony in GrC layer (Vos *et al*. 1999a; Hartmann & Bower 1998). Indeed low frequency oscillations in the GrC layer of the hemispheral lobes are phase locked with oscillations in the sensorimotor cortex (Courtemanche & Lamarre 2005; O'Connor *et al*. 2002; Ros *et al*. 2009). Further, it has been shown that while gap junctions promote synchrony in the GoC network under low input conditions (Dugue *et al*. 2009) they can trigger rapid network desynchronization in response to sparse, coincident mossy fibre input (Vervaeke *et al*. 2010). Network desynchronisation can lead to a reduction or even a pause in GoC firing as GoCs may be inhibited by sequential afterhyperpolarisations transmitted from neighbouring GoCs via gap junctions.

Precisely how oscillations in the GoC network interact with ongoing synaptic input and how GoC synchrony might affect GrC processing are still largely unknown. Oscillations have been shown to help bind neuronal ensembles segregated by distance (Singer & Gray 1995), can be used to recode information according to phase (O'Keefe & Recce 1993) and can contribute to neuronal representations of sensory stimuli (Stopfer *et al*. 1997); which, if any, of these functions GoC synchrony confers on the GrC layer *in vivo* is at this point an open question.

1.4.3 GoC mediated inhibition of GrCs

GoCs are the only interneuron directly regulating GrC activity. Most GoCs co-release GABA and Glycine (Simat *et al*. 2007), but GrCs are not sensitive to the latter (Kaneda *et al*. 1995; Dugue *et al*. 2005). GrC inhibitory post synaptic currents (IPSCs) are comprised of a fast direct component arising from the release of GABA onto GrC post synaptic densities that contain concentrated clusters of $GABA_ARs$ (typically containing γ2 subunits; Farrant & Nusser 2005) as well as a slowly-rising slowly-decaying spillover component mediated by release from adjacent synaptic terminals onto an extrasynaptic population of α_6 subunit containing $GABA_ARs$ (Rossi & Hamann 1998; Wall 2002; Bright *et al*. 2010). Spillover inputs have been shown to exist in the absence of direct GoC inputs (Rossi & Hamann 1998; Crowley *et al*. 2009).

The direct component of the GoC–GrC IPSC undergoes frequency dependent STD (Mapelli *et al*. 2009), conversely spillover undergoes frequency dependent build up due to summation. As such, at high frequencies of GoC firing the spillover component of the IPSC carries the majority of the charge (Crowley *et al*. 2009). To date the majority of characterisation of the GoC–GrC synapse has been performed using stimulating electrodes to trigger GoC firing (Rossi & Hamann 1998; Wall 2002; Crowley *et al*. 2009; Mapelli *et al*. 2009). The disadvantage of this approach is that it lacks specificity; the rate of GoC firing immediately prior to the stimulation cannot be controlled and the stimulation potentially triggers multiple GoCs simultaneously or activates other elements in the circuit which may affect GoC–GrC transmission.

The magnitude of the GoC–GrC input may be subject to modulation by second messengers. In juvenile rats it has been shown that glutamate released upon MF stimulation can reduce GABA release from GoCs via mGluR activation. The effect was frequency-dependent, reducing IPSC amplitude by a maximum of 54 % at 100 Hz MF stimulation (Mitchell & Silver 2000). If this mGluR mediated suppression of inhibition persists in the adult animal it could represent a potent means of controlling GrC excitability.

1.4.4 The effect of inhibition on GrC computation

Marr proposed that inhibition in the GrC layer serves predominantly to maintain GrC excitability within a fixed range in the face of widely variable levels of MF input (Marr 1969). If we assume that GrCs signal to PCs in a primarily rate-coded fashion this can be achieved quite simply by shifting the GrCs input–output (I–O) function to the left (**Fig. 1.5**), a linear subtractive operation (Silver 2010). However, it has been shown that, when delivered with a noisy excitatory input tonic inhibition or indeed phasic inhibition serves principally to alter the slope, or "gain" of the GrCs I–O function (Mitchell & Silver 2003), though it has been argued that the direct component of the GoC IPSC can perform a principally additive function (Crowley *et al*. 2009).

For Marr's assumption to be tenable GoCs would be expected to respond to inputs carrying similar information to that driving their target GrCs, however, *in vivo* evidence suggests this is not necessarily the case. For example the ventral paraflocculus receives MF input conveying vestibular, visuomotor, and eye movement information (Langer *et al*. 1985) however GoCs in this area respond only to eye movement over a very limited positional range (Heine *et al*. 2010) and in this and other regions GoC activity has been shown to correlate poorly with that of surrounding GrCs (Van Kan et al. 1997; Barmack & Yakhnitsa 2008) thus it is possible that the GoCs are performing contrast enhancement or an "and-not" operation manifested as a state and time-specific filtering of GrC activity. If GoCs respond to different MF inputs to the GrCs they inhibit then they will also confer a mixing of modalities. Additionally, if parallel fibre activity predominantly inhibits GoCs via mGluR2 rather than exciting them (Watanabe & Nakanishi 2003; Holtzman *et al*. 2011) then GoCs are poorly positioned to constrain GrC activity.

The GrC layer does not deal strictly with rate-coded inputs, indeed the most common GoC response to a tactile input is a pause in firing or a burst followed by a pause (Holtzman *et al*. 2006b). The timing of these bursts and pauses relative to the MF input to a GrC is therefore important in shaping the GrC output. If a burst of GoC inputs arrive directly before a MF–GrC input it might be expected to block or reduce the GrC's spiking output, if inhibition arrives immediately after excitation it might be expected to truncate the spiking and thus sharpen the GrC response. By contrast a pause immediately before a MF–GrC input might accentuate the signal, while a pause immediately after the MF input would accentuate the latter part of the signal.

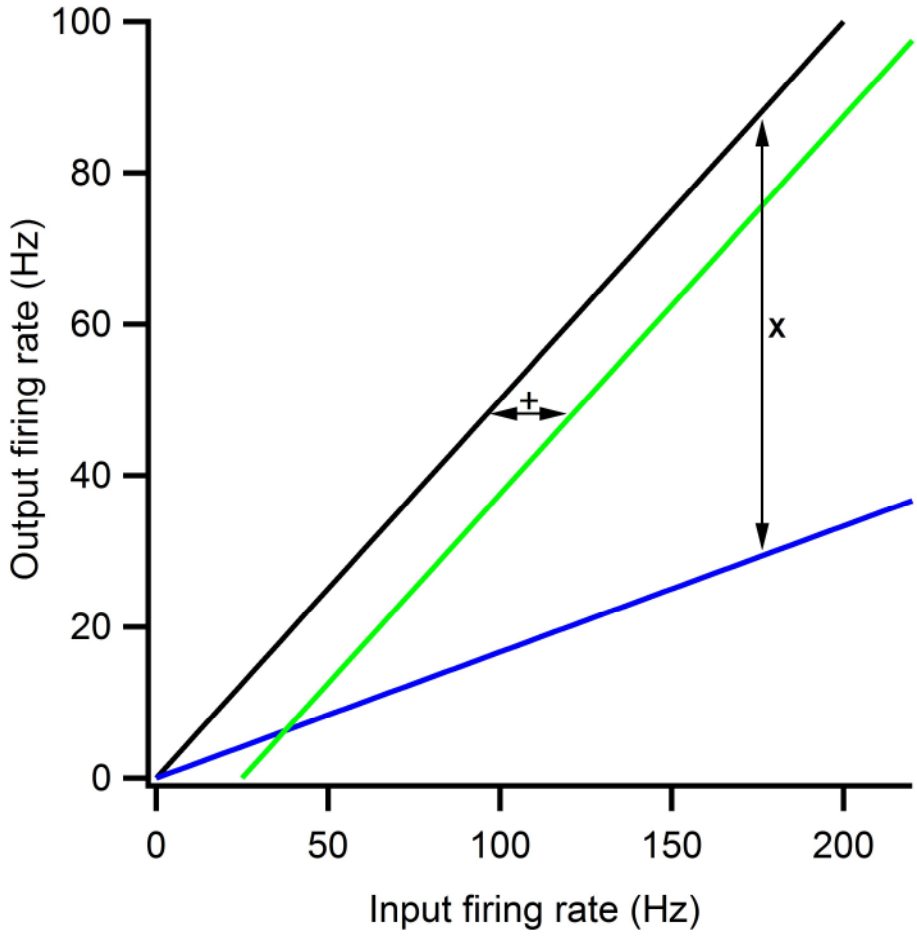

Fig 1.5: Rate coding. Processing of rate-coded information by a neuron can be described in terms of the relationship between the mean input rate and mean output firing rate (black). In general terms the effect of a second type of input, can function in one of two ways, it can either add an offset to the I–O function without changing its slope, serving to subtract baseline levels of excitation from a signal (green), or change the slope of the I–O function (a multiplicative function) effectively altering the sensitivity of the cell to changes in the excitatory input rate (blue).

1.5 Aims and outline of this study

This thesis aims to characterise the GoC–GrC synapse and investigate how changes in activity at this synapse can modulate the activity of single GrCs and in turn how these changes in GrC activity could affect the cerebellar cortex at the network level. In **Chapter Three** I present a characterisation of the GoC–GrC synapse using focal stimulation and paired GoC–GrC recordings. The results of the characterisation were utilised to produce average synaptic conductance waveforms for use in dynamic clamp experiments investigating the effect of changes in the rate or synchrony (**Chapter Four** & **Five**) of GoC activity on GrC processing of realistic MF input. Finally, in **Chapter Six** I have investigated how the relationship between GoC activity and GrC processing might be modulated by the activation of mGluR and nicotinic ACh receptors on the GoC.

Chapter Two

2. Materials and Methods

2.1 Slice preparation

Parasagittal (and in some cases coronal or lateral) slices of cerebellum were prepared from Sprague Dawley rats (postnatal day 25–35) in accordance with UK Home Office regulations as described previously (Silver *et al*. 1996): Rats were anaesthetised with isoflurane prior to decapitation with a guillotine. Heads were submerged in oxygenated (with 5% CO_2 /95% O_2) ice-cold slicing solution (**Table 2.1**) for the removal of the skin and fur surrounding the skull with a cut along the midline of the scalp. Craniotomies were performed with fine cuts from the base of the skull around the base of the crown leaving brains exposed. Any dura or arachnoid mater surrounding the brains was removed with fine forceps after which the brains were excised and placed in a fresh dish of oxygenated ice-cold slicing solution with a 5% Sylgard base. The brains were pinned to the dish and had their cerebellum removed with a single scalpel cut traversing the midbrain and pons. For parasaggittal slices, cerebellums were then placed on the cut surface before the removal of the brainstem and cerebellar hemispheres with three further scalpel cuts leaving the vermis. The vermis were then transferred to the oxygenated ice-cold slicing solution-filled slicing chamber of a Campden Integraslice 7550 PSDS equipped with a ceramic blade and cut into 220 µm thick parasaggital slices. Slices were stored in oxygenated slice incubation solution (**Table 2.1**) for 30 minutes at 30-31 °C followed by storage at room temperature for up to 6 hours.

Table 2.1: External solutions

Compound	**ACSF**	**Slicing**	**Incubation**
	Composition in mM		
NaCl	125	-	85
Sucrose	-	230	75
KCl	2.5	2.5	2.5
$NaHCO_3$	26	24	24
NaH_2PO_4	1.25	1.25	1.25
Glucose	25	-	25
Ascorbic acid	0.5	-	-
$CaCl_2$	2	0.5	0.5
$MgCl_2$	1	4	4

All solutions were pH 7.3, 315-320 mOsm, and equilibrated with 5% CO_2/95% O_2. Artificial cerebrospinal fluid (ACSF) was sometimes supplemented with various pharmacological agents depending on requirements. A list of drugs and concentrations utilised is given in **Table 2.2**. Specifics of use are given in the results section.

2.2 Electrophysiological recordings and analysis

For electrophysiological recordings cerebellar slices were transferred to a recording chamber where they were visualised with an Olympus BX50WI microscope. Slices were placed on a fine nilon mesh suspended on a platinum washer and held in place by fine nylon filaments stretched between the arms of a small U-shaped piece of platinum. In the recording chamber, brain slices were continuously perfused with oxygenated ACSF (**Table 2.1**) at 35–37°C (unless otherwise stated; temperature was measured and maintained with a feedback regulated automatic temperature controller; Warner instrument corporation). Perfusion was regulated by a peristaltic pump with a flow rate set to ~ 5 ml/min. For some experiments pharmacological agents were added to the perfusate a list of these agents and their concentrations is given in **Table 2.2**.

Table 2.2: Pharmacological compounds

Compound	Source	Method of application	Concentration (µM)
AP5	Tocris	Bath	10
NBQX	Tocris	Bath	50
GBZ (SR95531)	Tocris	Bath	10
Strychnine	Tocris	Bath	0.3
Nicotine	Sigma	Puff / Bath	100 / 10
GYKI 52466	Tocris	Bath	50
TTX	Tocris	Bath	1
DβE	Tocris	Bath	4
Methyllycaconitine	Tocris	Bath	0.04
Pancuronium	Tocris	Bath	10
Mecamylamine	Tocris	Bath	25
Choline	Sigma	Bath	1000
ACPD	Tocris	Bath	100
Furosemide	Sigma	Bath	100

The full names of the above compounds are given in the abbreviations section. All chemicals were obtained from Sigma-Aldrich (www.sigmaaldrich.com) or Tocris (www.tocris.com).

2.2.1 Visual identification of target cells

Slices were visualized with a 60x (numerical aperture 0.9) water-immersion objective using infrared differential interference contrast (DIC) optics (Olympus BX50W1) and a charge-coupled device camera. Contrast was optimised using a contrast enhancement box (C2400 Camera Controller, Hamamatsu).

The three cellular cerebellar layers were clearly distinguishable. The GrC layer was apparent as a cell dense band between the PC layer and the white matter. GrCs were identified as abundant spherical or ovoid bodies ~5–6 µm in diameter (Palay & Chan-Palay 1974). GoCs were identified as sparser, larger neurons within the GrC layer having spherical cell bodies ~10–30 µm in diameter. Cell types were further distinguished by their electrophysiological character (see below).

2.2.2 Data acquisition

Patch clamp experiments were performed using an Axopatch 700B (Molecular devices) connected to CV7B headstages. Data was low-pass filtered at 7–30 kHz and digitized at 50–100 kHz via an 18 bit DAC/ADC board (instrutech). Recordings were acquired and analyzed with IgorPro (WaveMetrics) using NeuroMatic (http://www.neuromatic.thinkrandom.com/). All traces displayed in the figures were further digitally filtered to 7 kHz using a binomial smoothing function in IgorPro.

2.2.3 Whole cell recordings

Fire-polished patch pipettes produced from borosilicate glass capillaries (outer diameter 1.5 mm, inner diameter 0.75 mm, length 10 cm; Sutter Instruments) were filled with the appropriate internal solution (**Table 2.3**). In order to keep the pipette tip free of debris, ~0.8 PSI of positive pressure was applied after submersion in the ACSF up until sealing.

Pipette resistance (R_{pip}), assessed by measuring the steady state current response upon the application of a square -5 mV pulse in voltage clamp ($V_c = I_{pip} \cdot R_{pip}$; R_{pip} was 4–5 MΩ for GoCs, 5–7 MΩ for GrCs). Liquid junction potentials were not compensated except in experiments using dynamic clamp (see below).

The pipette tip was positioned above the targeted cell with manipulators (SM-1 or SM-5; Luigs & Neumann) such that the outflow of the tip caused a dimple on the cells surface. Pipette offset was compensated then pressure was released after which a negative holding current was applied (-60 mV for GoCs, -70 mV for GrCs) resulting in the formation of a tight seal (R > 2 GΩ) on the cell's surface, at this point pipette capacitance was compensated. The membrane within the tip was then perforated either with gentle suction (most GrCs), a brief zap (1 V, 500 µs) or a combination of the two (most GoCs).

Membrane resistance, series resistance and cell capacitance (R_m, R_s, C_m) were assessed during or between recordings by measuring the current response ($I_m(t)$) to a transient, -5 mV voltage step. $I_m(t)$ is made up of an initial rapidly rising and decaying component followed by a steady state component corresponding to the resistive and capacitive

elements of the cell membrane. The time course of the response can be estimated using the following equation.

$$I_m(t) = \frac{V_C}{R_m + R_s} \cdot \left(\frac{R_m \cdot e^{-t/\tau}}{R_s} \right) \quad (1)$$

which at $t = 0$ reduces to:

$$I_m(0) = \frac{V_C}{R_s} \quad (2)$$

Table 2.3: Internal solutions

Compound	**GrC**	**GrC E_{Cl} = 0 mV**	**GrC E_{Cl} = -24 mV**	**GoC**
	Composition in mM			
KCH_3SO_4	110	-	-	150
$CsCH_3SO_4$	-	-	75	-
CsCl	-	135	-	-
NaOH	6	-	-	6
$MgCl_2$	3	2	2	4
$CaCl_2$	0.02	0.5	0.5	-
HEPES	40	0.5	0.5	10
BAPTA	0.15	-	-	-
EGTA	-	5	5	0.1
Na_2ATP	4	2	2	2
Na_2GTP	0.3	0.5	0.5	0.4
Phosphocreatine	-	-	-	10

Internal solution pH was set to 7.3 (with KOH for K^+ based solutions and CsOH for Cs^+ based solutions). GrC E_{Cl} = 0 mV and GrC E_{Cl} = -24 mV solutions were supplemented with 5 mM QX-314 to block Na^+ channel activity. For imaging experiments GoC intracellular solution was supplemented with 20 µM Alexa594 and 100 µM Fluo-5F. Intracellular solution was made up from 160 µl of 1.25x stock (frozen until required for use; max three months) and diluted at point of use with 40 µl of double distilled H_2O containing supplements as necessary. All chemicals were obtained from Sigma-Aldrich (www.sigmaaldrich.com) or Tocris (www.tocris.com).

Recordings were rejected if R_s > 30 MΩ or if R_s was unstable (> 25% change in the recording duration). R_s was not compensated in voltage clamp recordings. C_m was deduced from the slope of decay from maximal current to steady state according to the following equation:

$$\tau = C_m \cdot \left(\frac{R_m \cdot R_s}{R_m + R_s} \right) \quad (3)$$

C_m was used as a further criterion for cell identification. GrCs had a mean C_m of 3.8 ± 1.0 pF (N = 340) while GoCs had a mean C_m of 33 ± 11 pF (N = 180). Cells were also distinguished by their basal activity, in current clamp GrCs had a V_m ranging between -85 mV and -68 mV and were relatively stable, while GoCs had a V_m > -65 mV and fired spontaneously at 9 ± 5 Hz.

For current clamp recordings pipette capacitance was compensated to ~ 90%. Series resistance was compensated using a bridge balance circuit. Recordings were rejected in the event that V_m showed a marked change in stability (acceptable limits were determined according to cell type and experiment; in GrCs typically any change in V_m > 3 mV was cause for rejection).

2.2.4 Synaptic stimulation

In some experiments MF or GoC axons were activated with focal electrical stimulation. This was achieved with an ACSF-filled glass pipette (~ 7 MΩ tip size) placed in the white matter tract for stimulation of MFs or in the GrC layer for stimulation of GoC axons, typically 100–200 µm from the recording site. Electrical pulses (5–60 V, 20 µs) were delivered using an isolated stimulator (DS2A, Digitimer Ltd.) at a frequency < 1 Hz (to avoid receptor desensitisation) while the stimulating electrode was moved around the area of interest until a synaptic response was detected. Once a response was detected stimulation intensity was reduced while optimal stimulator position was assessed. Once optimal position and minimal stimulation threshold were found, stimulation intensity was increased by 5 V to ensure reliable stimulation for the course of the experiment. If the increase in intensity also increased the evoked synaptic response (indicating stimulation of additional axons) an alternative stimulation site was sought.

For paired recordings a 50 ms depolarising step (sufficient to elicit 1 action potential) was delivered to the presynaptic GoC. The average of at least 100 post synaptic responses was assessed to verify whether an input was present. A fixed rate of GoC firing was obtained through the delivery of brief precisely timed pulses (1 ms 0.5–1.5 nA).

2.2.5 Analysis of IPSCs

IPSCs were analysed by baseline subtracting a 5 ms window immediately prior to stimulation of the presynaptic cell. Synaptic events were considered successful if amplitude was > than 3 times the standard deviation (SD) of the mean background. Spontaneous inhibitory post synaptic currents (sIPSCs) were initially detected using a thresholding operation set to 5 SDs of the mean background. Detected IPSCs were then sorted and aligned to their 20% rise time (RT) and averaged. The averaged waveform was fitted with a Beckers function (Nielsen *et al*. 2004). The fit was then used to construct a template for the detection of further events with the NeuroMatic inbuilt event detection function. Finally, detected events were filtered by eye to ensure all had an amplitude at least 3 SDs of the noise and faster RTs than decay times. IPSCs obtained in paired recordings were aligned to the 20% rise time of the presynaptic action potential. Averaged IPSCs (> 100 events) were assessed for amplitude, 20–80% RT and weighted decay. Weighted decay was calculated by normalizing the peak of the IPSC to one and integrating for 100 ms (which is 3.5 times the slow decay constant of the mean IPSC) from the start of the IPSC. Decay time courses were not directly presented due to the difficulty in comparing decay times with differing numbers of exponentials and decay constants. Spillover only IPSCs were separated from direct IPSCs on rise time criteria (> 1ms vs < 0.8 ms; DiGregorio *et al*. 2002).

Averaged IPSCs derived from paired recordings were used to construct population averages for direct and spillover only IPSCs. These population averages were converted to conductances and fitted with a Beckers function (equation 4) to generate template direct and spillover only inhibitory inputs for use in dynamic clamp (see below).

2.2.6 Simulation of synaptic conductances

Simulated MF inputs modelled on recordings of MF–GrC synaptic input (N = 11; described in Rothman *et al*. 2009) comprised AMPAR and NMDAR components were generated for use in dynamic clamp and modelling experiments. AMPA conductances were described by the following equation:

$$G(t) = (1 - e^{-t/\tau r})^n [a_1 e^{-t/\tau d1} + a_2 e^{-t/\tau d2} + a_3 e^{-t/\tau d3}] \quad (4)$$

Where e is the base of the natural logarithm, τ_r and $\tau_{d1–3}$ are the time constants of the rising and decaying components respectively, $a_{1–3}$ are the amplitude components and t is time. The following values were computed from fits to MF–GrC AMPAR conductance data: n = 11 τ_r = 0.10 ms, a_1 = 2.23 nS, τ_{d1} = 0.45 ms, a_2 = 0.29 nS, τ_{d2} = 2.88 ms, a_3 = 0.08 nS and τ_{d3} = 21.67 ms. NMDA conductances were described by the following equation:

$$G(t) = (1 - e^{-t/\tau r})^n [a_1 e^{-t/\tau d1} + a_2 e^{-t/\tau d2}] \quad (5)$$

The following values were computed from fits to MF–GrC NMDA conductance data: n = 1, τ_r = 1.14 ms, a_1 = 0.11 nS, τ_{d1} = 8.1 ms, a_2 = 0.06 nS, τ_{d2} = 37 ms.

To simulate STD the amplitude of each simulated MF AMPA conductance was multiplied by a scale factor of 0.5 ($D \rightarrow D \cdot 0.5$) in accordance with Varela *et al*. 1997. Between inputs, D recovered exponentially back to its initial value of 1.0 with a time constant τ_D = 40 ms in accordance with Rothman *et al*. 2009.

Simulated GoC–GrC conductances were modelled on IPSCs recorded from GoC–GrC pairs as described in **Chapter 3.4**. Simulated direct GoC–GrC GABA conductances (fit from 25 pairs) were described by equation (4) the following values were computed from the fit to an averaged GoC–GrC IPSC waveform: n = 490, τ_r = 0.22 ms, a_1 = 0.35 nS, τ_{d1} = 4.22 ms, a_2 = 1.11 nS, τ_{d2} = 1.19 ms, a_3 = 0.07 nS and τ_{d3} = 19.93 ms. Simulated spillover GoC–GrC conductances (fit from 15 pairs) were also described by equation (4) the following values were computed from the fit to a averaged GoC–GrC IPSC

spillover waveform: n = 17, τ_r = 1.40 ms, a_1 = 3.06 nS, τ_{d1} = 0.53 ms, a_2 = 9.83e^{-4} nS, τ_{d2} = 0.71 ms a_3 = 0.04 nS and τ_{d3} = 150.11 ms. GoC–GrC inhibitory conductance waveforms were delivered at steady rates and were scaled according to rate based on an analysis of GoC frequency dependent STD (**Chapter 3.4**).

2.2.7 Dynamic clamp recordings

Dynamic-clamp recordings were made from GrCs using the GrC intracellular solution (**Table 2.3**). A liquid junction potential of +6.3 mV (as measured by; Rothman *et al*. 2009) was corrected prior to gaining whole-cell access. Cells were not used for dynamic clamp recordings if R_s exceeded 25 MΩ. During recordings resting V_m was maintained near −75 mV through the injection of small amounts of current. Conductance trains were injected with a 3-channel SM1 amplifier (Cambridge Conductance, UK). Simulated MF AMPAR and NMDAR-like conductances were injected into GrCs via dynamic clamp as described below.

The AMPAR component, followed a simple linear Ohmic relationship with voltage, while the NMDAR component introduced by the SM1 amplifier had a Boltzmann-like non-linearity that mimics the voltage-dependent Mg^{2+} block of the NMDA conductance measured in GrCs. This non-linearity introduced by the SM1 amplifier required scaling of the NMDAR conductance waveforms (by *B*) so that the final peak value, after leaving the SM1 amplifier, matched the measured value, as described by the following Boltzmann function:

$$B(V) = \frac{1}{1 + e^{-(V - V_{0.5})/k}} \qquad (6)$$

where $V_{0.5}$ = −12.8 mV and k = 22.4 mV (N = 6 cells; curve fit to data; Rothman *et al*. 2009). Excitatory conductance trains (of which there were multiple instances for each mean firing frequency) were injected in random order, with tonic inhibition and/or simulated GoC input. The simulated GABAergic conductance was linear and had a reversal potential of -75 mV. Some GrCs were excluded where an accurate measurement of a gain change was required due to their output spike rate being too low or absent in the presence of inhibition. This will tend to underestimate any gain change

reported. Cells were also discarded if the amplitude of their action potentials changed by more than 20% during an experiment.

2.2.8 Analysis of dynamic clamp data

Action potentials were detected using a threshold set at 0 mV. For assessment of GrC mean firing rate in response to rate coded inputs, GrC output firing rate was calculated in a variable window starting 100 ms after the onset of the stimulus train and is assumed to represent steady state firing.

For gain calculation, plots of GrC firing rate (F) versus simulated MF input rate (f) were fitted with a Hill equation of the form:

$$F(f) = \frac{F_{\max}}{1 + \left(f_{50\%} / f\right)^n} + F_0 \qquad (7)$$

where n is the exponent factor, F_0 is the firing rate offset, $F_{\max}$ is the maximum firing rate and $f_{50\%}$ is the value of f at which F reaches half maximum (Rothman *et al*. 2009). Fits to I–O relations were compared using the F-ratio for the separate and combined data sets. Fits were considered significantly different if $P < 0.05$. The gain was calculated from the average slope (F') of the fits between 5% and 75% its maximum value. An upper limit of 75% was used so that all computations of F' were limited to the range of the experimental data. Changes in gain (ΔGain) were computed as follows:

$$\Delta Gain = \left(\frac{F'_a - F'_b}{F'_b} \right) \qquad (8)$$

where a and b denote two conditions being compared. Additive offset shifts (x-offset) were defined as the difference between the half-maximum frequencies of the fits for the conditions being compared.

To assess the effect of synchronised simulated GoC input on the character of GrC spiking, cumulative distributions of GrC interspike intervals (ISIs) were assessed for statistical differences using the Kolmogorov-Smirnov test.

To assess the effect of synchronised simulated GoC input on the patterning of GrC activity spikes were placed in 1 ms bins. Autocorrelations were then performed using Igor Pro's inbuilt circular correlation function:

$$R_{xx}(j) = \sum_{n} x_n x_{n+j} \qquad (9)$$

Where R represents the discrete autocorrelation, j represents the lag and x_n is the signal (in this case representing the spike histogram). To make the autocorrelation circular (and thus negate boundary effects) the indexes $n + j$ were wrapped around when they exceeded the range of x.

Autocorrelations were assessed for significance using Z-score vertical scaling, Z-scores were obtained by subtracting the average spike count per bin of shuffled autocorrelations (ISI order was randomised), and dividing by the average SD of the shuffled autocorrelations. Significance was fixed at Z-score = 2. The synchronization strength (peak area above Z-score = 2; Dugue *et al*. 2008) and the difference between the second satellite peak and the second valley (Samonds & Bonds 2005) were calculated on autocorrelations. The oscillation score (Mureşan *et al*. 2008) was derived by removing the primary peak of the autocorrelation, smoothing (5 points) using the polynomial smoothing function in IgorPro (to reduce high frequency noise), applying a fast Fourier transformation (FFT; Muresan *et al*. 2008) and computing the average magnitude (M_{avg}) of the spectrum by integrating the whole frequency spectrum and taking its average:

$$M_{avg} = \frac{\int_0^{fc/2} \text{Magnitude}(f)\,\mathrm{d}f}{f\text{c}/2} \qquad (11)$$

Where *magnitude*(f) is the estimated magnitude of frequency f in the FFT computed spectrum and f_c is the reciprocal of the bin size used in the autocorrelation function (1 KHz in this case). The oscillation score is given by:

$$\frac{M_{peak}}{M_{avg}} \qquad (12)$$

Where M_{peak} is first and highest peak in the band of interest in the power spectrum.

2.3 Modelling and analysis

An integrate and fire (IF) model GrC developed by Jason Rothman and Volker Steuber (Rothman *et al*. 2009) and constrained to in house data was utilised for modelling experiments. The model is described by the following equation:

$$-C_m \frac{dV}{dt} = \frac{(V - E_L)}{R_m} + D(t)G_{AMPAR}(t)(V - E_{AMPAR}) + G_{GABAR}(t)(V - E_{GABAR}) + G_{NMDAR}(t)B(V)(V - E_{NMDAR}) \quad (13)$$

Where the reversal potentials for the leak E_L = -75 mV, D represents the scale factor for short term plasticity, E_{AMPAR} = 0 mV, E_{NMDAR} = 0 mV, and a membrane resistance R_m = 2 GΩ, B is described in equation 6 (Rothman *et al*. 2009), other parameters were varied in the course of the experiments. Action potentials were generated when the model's membrane potential V reached a threshold of -40 mV, at which time V was set to 32 mV for one integration time step (0.06 ms), then clamped to -63 mV for a refractory period of 2.0 ms. These parameters were based on measurements from 38 GrCs (Rothman *et al*. 2009). The model was implemented in the IGOR Pro envioronment by Jason Rothman. Modelling experiments were analysed in a similar fashion to patch clamp experiments

2.4 Imaging and analysis

2.4.1 Imaging setup

I utilised a 2-photon microscope consisting of a femtosecond tuneable Laser (MAI-TAI; Spectra-Physics; tuned to 850 nm), attached to a scanhead (Ultima, Prairie Technologies) and upright microscope (BX51, Olympus) with an infrared coated water-immersion objective (Olympus LumPLanFL/IR 60x/0.90W). Green and red fluorescence was collected selectively using emission filters (HQ 525/70m-2P for green light; Chroma Technology; HQ 630/100m-2P for red light; Chroma Technology), both

were amplified using GaAsP photomultipliers (Hamamatsu H7422). Images were acquired with PrairieView acquisition software. Laser intensity was controlled using a Pockels cell (Conoptics Model 302CE).

2.4.2 Fluorescence and Ca^{2+} imaging

GoCs identified in acute slices under DIC were patched with a pipette containing GoC internal solution (**Table 2.3**) supplemented with 20 µM Alexa594 (for GoC visualisation; Molecular Probes, Invitrogen; peak absorbtion 590 nm, peak emission 617 nm) and 100 µM Fluo 5F (for Ca^{2+} imaging; Molecular Probes, Invitrogen peak absorbtion 494 nm, peak emission 518 nm). After spatial equilibration of the dye (~10 minutes) the cell was imaged (red channel) to confirm appropriate morphology then images of the cell body were acquired in both channels (at a rate of 4 Hz) surrounding pressure application of 100 µM nicotine 60 µm from the cell body. ImageJ was used to calculate $\Delta F/F$ at the cell body by relating the intensity difference during stimulation to the average pixel intensity before stimulation. A significant Ca^{2+} response was judged as an increase in F of over 5 x SD above the mean. After completion of the experiment Z-stacks were taken (red channel; 21-25 µm at 0.5 µm Z directional steps). All Ca^{2+} imaging experiments were performed in the current clamp configuration.

2.5 General statistics

Data are represented as mean ± SD with number of cells (N) unless otherwise stated. Normality was assessed using a Kolmogorov-Smirnov test. Normally distributed groups were compared using a paired or unpaired two-tailed Student's T-test (with Welch correction if SDs were significantly different) or analysis of variance (ANOVA) for multiple comparisons. Non-normally distributed data was compared using a Mann-Whitney test, a Kruskal-Wallis test for multiple unpaired comparisons or a Freidman test for multiple paired comparisons. Where multiple comparisons were made an appropriate post hoc test was employed (Tukey-Kramer test for normally distributed data or the Dunn test for non-normally distributed data). Groups were considered significantly different at $P < 0.05$. Correlations were assessed for strength using Pearson's product moment correlation coefficient (r). Fits to data were achieved by minimising the sum of squares to the weighted data points. For linear regressions data

are presented with the goodness of fit (r^2) and a P value indicating if the slope is significantly different from zero (derived from an F-test). Where data sets were represented by a model of best fit models were compared for difference using the *F*-ratio for the separate and combined data sets. Models were considered significantly different at $P < 0.05$. All statistical analysis was performed using either Excel, Graphpad Prism or Igor Pro.

Chapter Three

3. Analysis of the Golgi cell–granule cell synapse

3.1 Introduction

GrCs receive two forms of inhibitory input: tonic inhibition, an approximately steady state conductance arising from the persistent release of GABA from glial cells via Best1 channels onto high affinity extrasynaptic δ subunit containing $GABA_A$Rs (Brickley *et al*. 1996; Farrant & Nusser 2005; Lee *et al*. 2010). And phasic inhibitory input arising from vesicular GABA release from presynaptic GoCs which acts on synaptic γ subunit containing $GABA_A$Rs to convey the direct component of the IPSC (Farrant & Nusser 2005) and extrasynaptic α6 subunit containing $GABA_A$Rs to convey the slow spillover component of the IPSC (Bright *et al*. 2011).

Changes in tonic inhibitory input have been shown to elicit a gain change in the I–O function of the GrC (Mitchell & Silver 2003; Rothman *et al*. 2009). However, the functional role of phasic inhibitory input to GrCs is less well understood.

In order to address this issue it is critical to have a good description of the GoC–GrC synapse. Several studies have perfomed a limited characterisation of the GoC–GrC synapse (Puia *et al*. 1994; Kaneda *et al*. 1995; Tia *et al*. 1996; Wall & Usowicz 1997; Rossi & Hamann 1998; Brickley *et al*. 2001; Wall 2002; Cathala *et al*. 2003; Wall 2003; Yaun & Atchison 2003; Carta *et al*. 2004; Dugue *et al*. 2005; Chiu *et al*. 2005; Wall 2005; Mameli *et al*. 2008; Mapelli *et al*. 2009; Crowley *et al*. 2009; Dugue *et al*. 2009; Bright *et al*. 2011). The majority of these studies either looked at spontaneous synaptic events (sIPSCs) or evoked synaptic inputs using a stimulating electrode (eIPSCs). The study of sIPSCs alone cannot provide a detailed description of a synaptic input due to issues with detection bias (smaller spillover events are typically lost in the noise), a lack of certainty as to whether detected sIPSCs arise from a single presynaptic source and an inability to control the rate of sIPSC activity (rendering an analysis of the frequency dependence of the synapse impossible). On the other hand, with focal stimulation the experimenter has a higher degree of control but cannot be sure that only a single axon is being activated, that stimulation of the surrounding cellular milieu does not affect the

synaptic input, or that the axon is being activated in a physiological fashion. Studies of the GoC–GrC synapse that have utilised paired recordings typically relied on a very small sample size (Dugue *et al*. 2005). I have performed characterisation of the GoC–GrC synapse first using a stimulating electrode for comparison with other studies and second using paired recordings to carefully characterise individual GoC–GrC inputs.

3.2 GrC inhibition

3.2.1 Basal inhibition in GrCs

GoCs fire spontaneously in slice at ~8 Hz at near physiological temperature (34ºC; Dieudonné, 1998; Forti *et al*. 2006). To investigate the properties of the resulting sIPSCs patch clamp recordings were made from GrCs using an internal solution containing a high concentration of Cl^- ions (GrC E_{Cl} = 0 mV intracellular solution; **Table 2.3**), such that GABAergic inputs would be visible as inward currents in the presence of blockers of ionotropic glutamatergic activity (50 µM GYKI52466 and 10 µM APV) at physiological temperature (35-37 °C). When recording in voltage clamp at a holding potential of -60 mV sIPSCs were visible as fast inward currents (**Fig. 3.1A** & **B** left) and occurred with a mean frequency of 4.6 ± 4.7 Hz, had a mean amplitude of -60.7 ± 23.8 pA (948 ± 371 pS), average 20–80% rise time (RT) of 0.21 ± 0.09 ms and mean weighted decay of 8.1 ± 4.3 ms (N = 11; **Fig. 3.2A**).

Application of 1 µM tetrodotoxin (TTX) to block action potentials reduced the frequency of sIPSCs but did not elicit a shift in holding current (I_{hold}; 0.38 ± 2.77 pA equivalent to a conductance of 5.9 ± 43.3 pS; N = 5; P = 0.78; **Fig. 3.1A**). Application of the $GABA_AR$ antagonist gabazine (GBZ; 10 µM) blocked sIPSCs and elicited an outward current shift of 27 ± 17 pA (N = 11) reflecting a suppression of tonic conductance of 420 ± 270 pS. GBZ application also reduced the SD of the noise of the recording (from 7.1 ± 4.2 pA to 2.6 ± 0.4 pA; Mann-Whitney U test P = 0.008) by preventing the stochastic opening of $GABA_ARs$ (**Fig. 3.1B**).

In accordance with previous studies (Brickley *et al*. 1996; Hamann *et al*. 2002) these results show that under resting conditions GrCs are subject to both a large tonic GABAergic inhibitory conductance and spontaneous phasic inhibitory input.

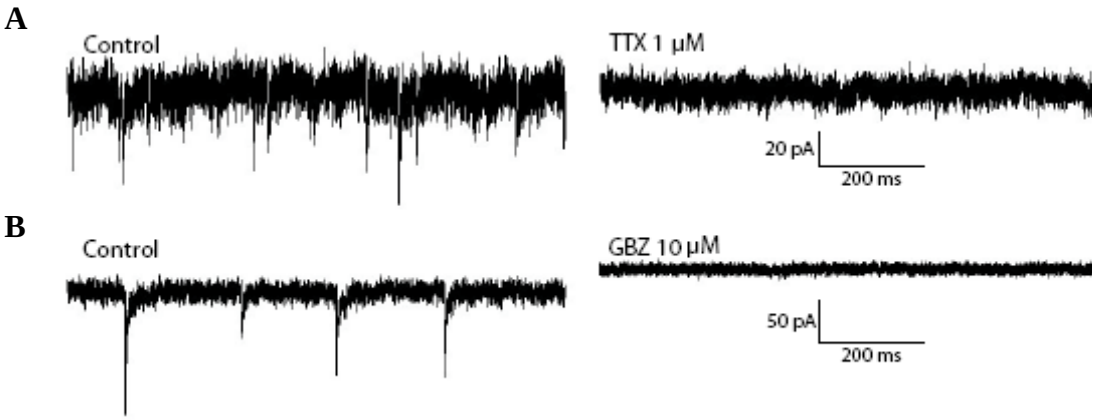

Figure 3.1: Spontaneous IPSCs in the GrC. Example traces recorded at -60 mV with GrC E_{Cl} = 0 mV intracellular solution at 35-37 °C showing sIPSCs (left) which were eliminated (right) by the application of either **A**. 1 µM TTX or **B**. 10 µM Gabazine (GBZ).

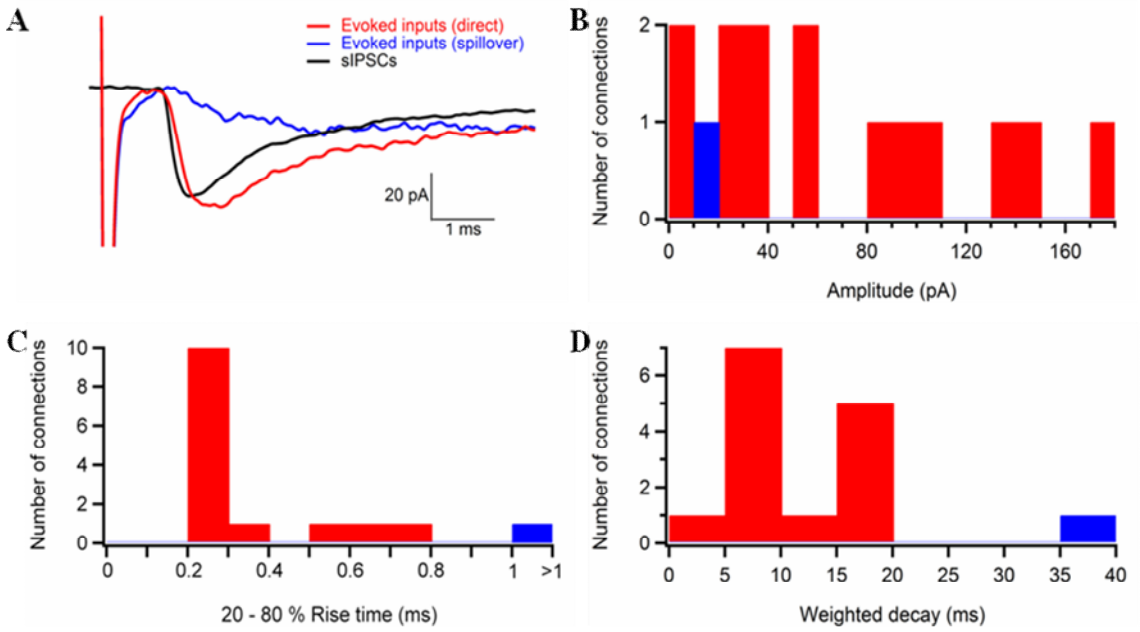

Fig. 3.2: Evoked GoC–GrC IPSCs. **A**. Evoked IPSCs in an example GrC were separated into successful (direct; red) and failed (spillover; blue) and averaged. Evoked IPSC waveforms are presented with averaged spontaneous IPSCs (black) from the same cell. **B**. Histogram of eIPSC amplitudes. **C**. Histogram of eIPSC 20–80 % RTs. **D**. Histogram of eIPSC weighted decays times. Evoked IPSCs were separated into direct (red; N = 14) and spillover only (blue; N = 1) connections based on RT criteria.

3.3 Analysis of the GoC–GrC synapse using synaptic stimulation

3.3.1 Evoked IPSC characteristics

IPSCs were evoked through electrical stimulation GoC–GrC synaptic connections. Evoked IPSCs typically comprised a rapidly rising, rapidly decaying direct component followed by a slowly decaying spillover component (**Fig. 3.2A**; red). Evoked IPSPs (average of 100 trials; N = 15) had a mean amplitude of -66.0 ± 55.0 pA (1031 ± 859 pS; similar to the amplitude of sIPSCs; T-test with Welch correction P = 0.74; **Fig. 3.2B**), mean 20-80% RT of 0.41 ± 0.27 ms (slower than that of sIPSCs; Mann-Whitney U test P < 0.005; **Fig. 3.2C**) and a mean weighted decay of 13 ± 8.6 ms (not significantly slower than that of sIPSCs; Mann-Whitney U test P = 0.077; **Fig. 3.2D**). Direct inputs failed 27.9 ± 27.5 % of the time revealing the slowly rising, slowly decaying spillover only waveform in isolation (**Fig. 3.2A**; blue). In three cells where stimulation of a directly connected GoC input regularly resulted in a failure of direct transmission (more than 50 % of the time), spillover events were isolated and averaged revealing a current with a peak amplitude of -15.9 ± 4.6 pA (248 ± 71.9 pS), mean RT of 3.9 ± 1.2 ms and a mean weighted decay of 25 ± 8.2 ms (**Fig. 3.2A**).

Some GoC–GrC connections have been shown to completely lack a direct component and can be considered spillover only connections (Rossi & Hamann 1998). Mean eIPSC waveforms could be separated into direct and spillover only connections based on RT criteria; 14 of 15 connections (93 %) showed rapid RT kinetics (0.35 ± 0.16 ms) the remaining, spillover only connection, exhibited a 20–80% RT with slower kinetics (1.2 ms; **Fig. 3.2C**).

Application of 1 µM TTX (N = 3) or 10 µM GBZ (N = 5) completely blocked evoked IPSCs (**Fig. 3.3**) confirming that eIPSCs are mediated by action potential dependent GABA release.

It has been suggested that the spillover component of the IPSC is conveyed primarily by distinct extrasynaptic α_6 subunit containing $GABA_A$Rs (Bright *et al*. 2011). To test this hypothesis I utilised the $GABA_A$R (and $Na^+/2Cl^-/K^+$ cotransporter) antagonist furosemide which has a 100 fold greater selectivity for α_6 subunit containing $GABA_A$Rs

over non-α_6 subunit containing $GABA_A$Rs. In three cells 100 µM furosemide reduced the mean evoked IPSC amplitude by on average 68 ± 11 % but failed to affect weighted decay (11.5 vs 11.2 ms; Mann-Whitney U test P = 0.96; **Fig. 3.4**). Therefore, in my hands, furosemide does not appear to selectively reduce spillover. Furosemide elicited an outward current shift of 15.9 ± 2.2 pA reflecting a suppression of tonic conductance of 248 ± 34.4 pS (59 % of total resting inhibition).

In accordance with previous data (Rossi & Hamann 1998; Crowley *et al*. 2009) these results confirm that eIPSCs are typically large and comprised of a rapidly rising, rapidly decaying direct component followed by a slowly decaying spillover component, that failure of the direct component can reveal the spillover component in isolation and that some GoC–GrC inputs are mediated purely by spillover.

3.3.2 Frequency dependence of eIPSCs

To investigate the degree to which sustained phasic input might contribute to the ongoing inhibitory conductance seen by a given GrC, trains of inhibitory inputs were triggered (10 shocks at 5, 10, 20, 33 or 50 Hz delivered interspersed by 2 second intervals; average of at least 20 trials; N = 8 direct connections; **Fig. 3.5**).

Short-term plasticity of the eIPSC was assessed by measuring the amplitude of successive eIPSCs. The amplitudes of the 1st, 2nd, 5th and 10th eIPSCs in each train are expressed as a percentage of the first amplitude of the first eIPSC (**Fig. 3.5A**). At frequencies above 5 Hz eIPSC amplitude depressed steadily with successive shocks. Depression occurred in a frequency-dependent manner with eIPSCs reaching 45.6 ± 8.9 % of their initial amplitude by the 10th shock delivered at 50 Hz (**Fig. 3.5B**).

Measuring the change in I_{hold} in 4 ms windows immediately preceding each consecutive shock (**Fig. 3.6A**) revealed a gradual build up of the slow components of the eIPSCs at all frequencies (**Fig. 3.6B**). The shift in I_{hold} 50 ms after the final shock (~20 times the average fast IPSC decay constant) was measured and used to estimate the conductance generated by the summation of the pure IPSC spillover at each frequency. The evoked conductance increased in a sub-linear fashion with stimulus frequency generating a maximum of 301 ± 57 pS at 50 Hz (72% of the magnitude of the resting tonic conductance; **Fig. 3.6C**).

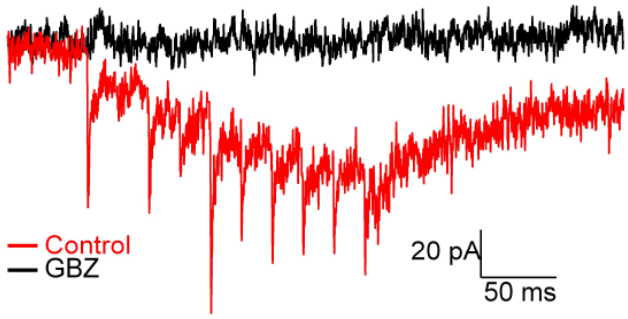

Fig. 3.3: Blockade of GoC–GrC eIPSCs with GBZ. Example trace showing bursts of eIPSCs triggered at 50 Hz (red) in an example GrC and again in the presence of 10 µM GBZ (black). Traces are the average of 20 trials, artefacts have been subtracted and traces have been baseline subtracted to allow direct comparison.

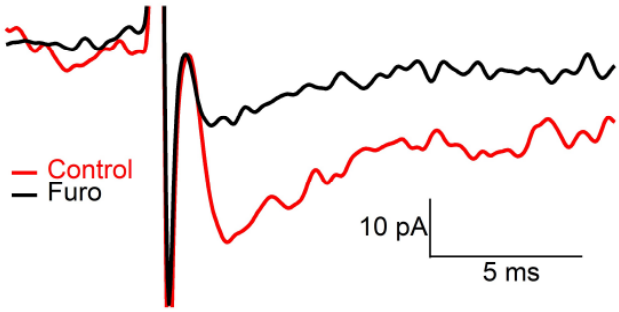

Fig. 3.4: Effect of furosemide on GoC–GrC eIPSCs. Example eIPSCs in the absence (red) and presence (black) of 100 µM furosemide. Traces are the average of 20 trials, IPSCs are baselined to allow direct comparison.

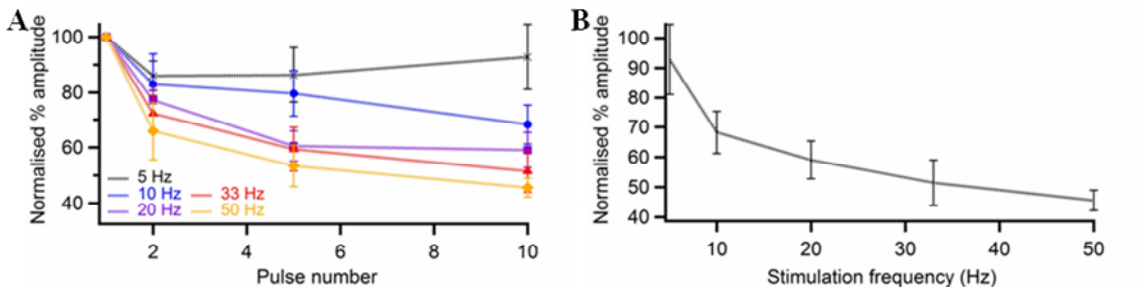

Fig. 3.5: Short term plasticity of GoC–GrC eIPSCs. **A**. Normalised mean amplitudes for the 1st, 2nd, 5th and 10th eIPSCs delivered at 5 (black), 10 (blue), 20 (purple), 33 (red) and 50 Hz (orange). **B**. Normalised mean eIPSC amplitudes for the 10th eIPSC at the same frequencies as above (N = 8). Error bars represent SEM

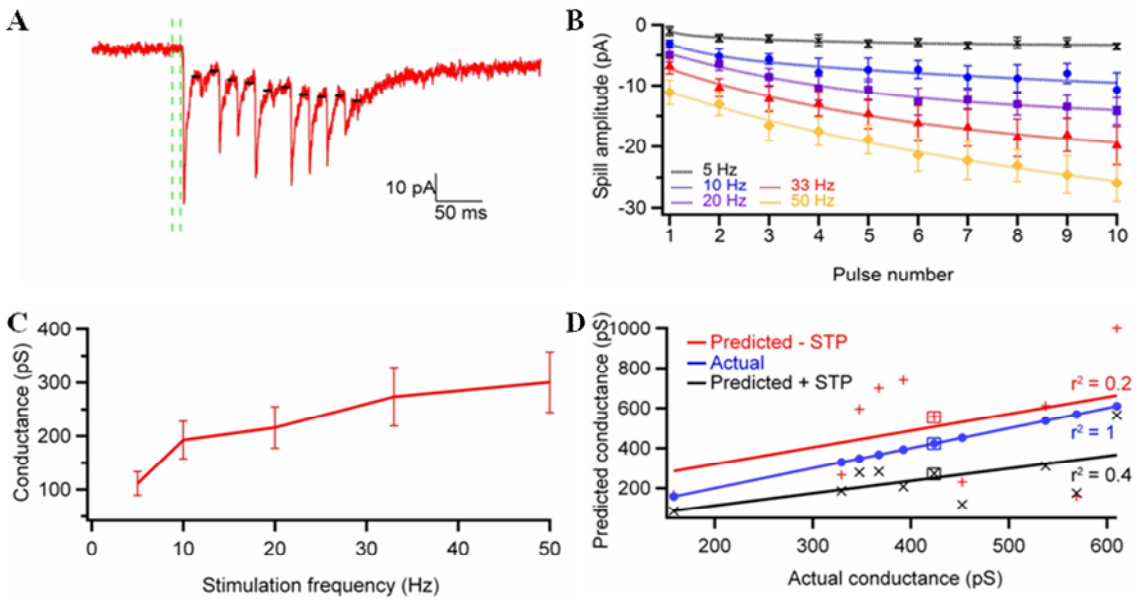

Fig. 3.6: Summation of GoC–GrC eIPSC spillover. **A**. Example figure showing how spillover was measured in a fixed 4 ms window (black) immediately preceding each consecutive pulse (green dotted lines indicate baseline). **B**. The build up of spillover current from 10 successive eIPSCs arriving at 5 (black), 10 (blue), 20 (purple), 33 (red) and 50 Hz (orange); lines represent double exponential fits to the data. **C**. Estimate of total spillover measured 50 ms after the last shock at the same stimulation frequencies (N = 8), error bars represent SEM. **D**. Spillover conductance elicited by 10 eIPSCs at 50 Hz (measured in a fixed 4 ms window 15 ms after the final pulse) plotted against itself (blue) and the predicted conductance for the same connections in the absence (red) and presence (black) of short term plasticity (N = 11). The spillover only connection is marked by the boxed symbol.

In order to better understand the mechanisms underlying the build up of spillover the total spillover conductance generated by 10 eIPSCs arriving at 50 Hz (measured in a fixed 4 ms window 15ms after the final pulse) was compared to the amount of spillover that would be generated by the same eIPSCs in the absence of any STD (the waveform of the first IPSC in the train was delivered 10 times at 50 Hz) and the presence of STD (the waveform of the first eIPSC in the train was delivered 10 times at 50 Hz, each iteration of the waveform was scaled according to the reduction in peak amplitude of the corresponding eIPSC; **Fig. 3.6D**). Actual trains of eIPSCs generated significantly more inhibitory conductance (418 ± 132 pS) than those modelled with STD (248 ± 133 pS; paired T - test; $P < 0.001$) but, generally, less than those modelled without (502 ± 283 pS; paired T - test; $P = 0.3$). However, actual data correlated weakly with modelled data without STD (Pearson's rank; $r = 0.39$; $P = 0.26$) but strongly with modelled data with STD (Pearson's rank; $r = 0.61$; $P = 0.06$). These results suggest that the spillover component of the eIPSC is subject to STD. A conclusion supported by the fact that the peak amplitude of the identified spillover-only eIPSC depressed by a similar amount to that of the direct IPSCs (**Fig. 3.6D** points marked by boxes). That the amount of spillover generated by 50 Hz trains was larger than predicted by modelled data including STD may imply that spillover may summate in a supralinear fashion.

These results show that GoC–GrC eIPSCs undergo frequency dependent short term depression (**Fig. 3.5**) and summation of spillover (**Fig. 3.6B**, **C**). The spillover component of the eIPSC is subject to STD; however, the inhibitory conductance generated by a 50 Hz train is larger than would be expected were the whole eIPSC waveform to depress to the same level as the peak of the direct component (**Fig. 3.6D**). It is possible that the spillover component may depress less than the direct component of the IPSC or that spillover sums in a supralinear fashion.

3.4 Analysis of the GoC–GrC synapse using paired recordings

Focal electrical stimulation has been widely utilised to characterise synaptic connections. However, where the target axons exist in a dense overlapping plexus (as with GoC axons), one cannot be sure of only stimulating a single axon, further, one may unintentionally stimulate additional modulatory inputs and/or the large electrical pulse used to evoke axonal activity may elicit a signal in the axon quite different from that conveyed by a typical action potential. As such the usefulness of this technique for

detailed quantitative analysis of synapses is limited; therefore the above experiments were repeated using paired GoC–GrC recordings.

3.4.1 Unitary IPSC characteristics

Paired recordings were made between single GoCs and GrCs within a radius of ~100 µm. IPSCs from 100 or more trials were aligned to the presynaptic action potential and averaged (**Fig. 3.7A**). IPSCs from paired recordings (N = 69) had a mean amplitude of -17.3 ± 20.8 pA (270 ± 325 pS; **Fig. 3.7B**; significantly smaller than the recorded amplitudes for both eIPSCs and sIPSCs; Kruskal-Wallis test $P < 0.0001$; post hoc Dunn test $P < 0.001$ in both cases), mean 20–80 % RT of 2.1 ± 3.2 ms (**Fig. 3.7C**; significantly slower than eIPSCs and sIPSCs; Kruskal-Wallis test $P < 0.0001$; Dunn test $P < 0.05$ and $P < 0.001$ respectively) and a mean weighted decay of 23 ± 16 ms (**Fig. 3.7D**; also significantly slower than both eIPSCs and sIPSCs; Kruskal-Wallis test $P < 0.0001$; Dunn test $P < 0.05$ and $P < 0.001$ respectively).

IPSCs from GoC–GrC pairs fell into two distinct classes based on RT criteria; direct IPSCs (20-80 % RTs < 0.8 ms), and slow spillover only events (RT > 1 ms; **Fig. 3.7C**). Direct IPSCs (N = 44; 64%) had a mean amplitude of -24.4 ± 23.2 pA (381 ± 362 pS), mean 20–80 % RT of 0.39 ± 0.15 ms and a mean weighted decay of 15 ± 7.4 ms. In a subset of direct connections (where IPSCs were reliably detectable above the noise on a single trial basis) the direct component had a failure rate of 22.5 ± 19.4 % (N = 22; lower than but not significantly different to the failure rate of eIPSCs; Mann-Whitney U test $P = 0.86$). Spillover only IPSCs (N = 25; 36%) had a mean amplitude of 4.7 ± 3.3 pA (73.4 ± 51.6 pS), mean 20–80 % RT of 5.1 ± 3.8 ms and mean weighted decay time of 38 ± 14 ms.

Paired GoC–GrC IPSCs have much smaller amplitudes than eIPSCs and sIPSCs (**Fig. 3.7B**). This may indicate that the recorded eIPSCs and sIPSCs represent combined input from multiple GoCs or that detection is biased to select for larger events. Additionally, the detection of a greater proportion of spillover only inputs than reported in previous studies (Rossi & Hamann 1998; Wall 2002; Crowley *et al*. 2009) implies that the prevalence and therefore importance of spillover only connections is greater than previously thought.

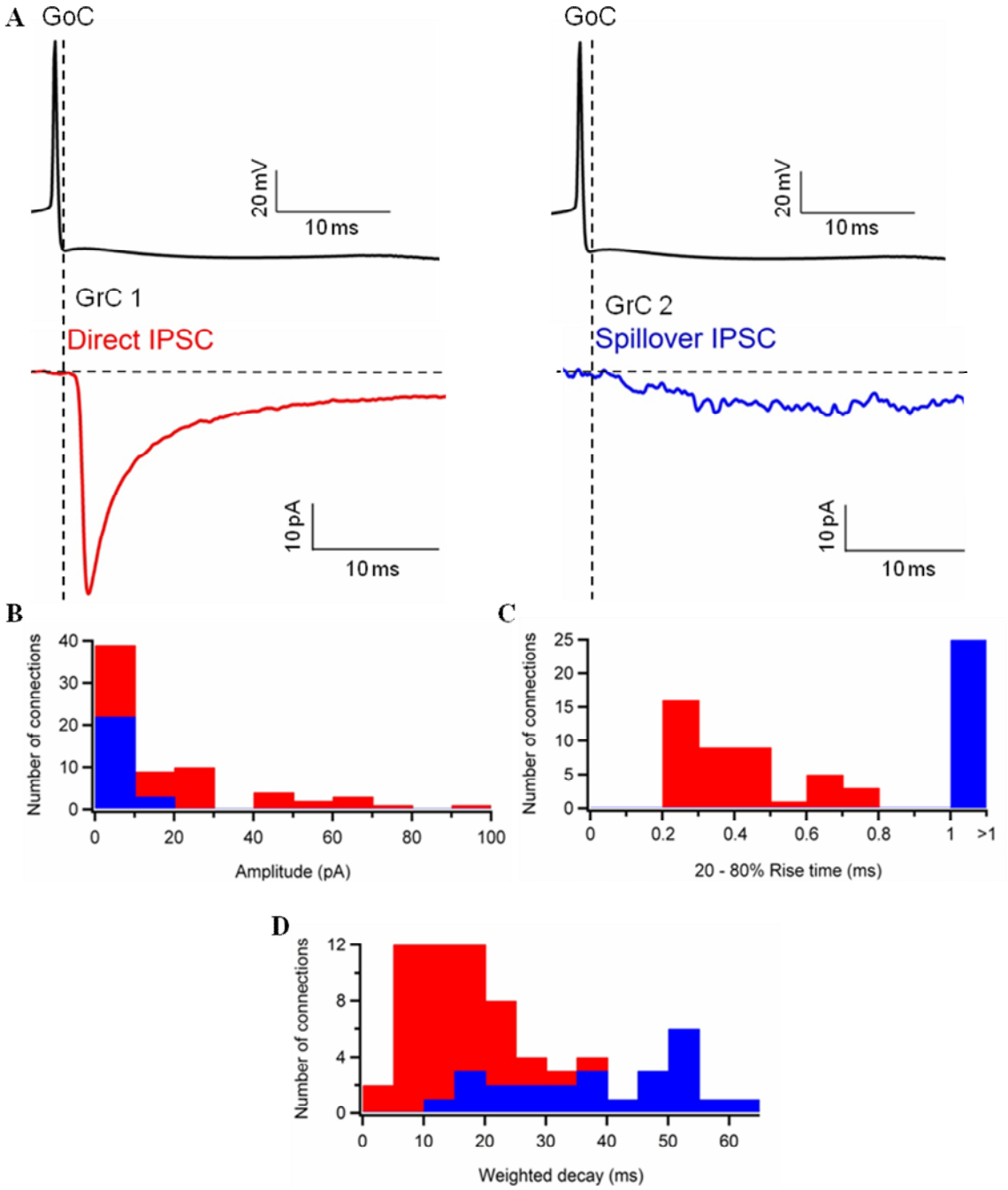

Fig. 3.7: Paired GoC–GrC IPSCs. **A**. Averaged presynaptic action potentials and postsynaptic IPSCs from paired recordings with different postsynaptic GrCs but the same presynaptic GoC. GrC 1 (left; red) exhibits a typical direct IPSC waveform, GrC 2 (right; blue) exhibits a spillover only synaptic response. **B**. Histogram of IPSC amplitudes from paired recordings. **C**. Histogram of IPSC 20–80 % RTs. **D**. Histogram of IPSC weighted decays. Direct IPSCs are shown in red, spillover IPSCs are in blue.

3.4.2 Frequency dependence of unitary GoC inputs

To investigate the degree to which sustained phasic input from a single GoC might be able to alter the inhibitory conductance received by a postsynaptic GrC, trains of presynaptic action potentials were triggered using square 1 ms current injections (12 pulses at 0.5–2 nA; **Fig. 3.8**). Short term plasticity was assessed by measuring the amplitude of successive IPSCs delivered at 5, 10, 20 and 50 Hz (N = 6 direct connections). The 1st, 2nd, 5th and 10th stimuli in each train are expressed as a percentage of the first IPSC (**Fig. 3.9A**). Plotting the normalised % amplitude against stimulation frequency (**Fig. 3.9B**) reveals that at stimulation frequencies of 20 Hz and above paired IPSCs depress to a greater extent than eIPSCs, reaching a maximum of 23.2 % of their initial amplitude within 12 pulses at 50 Hz.

As for eIPSCs, measuring the change in I_{hold} in a fixed window following each IPSC revealed a rate-dependent summation of the slow components of the IPSCs (N = 6; **Fig. 3.10A**). The shift in I_{hold} 50 ms after the presynaptic action potential (20 times the average fast IPSC decay constants measured for eIPSCs) was measured and used to estimate the peak conductance generated by the summation of pure IPSC spillover at each frequency (**Fig. 3.10B**).

When IPSCs were triggered at high rates (50 Hz) the peak conductance generated by the summation of IPSC spillover was not significantly different between direct connections and spillover only connections (103 ± 80 pS (N = 34) vs 100 ± 89 pS (N = 16); T-test P = 0.9; **Fig. 3.8**) implying that at high GoC firing rates the two connection types are functionally similar.

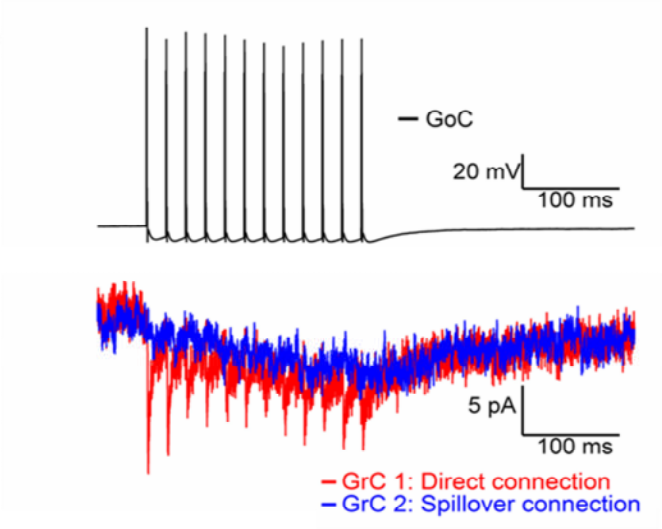

Fig. 3.8: A 50 Hz train of paired GoC–GrC IPSCs. Example trace showing action potentials triggered at 50 Hz in a presynaptic GoC and responses in two separate postsynaptic GrCs, one receiving a direct IPSC (red) and the other a spillover-only input (blue; same cells as in **Fig. 3.7**). Traces are the average of 50 trials.

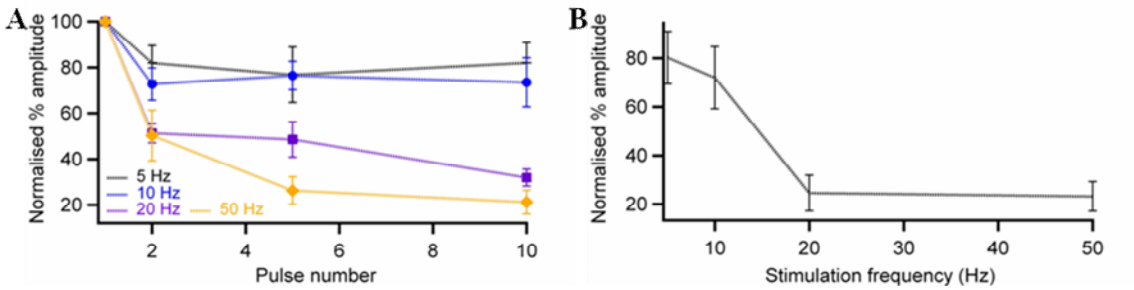

Fig. 3.9: Short term plasticity of paired GoC–GrC IPSCs. **A**. Normalised mean IPSC amplitudes for the 1st, 2nd, 5th and 10th IPSCs in trains delivered at 5 (black), 10 (blue), 20 (purple), and 50 Hz (orange). **B**. Normalised mean IPSC amplitudes for the 12th pulse at the same frequencies as above (N = 6). Error bars represent SEM. All connections presented are direct.

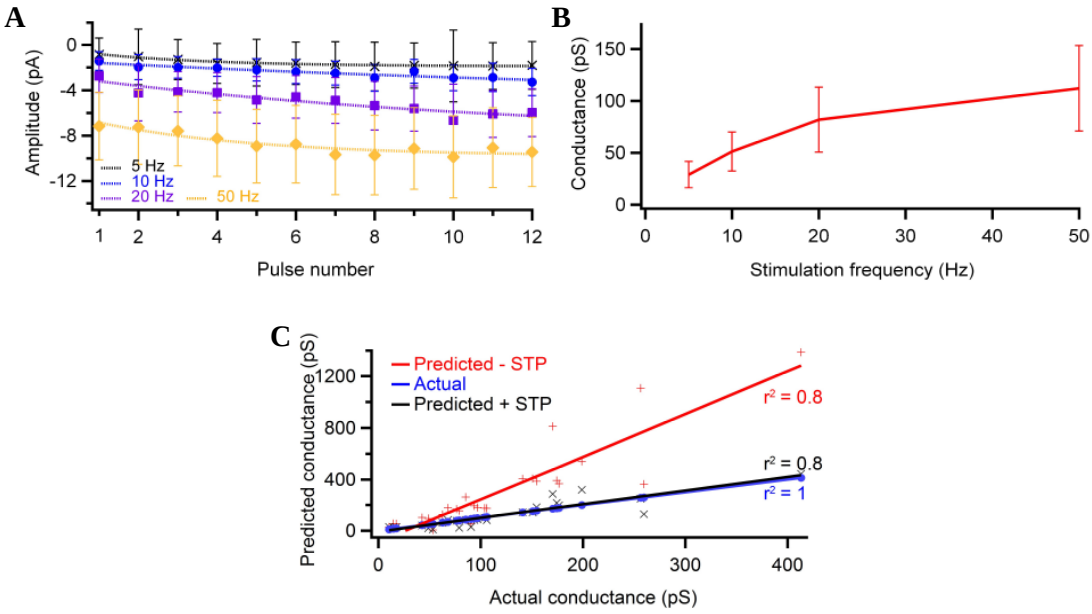

Fig. 3.10: Summation of spillover at individual GoC–GrC synapses. Spillover was measured as in **Fig. 3.6A**. **A**. The gradual build up of spillover current in response to 12 IPSCs arriving at 5 (black), 10 (blue), 20 (purple) and 50 Hz (orange) lines represent double exponential fits to the data. **B**. Estimate of uncontaminated spillover measured 50 ms after the last pulse at the same frequencies as in **A** (N = 6), error bars represent SEM. **C**. Spillover conductance elicited by 8 pulses at 50 Hz (measured in a fixed 4 ms window 15ms after the 8th pulse) vs predicted conductance in the absence (red) and presence (black) of short term plasticity (N = 26).

In order to better understand the mechanisms underlying the build up of spillover at unitary synapses the spillover conductance generated by 8 IPSCs at 50 Hz (measured in a fixed 4 ms window 15 ms after the 8th pulse) was compared to the amount of spillover predicted to be generated by the same IPSCs in the absence of STD (the waveform of the first IPSC in the train was delivered 8 times at 50 Hz) and the presence of STP (the waveform of the first IPSC in the train was delivered 8 times at 50 Hz, each iteration of the waveform was scaled according to the reduction in peak amplitude of the corresponding paired IPSC; **Fig. 3.10C**). Spillover connections were excluded from this analysis due to difficulty in accurately assessing the amplitude of individual IPSCs in 50 Hz trains and estimating plasticity. Actual trains of IPSCs generated a similar mean inhibitory conductance (121 ± 90 pS) to those modelled with STD (121 ± 108 pS; paired T-test $P = 0.9$) and significantly less than those modelled without (313 ± 332 pS; paired T-test $P < 0.001$). Actual data correlated well with modelled data lacking STD (Pearson's rank; $r = 0.89$; $P < 0.001$) and modelled data with STP (Pearson's rank; $r = 0.93$; $P < 0.001$). These results strongly imply that spillover is subject to STD to the same extent as the direct component of the IPSC and that spillover does not summate in a supralinear fashion at single synapses.

GoC–GrC IPSCs undergo more rapid and extreme frequency dependent STD than eIPSCs (**Fig. 3.9**). There is a frequency-dependent build up of spillover, but it is less pronounced than for eIPSCs (**Fig. 3.10A**, **B**). The build up of spillover and STD of the IPSCs mean that at high input rates spillover connections and direct connections generate a similar amount of charge (**Fig. 3.8**). In paired recordings spillover is scaled by STD to the same extent as the peak amplitude of the direct component of the IPSC and sums linearly at 50 Hz (**Fig. 3.10A**, **C**).

3.5 Discussion

3.5.1 Characterisation of the GoC–GrC synapse

Spontaneous IPSCs are detectable in GrCs in the absence of synaptic stimulation and occurred with a mean frequency of 4.6 ± 4.7 Hz; higher than reported in most previous studies (0.04 to 1.5 Hz; Tia *et al.* 1996; Wall & Usowicz 1997; Rossi & Hamann 1998;

Brickley *et al*. 2001; Wall 2002; Yaun & Atchison 2003; Carta *et al*. 2004; Chiu *et al*. 2005; Wall 2005) on account of the use of physiological recording temperatures in this study (at sub physiological temperatures GoCs fire at lower rates and release probability is substantially reduced; Dieudonne 1998; Volgushev *et al*. 2004). Studies carried out at or near physiological temperature have yielded mixed values for basal sIPSC frequency (0.7–10.5 Hz; Bright *et al*. 2011; Mameli *et al*. 2008) partially due to the use of animals of different age and species (GoCs in mice, as used by Bright *et al*. 2011, tend to be less active). The mean amplitude (-60.7 ± 23.8 pA) and RT (0.21 ± 0.078 ms) of sIPSCs recorded in this study were respectively greater, and faster than those recorded in studies performed at room termperature, however the mean IPSC amplitude was smaller than that reported by Mameli *et al*. 2008 (95 ± 13.5 pA) and Rossi & Hamann 1998 (92 ± 17.9 pA). This discrepancy may be due to differences in recording conditions, animal age, sIPSC detection criteria or the relatively small sample size in my study (N = 11).

In accordance with previous studies (Rossi & Hamann 1998) sIPSCs were sensitive to both TTX and GBZ (**Fig. 3.1**). GBZ application also revealed a tonic inhibitory conductance of 420 pS, somewhat smaller than the 700 pS recorded in Hamann *et al*. 2002 perhaps due to their use of older animals (tonic inhibition increases with age; Brickley *et al*. 1996). TTX did not affect tonic inhibition in agreement with Rossi *et al*. 2002 but in contrast to Bright *et al*. 2011, the disparity may be due to the use of mice in the latter study.

Evoked IPSCs had similar amplitudes to sIPSCs but slower kinetics (**Fig. 3.2**; in agreement with Rossi & Hamann 1998 and Wall 2002). Spillover inputs were not detected among the sIPSCs however this would not fully account for the kinetic discrepancy. Notably, mean sIPSC waveforms were the average of all sIPSCs recorded in a cell, as the majority of GoC–GrC connections are fast and direct the average sIPSC waveform was conferred with a fast RT. Further, averaged eIPSC waveforms would have included failures of release resulting in spillover-only input increasing the average weighted decay.

Evoked IPSC amplitudes recorded in this study (-66.0 ± 55.0 pA) were larger than those reported by Wall 2002 (~ 30 pA) but smaller than those reported in Rossi & Hamann 1998 (138 ± 18.3 pA). These discrepancies are likely to arise, at least in part, from age

differences in the animals used (Wall 2002 used P40 rats while Rossi & Hamann 1998 used P12; GoC–GrC IPSC amplitude reduces with age; Tia *et al*. 1996), however, differences in recording conditions and eIPSC detection criteria may also have contributed. RTs recorded in the present study were faster than in the aforementioned studies on account of my use of physiological recording temperatures.

Data from paired recordings revealed that unitary GoC–GrC inputs have much smaller amplitudes than eIPSCs and sIPSCs (**Fig. 3.7B**). This may indicate that the recorded eIPSCs and sIPSCs represent combined input from multiple GoCs or that detection is biased to select for larger IPSCs. As mentioned, sIPSC waveforms do not include failures of transmission and detection is biased to favour larger inputs. Further, it is known that GoCs fire in synchrony at rest (Dugue *et al*. 2009), thus it is possible that some sIPSCs represent near-simultaneous input from multiple GoCs. With regard to eIPSCs, it may be extremely difficult to stimulate a single GoC axon as GoC axons form dense overlapping plexuses in the GrC layer. It is also possible that stimulation of a single GoC may recruit activity in neighbouring GoCs via gap junctions. Further, the depolarisation of the axon elicited by a stimulating electrode may differ from an endogenous action potential leading to more Ca^{2+} at the GoC synaptic terminal and therefore more transmitter release (although failure rate was similar for paired IPSCs and eIPSCs the paired IPSC sample was biased to larger IPSCs which may have had lower than average failure rates). It is also possible that stimulation activated other elements in the cellular mileu that may have boosted the eIPSC amplitude. Additionally, in paired recordings IPSCs were averaged from at least 100 events allowing for the detection of very tiny events which would not be visible above noise on single trials while eISPCs were detected by eye and thus had to be visible on a single trial basis. The increased ability to detect very small spillover events can also account for the slower mean RTs and weighted decays in IPSCs from paired recordings. Direct IPSCs detected in paired recording had similar RTs and weighted decays to eIPSCs but expressed slower kinetics than sIPSCs. That unitary IPSCs from paired recordings were significantly smaller than eIPSCs may imply that other studies which have characterised putative single inputs using minimal stimulation may have overestimated the weight of single synaptic inputs.

The mean amplitude of IPSCs (17.3 ± 20.8 pA) in my paired recordings was smaller than the mean amplitude of IPSCs from paired recordings reported in Dugue *et al*. 2005

(53 ± 58 pA) but loosely comparable to the value reported in Crowley *et al*. 2009 (mean amplitude of successes = 32 ± 18 pA, failure rate = 0.58 ± 0.24). The discrepancy with results from Dugue may be partly due to differences in detection criteria, indeed 36 % of connections identified in my study were purely mediated by spillover, no small spillover-only connections were detected in Dugue *et al*. 2005 (N of 6 connections). Crowley *et al*. 2009 also reported a lower frequency of spillover connections (12 %) than I detected. The discrepancy may result from the use of the cell-attached technique in their presynaptic paired recordings. As GoCs tend to fire in synchrony in slice (Dugue *et al*. 2009; Verveake *et al*. 2010) the resultant postsynaptic waveforms may not correspond directly to the recorded presynaptic action potential, this could also account for the difference in the reported failure rate.

The results presented here differ from previous published data in terms of IPSC amplitude and the proportion of connections that can be considered spillover only, most likely due to the use of more sensitive recording techniques. However, I confirm the key assertion of previous studies that the majority of the charge from GoC IPSCs is conveyed by the slow component of the IPSC (Rossi & Hamann 1998; Crowley *et al*. 2009) as indicated by the high weighted decay values obtained for paired IPSCs and eIPSCs.

A potential source of error in this and previous studies results from the use of high Cl^- internal solutions which have been shown to slow the decay timecourse of IPSCs through direct actions on the $GABA_A$Rs (Houston *et al*. 2009). However, the bias is likely to be small as the majority of inhibitory charge is conveyed by the slow component of the IPSC (Rossi & Hamann 1998; Crowley *et al*. 2009) which is thought to be more sensitive to the timecourse of GABA in the synaptic cleft than receptor kinetics. Further, Mapelli *et al*. 2009 who used physiological Cl^- levels in their recordings note a very substantial spillover component.

It is impossible to be certain that the paired IPSCs in this study were not partially contaminated by input from neighbouring GoCs connected via gap junctions that were activated during stimulation of the presynaptic cell; however, single action potentials are not transmitted well by GoC gap junctions (Dugue *et al*. 2009; Verveake *et al*. 2010) and the small mean amplitude size recorded implies that contamination was likely to be limited.

It has been suggested that spillover is selectively mediated by α6 subunit containing $GABA_A$Rs, however, in agreement with Tia *et al*. 1996, Brickley *et al*. 2001, Rossi *et al*. 2002, Crowley *et al*. 2009 and Bright *et al*. 2011, in this study furosemide reduced the IPSC amplitude (by 68 %) and did not selectively diminish any component of the eIPSC (**Fig. 3.4**). Wall 2002 found a heterogenous contribution of the furosemide-sensitive receptors to GrC IPSCs. Similar results might have been obtained in this study had a larger sample of GrCs been tested, however Wall 2002 utilised puff application to apply furosemide rather than bath application, which might have been a less reliable delivery mechanism. Furosemide application produced a reduction in the tonic inhibitory conductance of 59 %, a little larger than the 43 % reduction noted by Rossi *et al*. 2002, however the sample size in this study was small (N = 3).

3.5.2 The frequency dependence of GoC–GrC synapse

Evoked IPSCs depressed steadily at frequencies greater than 5 Hz to a maximum of 45.8 % of their initial amplitude at 50 Hz (approximately the fastest GoC firing rate observed in rats *in vivo*; Holtzman *et al*. 2006b; **Fig. 3.5**). The magnitude of STD was similar to levels reported in other studies (Crowley *et al*. 2009; Mapelli *et al*. 2009). IPSCs in paired recordings underwent greater frequency-dependent STD (at frequencies above 10 Hz) than eIPSCs, depressing to 23.2 % of their initial amplitude at 50 Hz (**Fig. 3.9**). The discrepancy between the STD observed with paired IPSCs and eIPSCs may result from the small sample number in both data sets (8 and 6 cells respectively). It is possible however that stimulation of other elements in the cellular mileu with the stimulating electrode may have altered eIPSC plasticity. Alternatively, it is possible that action potentials evoked by stimulation are transmitted more reliably than those evoked by somatic depolarisation (although failure rate was similar for paired and evoked IPSCs) or that successive stimuli resulted in the activation of additional GoC axons by increasing local K^+ release. Finally, dialysation of the presynaptic cell may have affected the properties of the presynapse. This is unlikely however as the GoC axon is long, has a high resistance and typically takes several minutes to fill. These ideas could be tested to some extent by looking at the coefficient of variation and failure rate of paired IPSCs and eIPSCs when delivered at high rates, this was not done as some paired IPSCs were not detectable above noise on a trial by trial basis.

In accordance with a recent study (Crowley *et al*. 2009) delivering eIPSCs at frequencies of 5 Hz or above resulted in a build-up of spillover. The build up of spillover could be fitted with a double exponential function (**Fig. 3.6B**). IPSCs evoked in paired recordings also elicited a build up of spillover that could be fitted with a double exponential function but which was much smaller in magnitude (**Fig. 3.10A**). The amount of spillover generated increased with stimulation frequency. Paired IPSCs could produce an average conductance of ~ 100 pS (roughly a quarter of the size of the total resting inhibitory conductance; **Fig. 3.10B**) while eIPSCs could produce an average conductance of ~ 300 pS (roughly three quarters the size of the total resting inhibitory conductance; **Fig. 3.6C**) when delivered at 50 Hz.

The inhibitory conductance produced by a 50 Hz train of eIPSCs was larger than would have been predicted in the event that spillover sums linearly were the full eIPSC waveform scaled to the same extent as the peak amplitude by STD (**Fig. 3.6D**). By contrast, in paired recordings, a 50 Hz train of IPSCs matches almost exactly the conductance that would have been predicted in the event that spillover sums linearly, and the full IPSC waveform is scaled to the same extent as the peak amplitude by STD (**Fig. 3.10C**). It is possible that the spillover component of the eIPSCs was less susceptible to STD, perhaps because the larger release events triggered by stimulation allowed GABA to reach more distant receptor sites that were less prone to STD, however, that actual data correlated better with modelled data with STD than without, and that the single evoked spillover only input underwent depression (**Fig. 3.6D**) suggests that the spillover component of eIPSCs undergoes at least some STD. Electrical stimulation excites cells within a small radius of the stimulating electrode. Repeated stimulation, such as occurred in these 50 Hz trains could have elicited significant K^+ release which may in turn have lead to the recruitment of additional GoC axons, increasing the inhibitory conductance towards the end of the train. A further possibility is that eIPSC spillover sums supralinearly due to the saturation of GABA uptake mechanisms, this possibility is supported by the fact that the disparity between recorded inhibitory conductances and simulated inhibitory conductances with STD was greatest when the inhibitory conductance was largest.

3.6 Conclusions

Previous studies have grossly overestimated the size of individual GoC–GrC inputs and underestimated the proportion of spillover only inputs due to coarse methods of investigation. I have presented a careful description of the GoC–GrC synapse including a quantification of frequency dependent plasticity and summation of spillover, I have also identified a potentially non-linear build up of spillover in response to large synaptic inputs delivered at high rates. This description of the GoC–GrC synapse has allowed the investigation of the effect of GoC input on GrC processing of MF input as described in **Chapters 4** and **5**.

Chapter Four

4. The effect of phasic inhibition on rate coding in granule cells

4.1 Introduction

Broadly speaking GrCs receive two types of MF input: Transient bursts of MF input, typically signalling the onset (and perhaps the offset) of sensory stimuli (such bursts of MF EPSCs have been recorded in GrCs in response to discrete tactile input to the skin or whiskers; Jorntell & Ekerot 2006; Rancz *et al*. 2007) the precise timing of which is thought to be essential for regulating appropriately timed responses. And rate coded MF input that conveys information on some continuous sensory variable such as joint angle (Van Kan *et al*. 1993; Jorntell & Ekerot 2006) or head velocity in a preferred direction (Arenz *et al*. 2008). For such rate coded inputs it is the mean firing rate that is thought to carry the salient information, while the precise timing of individual inputs presumably has limited importance.

Processing of rate-coded information by a GrC can be described in terms of the relationship between mean MF input rate and mean GrC output firing rate. In general terms a second type of input, for example a GoC input, might be expected to alter the GrC I–O function in one of two ways; either by adding an offset to the I–O function without changing its slope, serving to subtract baseline levels of excitation from a signal (an additive operation), or by changing the slope of the I–O function effectively altering the sensitivity of the cell to changes in the excitatory input rate (a multiplicative operation; **Fig. 1.5**). Additive operations have been shown to be important for computing with population codes (Ma *et al*. 2006) while multiplicative operations have been shown to be involved in many neuronal operations from regulating bending behaviour in the medicinal leech (Baca *et al*. 2008) to scaling of visual responses in the monkey parietal cortex relative to head and eye position (Andersen *et al*. 1985; Brotchie *et al*. 1995).

Changes in tonic inhibitory input have been shown to elicit a gain change in the I–O function of the GrC (Mitchell & Silver 2003; Rothman *et al*. 2009), however little

evidence exists to suggest that tonic inhibition changes over a timescale that would be relevant to GrC computation. The extent to which phasic inhibition arising from GoCs can regulate GrC processing is not well understood. It has been suggested that the direct component of the GoC–GrC IPSC can mediate an additive shift to the GrC I–O function while the build up of spillover instigates a gain change (Crowley *et al*. 2009) My characterisation of the GoC–GrC synapse has allowed me to model realistic synaptic conductances which can be used in dynamic clamp experiments (Economo *et al*. 2010) to analyse the computational effects of GoC mediated inhibition in unprecedented detail.

The majority of inputs to the GoC will principally serve to alter its mean firing rate. Consequently I have investigated the effect of changes in mean GoC firing rate on the GrC I–O function.

In the slice (Dugue *et al*. 2008; Verveake *et al*. 2009) and under certain conditions *in vivo* (Vos *et al*. 1999a; Dugue *et al*. 2008) GoCs fire in loose synchrony. In addition to altering their firing rate, input to GoCs can disrupt (Verveake *et al*. 2009) or possibly enhance (Vos *et al*. 1999a) GoC synchrony. Therefore I have also investigated how GoC synchrony can affect the gain and pattern of GrC firing in response to rate coded MF input.

4.2 The effect of activity at the GoC–GrC synapse on GrC processing

In order to investigate the effect of GoC inputs on GrC computation, data from paired recordings was used to construct averaged synaptic conductances for direct (average of 25 connections) and spillover only (average of 15 connections) GoC inputs. GoC inputs were aligned to their 20 % RTs and averaged (**Fig. 4.1A**). The resultant direct inhibitory conductance waveform had a peak amplitude of 465 pS, a 20–80 % RT of 0.31 ms, and a weighted decay of 37.1 ms. The spillover inhibitory conductance waveform had a peak amplitude of 41 pS, a 20–80 % RT of 2.6 ms and a weighted decay of 381.7 ms.

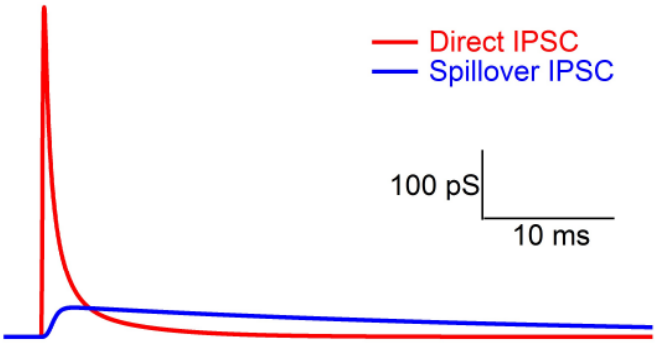

Fig. 4.1: Simulated GoC inputs. Simulated GoC–GrC synaptic conductances derived from the average of 25 direct GoC–GrC connections (Red) and 15 spillover connections (Blue) that were utilised as inhibitory inputs in dynamic clamp (and modelling) experiments.

Poisson-distributed trains of MF-like excitatory input with fixed mean rates were simulated to provide excitatory drive to GrCs. Four independent MFs inputs with similar mean rates were combined to produce excitatory synaptic trains for each of the selected excitatory input frequencies (**Fig. 4.2A**). Six input trains were created for each frequency so that the structure of a given excitatory train would not bias estimates of GrC firing rate.

The amount of tonic inhibition to which mature GrCs are subject is thought to be greater than the amount of phasic inhibition (Rossi *et al*. 2003). It is not known exactly how many GoCs contact a single GrC. Estimates have ranged from ~ 4 (Rossi & Hamann 1998) to 2.6 ± 0.55 direct synaptic contacts from GoC axon terminals (Jakab and Hamori 1988) with perhaps the same number of spillover only inputs (Rossi & Hamann 1998). For the following experiment, phasic inhibition was presumed to arise from 4 GoCs (a modest estimate), two making direct contacts, the other two spillover only. The total resting inhibitory conductance to which GrCs are subject (420 ± 270 pS), was presumed to include inhibitory input from four GoCs firing at ~ 8 Hz (Dieudonné, 1998; Forti *et al*. 2006). In order to obtain an estimate of the tonic inhibitory conductance I measured the amount of inhibitory conductance expected to arise from four GoCs firing at 8 Hz and subtracted it from the measured total inhibitory conductance, which left an estimated tonic conductance of 200 pS. As shown in **Fig. 4.2A**, the four GoC inputs were desynchronised and delivered at 0 (red; off), 10 (purple; ~ resting rate), or 50 Hz (blue; high rate) on top of the estimated tonic conductance. The sizes of the individual synaptic inputs were scaled according to plasticity data from paired recordings (by 0.85 for 10 Hz and by 0.3 for 50 Hz).

Dynamic clamp was utilised to inject excitatory input trains (four simulated MFs firing at 10, 30, 50, 70, 90 or 120 Hz) in conjunction with 0 Hz, 10 Hz and 50 Hz inhibitory input into patch clamped GrCs (N = 19). The order in which the trains were delivered and the specific excitatory trains used were randomised to eliminate bias. The spiking outputs for each trial were measured in a 250 ms window 100 ms after the start of the excitatory train and averaged across GrCs. Average spiking frequencies were plotted against input frequency and fitted with a Hill function to produce an I–O curve corresponding to each of the examined inhibitory regimes (**Fig. 4.2B**). Each fit was significantly different from the others (F-test; $P < 0.0001$ in all cases). Increasing the frequency of inhibition dramatically reduced the slope of the GrC's I–O function, 10 Hz

inhibition caused a gain reduction of 45 % relative to 0 Hz inhibition, while 50 Hz inhibition caused a gain reduction of 80 % relative to 0 Hz inhibition and 63 % relative to 10 Hz inhibition (**Fig. 4.2C**). Additionally, 10 Hz and 50 Hz inhibition produced an additive shift in the GrC I–O function (x offset) of 28.7 and 6.5 Hz respectively relative to tonic inhibition alone (**Fig. 4.2D**).

The rate of GoC firing has a strong effect on the slope of the GrC I–O function, therefore GoCs are well suited to regulate GrC gain.

4.3 The effect of GoC synchrony on GrC processing of rate coded signals

GoCs fire in loose synchrony at around 8 Hz in slice (Dugue *et al*. 2008; Verveake *et al*. 2009; Vos *et al*. 1999; Dugue *et al*. 2008). However, to date, no study has shown how this temporal patterning of the inhibitory input GrCs receive will affect their processing of MF information. With regard to rate-coded MF input it is unclear to what extent inhibitory synchrony might affect the I–O function of the GrC. Nor is it known whether the synchronised inhibitory input will be sufficient to pattern the GrC spiking activity, effectively imposing a temporal structure to their output.

4.3.1 The effect of synchrony on the GrC I–O function

To investigate whether GoC synchrony can affect the slope or offset of the rate coded GrC I–O function and thus interfere with rate coding, I used dynamic clamp to inject simulated, Poisson-distributed, inputs from 4 MFs at a range of mean rates (as above) in conjunction with inhibitory input arising from 8 GoCs; 5 making direct contacts, 3 spillover only (a high end estimate of the number of GoCs contacting a GrC to maximise any detectable effect), firing at 8 Hz (scaled to 0.8) either perfectly synchronised or totally desynchronised (in conjunction with 20 pS tonic inhibition such that mean inhibition totalled 420 pS) and recorded the GrC spiking output (**Fig. 4.3A**).

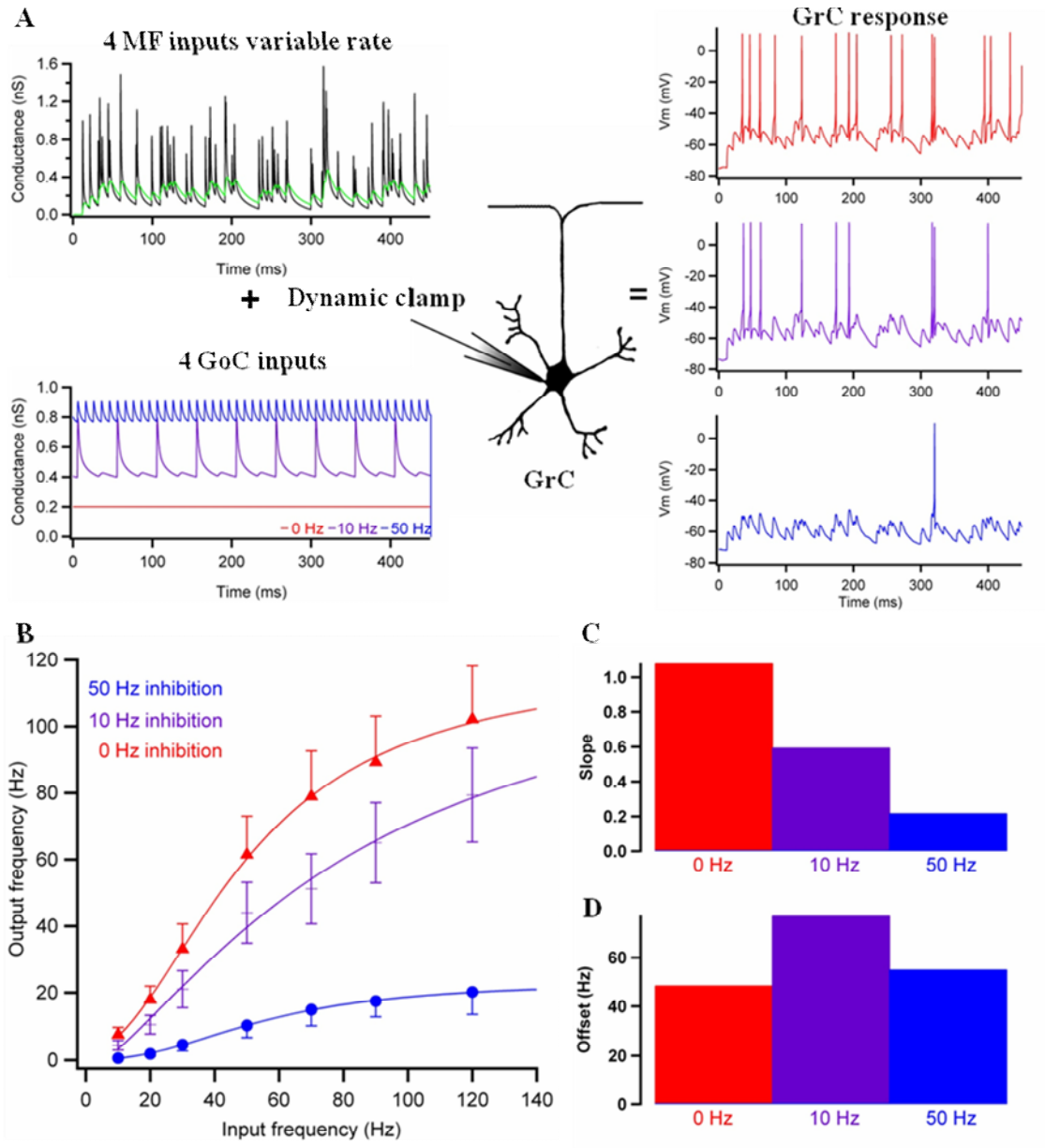

Fig. 4.2: The effect of GoC inhibition on the GrC I–O function. **A**. Schematic representation of the experimental protocol; trains of MF input (encompassing a range of rates) comprised of AMPA and NMDA waveforms (top left) were injected into GrCs using dynamic clamp (centre) in conjunction with GABAergic input from 4 GoCs at 0 Hz (tonic inhibition alone; red), 10 Hz (purple) and 50 Hz (blue), GrC spiking responses (right) were recorded for each case. **B**. Averaged I–O curves from 19 GrCs for 0, 10 and 50 Hz inhibition, data is fitted with a Hill function, error bars represent SEM. **C**. Quantification of the slope of the GrC I–O curves for 0 Hz, 10 Hz and 50 Hz inhibition. **D**. Quantification of the x-offset of the GrC I–O curves for 0 Hz, 10 Hz and 50 Hz inhibition.

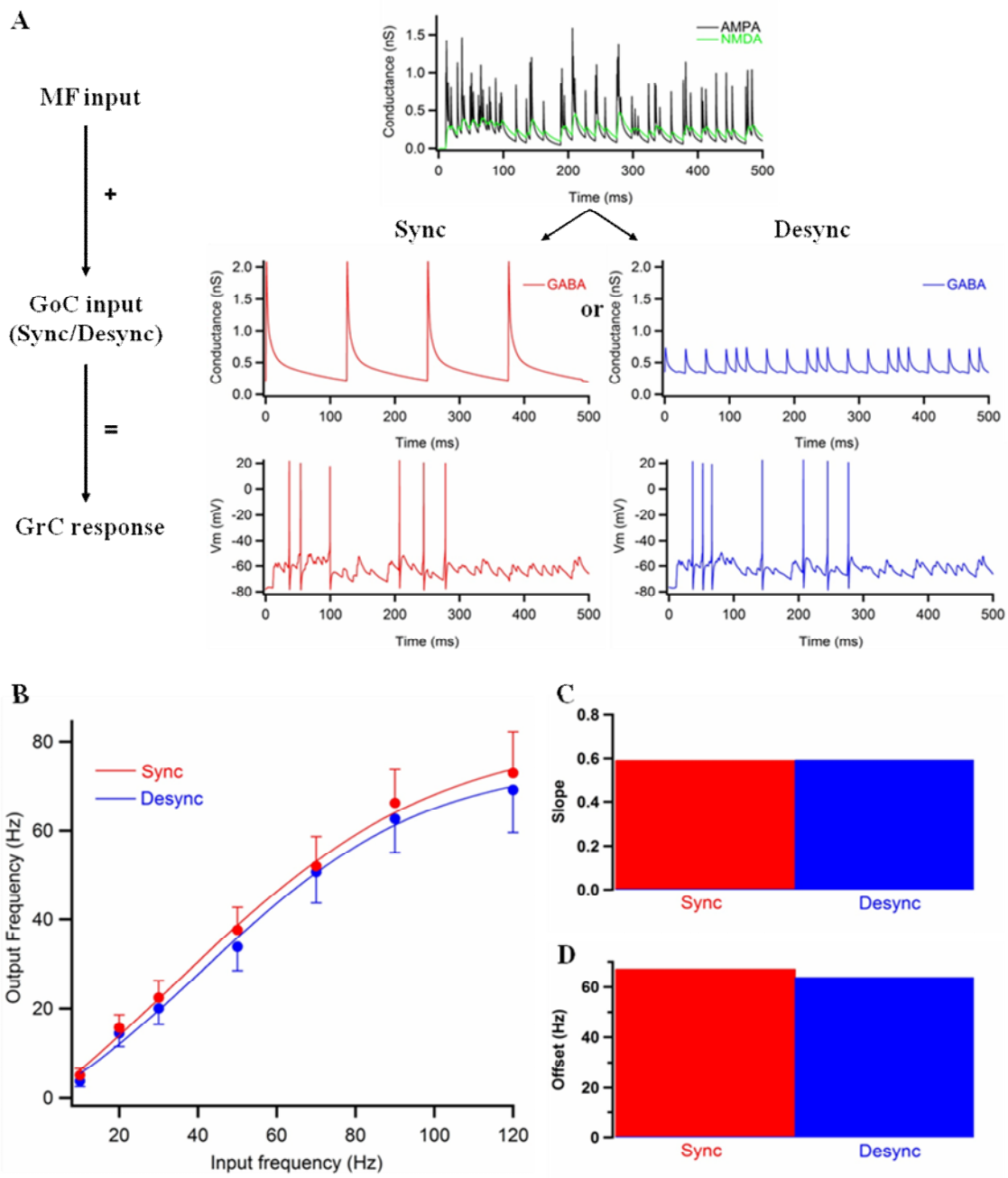

Fig. 4.3: The effect of GoC synchrony at 8 Hz on the GrC I–O function. **A**. Conductances used to investigate the effect of synchrony on the GrC I–O function. Simulated MF activity of variable rates was injected into GrCs in conjunction with inhibitory input from 8 GoCs (5 direct, 3 spillover only) firing at 8 Hz (scaled to 0.8) in prefect synchrony (red) or total asynchrony (blue). GrC spiking responses (bottom) were recorded and used to construct I–O curves. **B**. Mean GrC I–O curves (N = 41) obtained in the presence of synchronised (red) and desynchronised inhibition (blue). Fits represent a Hill function. Error bars represent SEM. **C**. Quantification of the slope of the Hill fits. **D**. Quantification of the x-offset of the Hill fits

The synchrony of inhibition did not affect the slope or offset of the GrC I–O function (**Fig. 4.3**; F-test P = 0.32). To test if the lack of effect of inhibitory synchrony was a function of the frequency of inhibitory input I repeated the above experiment using 15 Hz inhibitory input (15 Hz is the highest rate at which GoC synchrony can occur in an in lab model of GoC synchrony in the absence of specific excitatory drive; Verveake *et al*. 2009). GoC inputs were scaled to 0.6 and produced a mean conductance of 560 pS. As before I–O curves were constructed from the GrC spiking responses (this time measured in a 200 ms window; **Fig. 4.4**).

As with inhibition at 8 Hz the synchrony of inhibition failed to significantly affect the GrC I–O function (F-test P = 0.36). Thus synchrony of inhibition does not affect the slope or offset of the GrC I–O function when measured over a sufficiently large timescale and would not be expected to interfere with slow rate coded operations.

4.3.2 The effect of GoC synchrony on the pattern of GrC output

Given that the synchrony of inhibition failed to significantly affect mean GrC firing rate in response to rate coded MF input I investigated the effect of synchronised inhibition (delivered at 8 Hz) on the distribution of ISIs at MF input rates of 90 and 120 Hz (**Fig. 4.5**).

Inhibitory synchrony failed to significantly affect the distribution of ISIs elicited by MF input at either 90 (Kolmogorov-Smirnov test P = 0.11) or 120 Hz (Kolmogorov-Smirnov test P = 0.89).

In order to more carefully analyse the effect of inhibitory synchrony on the pattern of GrC responses to rate coded input I constructed several 1.5 second trains of 50 Hz poisson distributed MF input (4 MF each with a mean firing rate of 50 Hz were randomly selected from a bank of 98 to make each train) which I injected into GrCs using dynamic clamp with inhibition arising from 4 simulated GoCs (3 direct, 1 spillover only) firing at 8 Hz (GoC conductance waveforms were scaled to 0.8) either perfectly synchronised or perfectly desynchronised with 200 pS tonic inhibition to make the mean inhibitory conductance equal to 420 pS (**Fig. 4.7A**).

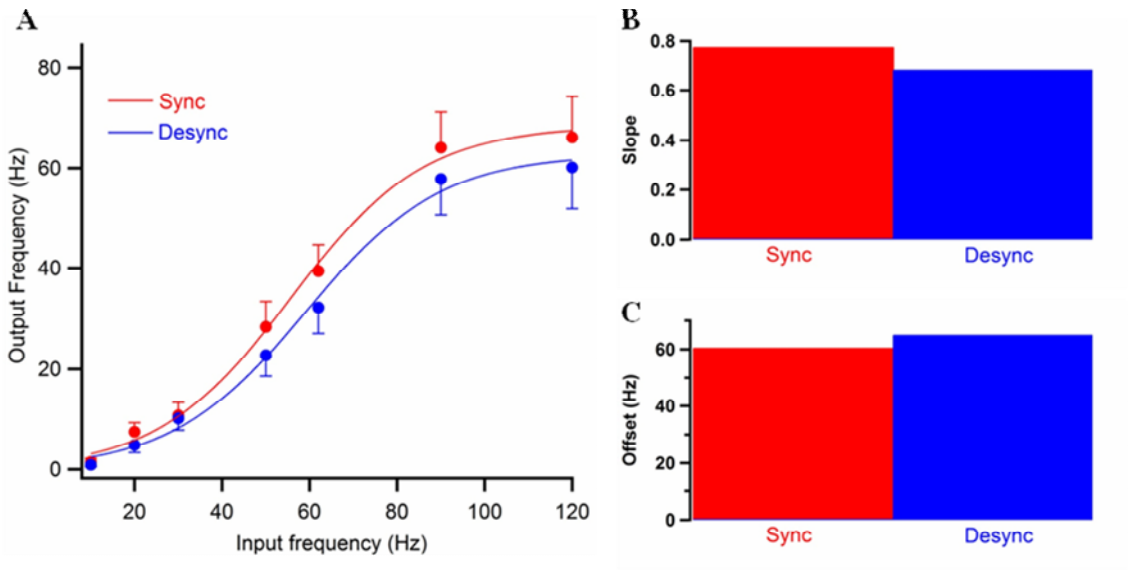

Fig. 4.4: The effect of GoC synchrony at 15 Hz on the GrC I–O function. **A**. Mean GrC I–O curves (N = 34) in the presence of synchronised (red) and desynchronised inhibition (blue). Fits represent a Hill function. Error bars represent SEM. **B**. Quantification of the slope of the Hill fits. **C**. Quantification of the x-offsets of the hill fits.

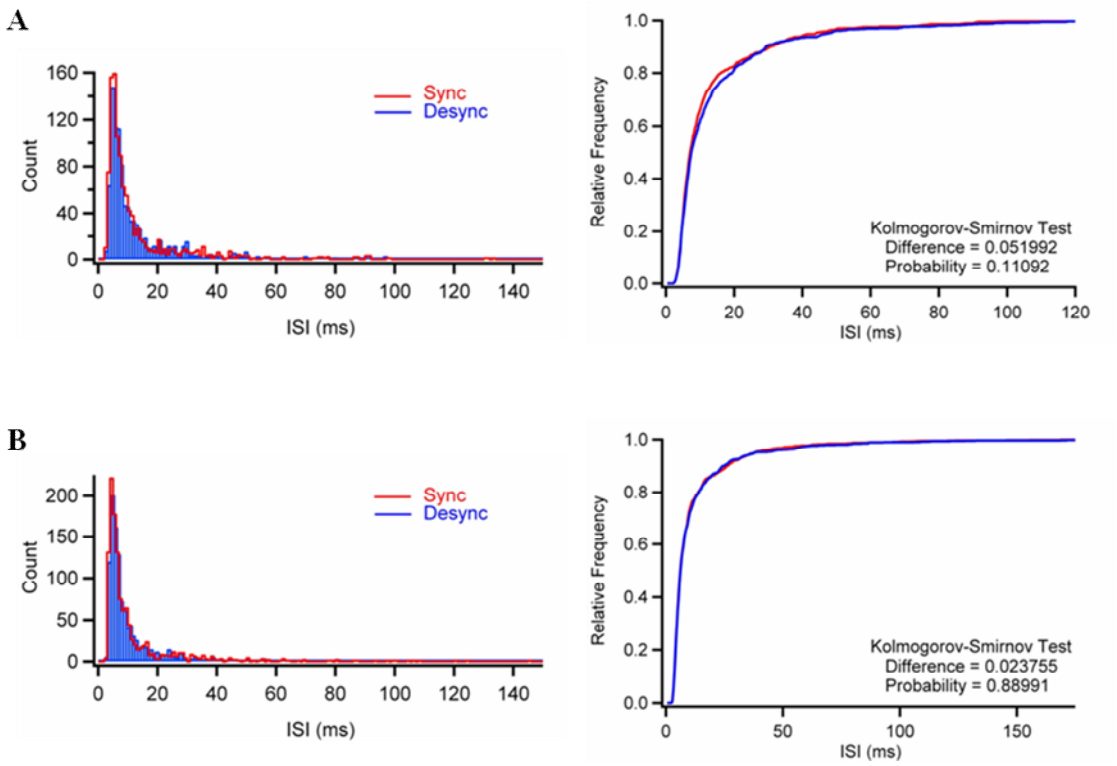

Fig. 4.5: The effect of GoC synchrony on GrC ISIs at high rates of MF input. **A**. Left, histogram of GrC ISIs elicited with a MF input rate of 90 Hz and inhibitory input from 8 simulated GoCs firing at 8 Hz either perfectly synchronised (red) or totally desynchronised (blue). Right cumulative distribution of GrC interspike intervals displayed on left. **B**. As for **A** but with a MF input rate of 120 Hz (N = 41).

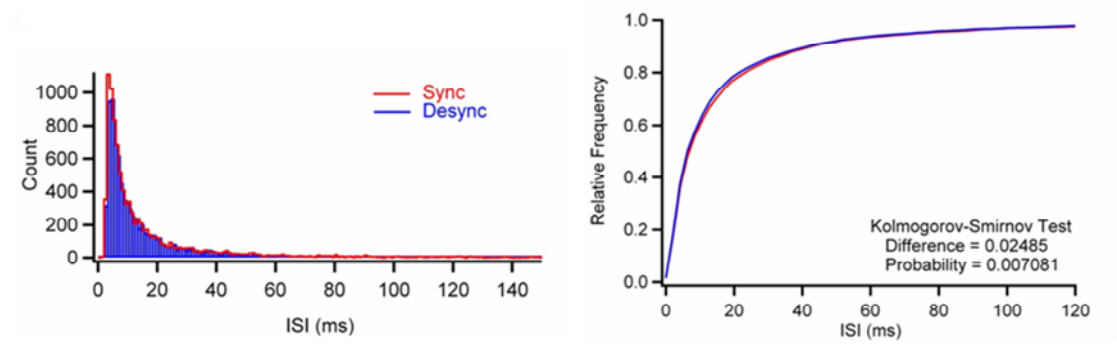

Fig. 4.6: The effect of GoC synchrony on GrC ISIs at moderate rates of MF input. Left, histogram of GrC ISIs with a MF input rate of 50 Hz and inhibitory input from 4 simulated GoCs firing at 8 Hz either perfectly synchronised (red) or totally desynchronised (blue). Right cumulative distribution of GrC interspike intervals displayed on left (N = 24 cells; 168 experiments).

GrCs fired at a mean rate of 49.8 ± 45.9 Hz with synchronised inhibition and 45.1 ± 45.0 Hz with desynchronised inhibition (N = 24 measurements made in a 1.25 second window; paired T-test $P < 0.05$). Inhibitory synchrony caused a very small but statistically significant change in the distribution of ISIs (Kolmogorov-Smirnov test difference = 0.025, $P < 0.01$; **Fig. 4.6**).

Given that inhibitory synchrony has little effect on the average firing rate or distribution of ISIs, if it is having a notable effect on GrC output it must be doing so by altering the order of ISIs, effectively patterning the GrC response. Several methods have been developed to detect patterns in cellular activity, the main categories of which are; spectral analyses (such as with a FFT) and analyses of the autocorrelation histogram. FFTs suffer from bias and variance problems (Jarvis & Mitra 2001) and do not directly quantify the strength of an oscillation, for this one must divide spectral magnitude of a particular frequency of oscillation by the average magnitude of the whole spectrum however this strategy is biased by the basal firing rates of neurons (Mureşan *et al*. 2008). Therefore I performed autocorrelations on the spike histograms obtained from the individual experiments (n = 168 from 24 cells; **Fig. 4.7**; a circular correlation function was utilised to avoid boundary effects). On average there was no clear pattern in the autocorrelation output with either synchronised or desynchronised inhibition (Z-score = 0.36 and 0.26 respectively; significance is judged as a Z-score value of 2 or more; **Fig. 4.8**; Dugue *et al*. 2008) implying that there is no clear patternation of GrC spiking at the single cell level.

However, GrCs don't act in isolation, oscillatory behaviour may occur at the GrC network level. PCs typically receive input from as many as 150,000 GrCs (Harvey & Napper 1991), and given that each GoC is expected to contact up to thousands of GrCs (Kanichay 2008) and that GoCs in close proximity tend to fire in synchrony (Vos *et al*. 1999; Dugue *et al*. 2008; Verveake *et al*. 2009), PCs are likely to receive input from a large population of GrCs sharing common inhibitory input, perhaps across a population of GrCs a clear signal can by generated and conveyed to a target PC.

To test this possibility I treated each experiment (n = 168) as if it represented the activity of an individual GrC within a fixed 1.5 second timecourse. Each "GrC" received unique MF input but GrCs shared common inhibitory input with the other GrCs. GrC's were randomly assigned to groups of variable size and the spiking output

of given groups was summed and assessed for patternation using autocorrelation analysis (**Fig. 4.7A**). Patterns in the spiking output of groups of GrCs were assessed for significance using Z-score criteria. Z-scores were averaged across groups of equal size.

With groups containing as few as 21 GrCs receiving common synchronised inhibition a significant pattern could be observed in the autocorrelation output, peaking at intervals of 125 ms to reveal an oscillation at 8 Hz (**Fig. 4.7B** & **4.8A**; average Z-score = 2.8). The significance of the correlation increased with group size (**Fig. 4.8A**). With a group sizes of 56 or more GrCs a pattern was detectable within the autocorrelation histogram of the GrCs receiving desynchronised inhibition (**Fig. 4.7B** & **4.8A**; average Z-score = 2.3) such an oscillation would never be detected *in vivo* as GoCs would never fire in a perfectly desynchronised fashion in the way that they have been constrained to in this experiment.

The strength of oscillations can be quantified in a number of ways. The synchronisation strength is defined as the area of the autocorrelation above a Z-score of 2 (**Fig. 4.8B**; Dugue *et al*. 2008). For GrCs receiving synchronised inhibition synchronisation strength increased with group size up to 84 GrCs before levelling out. For GrCs receiving desynchronised inhibitory input synchronisation strength remained low. However, synchronisation strength can be biased by oscillation frequency and basal firing rate.

The difference between the second satellite peak and the second valley in an autocorrelation has also been used to estimate oscillation strength (Samonds & Bonds 2005). Autocorrelation trough to peak height also increased with group size (**Fig. 4.8C**). The relationship between autocorrelation trough to peak height and group size could be well approximated with a double exponential function for cells receiving synchronised or desynchronised inhibition (not shown). However, as with synchronisation strength, this measure is sensitive to basal firing rate and does not work well with small data sets.

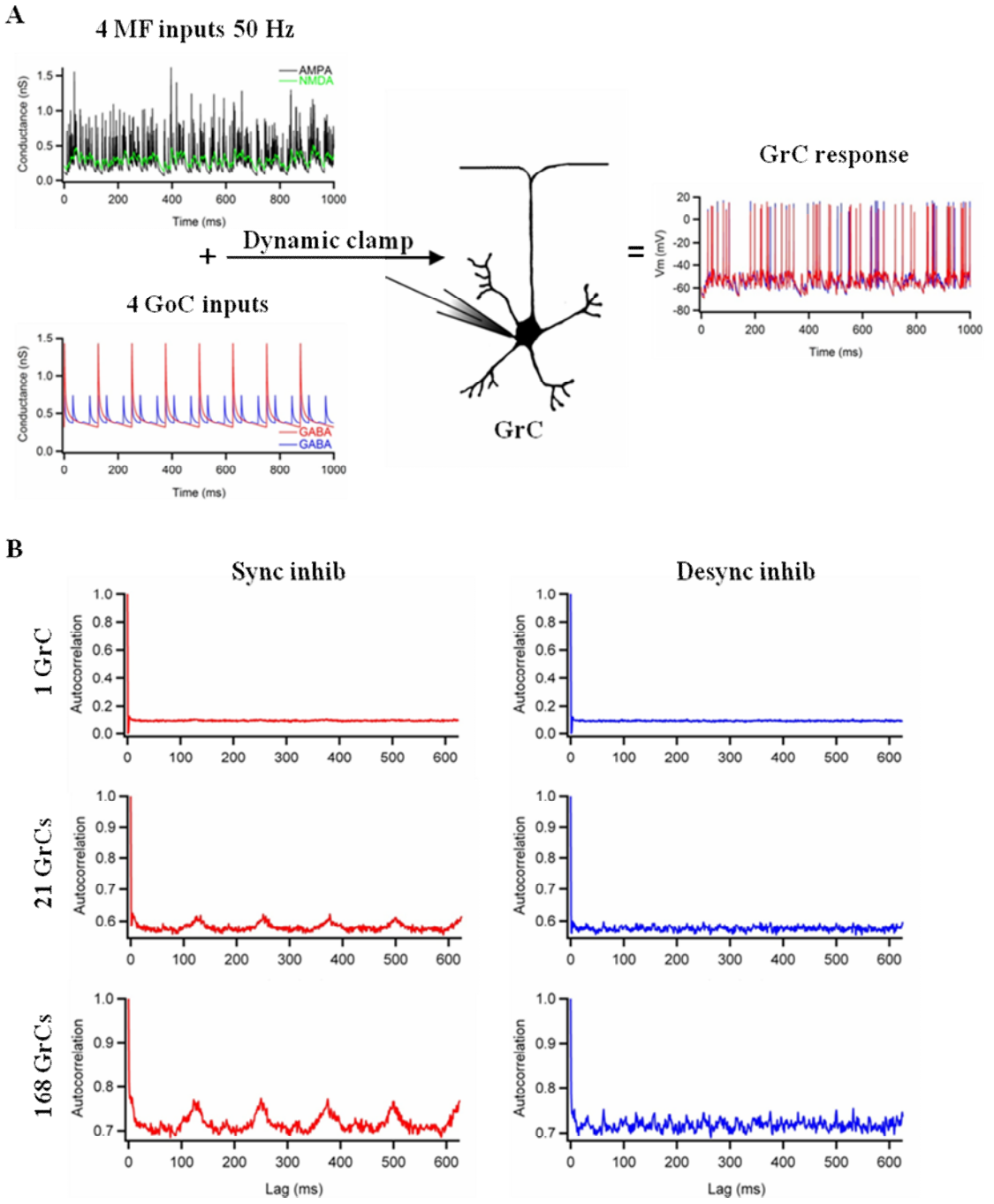

Fig. 4.7: Patterning of GrC firing by GoC oscillations. **A**. Excitatory conductance trains comprised of input from 4 randomly selected MFs with a mean firing rate of 50 Hz (top left) were injected via dynamic clamp with synchronised (red) or desynchronised (blue) inhibitory input from 4 GoCs (3 direct, one spillover; bottom left) firing at 8 Hz. The GrC spiking response was recorded (right). **B**. Average normalised circular autocorrelations of the spike histograms for single GrCs (average of 168 groups; top), groups of 21 GrCs (average of 8 groups; middle) and a group of 168 GrCs (bottom) with synchronised (red; left) and desynchronised (right; blue) inhibition.

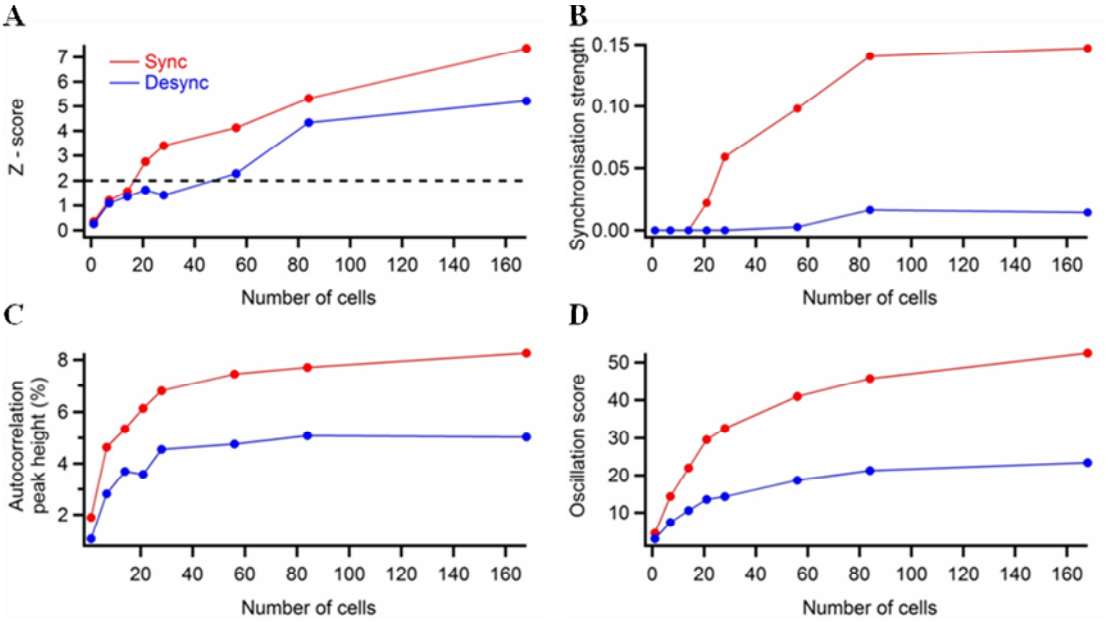

Fig. 4.8: Quantification of oscillations in GrC firing. Different measures of the strength and significance of oscillations in the firing pattern of groups of GrCs (x-axis) receiving either synchronised (red) or desynchronised (blue) inhibition. **A**. Z-score, dotted line represents significance. **B**. Synchronisation strength (area of the first satellite peak in the autocorrelation above a Z-score of 2). **C**. Height of the second satellite peak in the autocorrelation (measured from 2nd peak to 2nd trough) expressed as a % of the total autocorrelation. **D**. Oscillation score for different sized groups of GrCs.

The oscillation score measure was developed to overcome the shortcomings of the afore-mentioned methods (Mureşan *et al*. 2008) and does not rely on measurements of peak sizes or areas of the autocorrelation that can be biased by firing rate or spike number. Oscillation peak was judged at 7.8 Hz with synchronised inhibition and 32.1 Hz with desynchronised inhibition. Oscillation score increased with group size for cells receiving synchronised or desynchronised inhibition (**Fig. 4.8D**). Both relationships were well-approximated with a double exponential function (not shown). An oscillation score above 35 at 8 Hz is estimated to represent a strong oscillation (**2.3.8**; Mureşan *et al*. 2008).

These results show that while synchronised inhibition may not noticibly pattern the activity of individual GrCs, across a population of GrCs it can instil a clear temporal signal.

4.4 Discussion

4.4.1 GoC activity and the GrC I–O function

In order to investigate the effect of GoC mediated inhibition on GrC activity IPSCs recorded from GoC–GrC pairs were sorted by type, averaged and converted to conductances to give representative direct and spillover conductance waveforms. The waveforms were produced from limited data sets, so the amplitude of the direct GoC–GrC conductance is slightly larger than the mean amplitude reported for direct IPSCs in **Chapter 3**. In contrast the amplitude of the spillover conductance waveform is lower than the mean amplitude of spillover inputs reported in **Chapter 3** because spillover IPSCs were aligned to their 20 % RT. As spillover IPSCs had highly variable RTs, IPSC peaks were not well aligned creating a smoothed waveform with a less well defined peak than most individual spillover connections (**Fig. 4.1A**). In spite of these minor short-comings, the GoC–GrC conductance waveforms presented here are far more accurate than others utilised in previous studies of GrC computation (Mitchell & Silver 2003; Crowley *et al*. 2009).

I used the GoC–GrC conductance waveforms to investigate the effect of changes in GoC firing rate on GrC computation. The activity of 4 GoCs (two making direct inputs, 2 spillover) were simulated. Despite the fact that the resting level of inhibition to which

GrCs are subject was not sensitive to TTX in the present study and is therefore presumably action potential-independent, the view was taken that the ongoing activity of afferent GoCs (~ 8 Hz at rest) would likely contribute to the resting inhibitory conductance to which GrCs are subject (as activation of single GoCs had been shown to appreciably increase the inhibitory conductance seen by GrCs). The subsequent finding that tonic inhibition is mediated by GABA release through Best1 channels on astrocytes (Lee *et al*. 2010) could suggest that basal inhibition may not fall much below the observed levels even upon GoC silencing. Because of this, the scenario presented with 0 Hz inhibition wherein only a tonic inhibitory conductance of 200 pS was injected may not be a realistic representation of silenced GoC firing (**Fig 4.2B**, **C**). However other studies have demonstrated a significant action potential dependent component of the resting inhibition that GrCs receive (Bright *et al*. 2011).

Although individual IPSCs were shown to sum linearly in the previous chapter, delivery of eIPSCs at high frequencies revealed a supra-linear buildup of spillover (**Fig. 3.6**). As this effect has not been studied in sufficient detail to allow a meaningful quantification and it is not clear if the effect is physiological it was ignored for the sake of these experiments. Supra-linear buildup of spillover would tend to exaggerate the gain change elicited by increases in GoC firing rate.

Experiments investigating the effect of GoC firing frequency on GrC gain used a range of MF firing rates with a constant rate of inhibitory input. It is not clear that MF firing rate and GoC firing rate are truly independent, however, quantitive immunostaining has suggested that the probability of a GoC receiving common MF input to a GrC it is inhibiting is quite small (Kanichay 2008). Further, it has been demonstrated that some GoCs respond only to specific modalities or even sub-modalities in regions of the cerebellar cortex that receive multimodal MF input (Heine *et al*. 2010), several studies have detected GoC activity that is at odds with that of the majority of surrounding GrCs (Van Kan *et al*. 1993; Barmack & Yakhnitsa 2008; Heine *et al*. 2010) and GrCs in the C3 zone receive the majority of inhibitory input when tactile stimulation is applied to regions adjacent to those that evoke the majority of MF input (Jörntell & Ekerot 2006). Therefore it is not clear how GoC activity would be altered in the face of greatly variable MF input to surrounding GrCs. In truth, the degree to which the activity of a GoC is related to that of the GrCs it inhibits is probably variable. By treating GoC and GrC activity as independent in these experiments I have shown the relationship between

GoC mediated inhibition and the GrC I–O function. If future experiments inform us as to how GrC and GoC activity co-vary then these experiments could be useful as a framework to help discern precise GrC I–O functions.

A very clear gain change was observed upon increases in GoC firing rate (**Fig 4.2C**) suggesting that GoCs represent a suitable device for regulating the gain of GrC responses. Therefore, GoCs are well suited to maintain GrC activity to within a sensible dynamic range in the face of widely varying MF input and may allow GrCs to perform computational operations reliant on multiplication (e.g. coordinate transfer; Andersen *et al*. 1985; Brotchie *et al*. 1995).

GoC firing at 10 Hz produced an additive shift in the GrC I–O function. It has been suggested previously that the direct component of the IPSC could elicit additive offsets in the GrC I–O function (Crowley *et al*. 2009). However, this study utilised very large, unphysiological, "direct only" GoC–GrC conductance waveforms with nominal tonic inhibition (0.1–0.3 pS) and fixed rate inhibitory input that was often delivered exactly in phase with fixed rate excitatory input (which would serve to reduce noise and therefore gain; Mitchell & Silver 2003).

In addition to altering the gain of the GrC I–O function, increased rates of GoC firing seem to scale the maximal firing output of the GrC (**Fig 4.2C**) this may arise from the increased inhibitory conductance suppressing voltage fluctuations in the GrC (Mitchell & Silver 2003).

4.4.2 The effect of GoC synchrony on GrC processing of rate coded information

GoCs fire in loose synchrony in slice (Dugue *et al*. 2009; Verveake *et al*. 2010) and *in vivo* (Vos *et al*. 1999a) in phase with oscillations in the local field potential (Dugue *et al*. 2009) which have been observed extensively in the cerebellar cortex (Hartmann & Bower 1998; D'Angelo *et al*. 2001; Courtemanche & Lamarre 2002; Courtemanche & Lamarre 2005; Dugue *et al*. 2008; Courtemanche *et al*. 2009).

To investigate the effect of synchronised inhibition on GrC processing of rate coded MF input I utilised Poisson distributed MF input in conjunction with perfectly synchronised or perfectly desynchronised fixed rate inhibitory input (**Fig. 4.3A**). Perfectly

synchronised and desynchronised inhibition were utilised for clarity. In reality GoC firing is likely to be synchronised only to within a few milliseconds (Vos *et al*. 1999a; Dugue *et al*. 2009; Verveake *et al*. 2010), while reducing the level of GoC synchrony may affect my results quantitatively it would not be expected to alter my observations qualitatively. The inhibitory waveforms utilised were fixed and did not vary with MF–GrC input. It is not clear that GoC synchrony and rate would be conserved in the face of variable network activity, indeed field potential oscillations tend to be lost upon initiation of many motor behaviours (Hartmann & Bower 1998), however, as discussed above the activity of GoCs does not necessarily co-vary with that of the GrCs they inhibit.

To date, there has been no direct demonstration as to how synchronisation of inhibitory input might affect GrC processing of rate coded MF input. If the cerebellum is processing a rate coded signal conveying information on a sensory variable such as joint angle (Van Kan *et al*. 1993) or head velocity in a preferred direction (Arenz *et al*. 2008) then it is not immediately clear how a temporally-variant, inhibitory signal would be of use. It is interesting to note then, that the synchronisation of inhibition has little effect on the gain of the GrC I–O function, at least when measured over a sufficiently gross time scale and at the inhibitory frequencies investigated (250 ms with 8 Hz inhibition and 200 ms with 15 Hz inhibition; **Fig. 4.3** & **4.4**). The gross time scale was necessary to accurately compute the GrC I–O function in response to a Poisson distributed excitatory train.

That the gain and offset of the GrC I–O function are largely unchanged by inhibitory synchrony demonstrates that gain changes primarily relative to net inhibitory conductance rather than the noise or the distribution thereof (at least in the presence of a noisy excitatory input: Mitchell and Silver 2003), suggesting that a steady state conductance might be just as suitable as synaptic input for regulating gain. The precise timing of inhibitory inputs is likely to be more relevant to other computations.

In the afore-mentioned experiments gain was measured over a large time window (several inhibitory cycles). It is possible that GrC gain and firing is altered substantially over the course of an inhibitory cycle. To see if the GrC firing rate changes throughout the course of the inhibitory cycle I injected GrCs with long 50 Hz MF input trains in conjunction with synchronised or desynchronised inhibition via dynamic clamp and

performed autocorrelations on the GrC spike output. Individually no pattern in the GrC autocorrelation was detectable (**Fig. 4.7** & **4.8**) implying an absence of significant oscillatory activity. It is possible that an oscillation may have been detectable with more sensitive methods of analysis, for example it is possible to more accurately assess autocorrelations by fitting them with a Gabor function (Konig 1994) however this was not attempted in the present study due to the non-sinusoidal nature of the patterns in the autocorrelations presented (the Gabor function only works with sinusoidal waveforms; **Fig. 4.7**).

Neighbouring GrCs (particularly in the sagittal plane; Hámori & Szentágothai 1966) are likely to share common GoC input and neighbouring GoCs tend to fire in loose synchrony (Dugue *et al*. 2008; Verveake *et al*. 2009). Thus it is probable that neighbouring GrCs receive varied MF input but common inhibitory input. Populations of GrCs (above 21; **Fig. 4.7** & **Fig. 4.8**) receiving common synchronised inhibition showed clear oscillatory activity, revealing that GoC synchrony can pattern activity in the GrC layer without need for synchronised MF input. This patterning may underlie the oscillations in the GrC layer field potential noted *in vivo* (Hartmann & Bower 1998; D'Angelo *et al*. 2001; Courtemanche & Lamarre 2002; Courtemanche & Lamarre 2005; Dugue *et al*. 2008; Courtemanche *et al*. 2009).

The strength of the oscillations in the GrC layer will depend on the average GrC firing rate, the regularity of the MF input and the degree of synchrony in the GoC population. I used a steady MF input rate of 50 Hz (a comparatively high rate of firing for rate-coded MF inputs in the vestibular cerebellum; Arenz *et al*. 2007), however, at higher MF firing rates patterning may be clearer. Were GrCs receiving slower or less reliable patterns of MF input than those used here the clarity of the GoC mediated signal may be compromised. However, it is likely that it would still be detectable over a sufficiently large GrC population.

Large groups of GrCs are unlikely to receive identical synchronised or desynchronised inhibition from exactly the same set of GoCs *in vivo*, however I used inhibitory conductances from only 4 simulated GoCs in these experiments (likely fewer than the number of inhibitory inputs a GrC receives; Rossi & Hamann 1998), and synchronisation of the GoC network implies that it may not matter whether the GrCs are receiving input from the same GoCs as it has been demonstrated that GrCs receive

IPSCs in phase with the spiking of neighbouring GoCs even when no direct synaptic connection can be demonstrated (Dugue *et al*. 2008)

PCs typically receive input from as many as 150,000 GrCs (Harvey & Napper 1991) with the most efficacious input arising from GrCs positioned directly beneath (Isope & Barbour 2002; Sims & Hartell 2005; Sims & Hartell 2006) thus PCs are likely to receive significant synaptic input from a large population of GrCs that share common inhibitory input. The extent to which a PC could detect such oscillations however may depend on the clustering (Heck *et al*. 2003) and synaptic weight (Sims & Hartell 2005) of such inputs as well as the ongoing activity of the cell (Phoka *et al*. 2010) and the timecourse for integration. The detectability of oscillations in the GrC layer may vary with the frequency of synchronised GoC firing (4–30 Hz; D'Angelo *et al*. 2001; Courtemanche & Lamarre 2005). Signalling at the parallel fibre–PC synapse is mediated by both a fast AMPAR/NMDAR and a much slower mGluR mediated component (Tempia *et al*. 1998). The former may reliably convey oscillations in the parallel fibre input while the latter component may convey a signal that is insensitive to the comparatively fast oscillations in the GrC layer allowing the unperturbed transmission of rate-coded signals.

There has been little direct study of how oscillations in the GrC layer affect overlying PCs, however, it has been shown that oscillations in the GrC layer local field potential, which are associated with bursts of GrC multiunit activity (Courtemanche *et al*. 2002; Hartmann and Bower 1998) are also associated with increased simple spike output in some PCs (though PC activity increases slightly ahead of the peak local field potential; Courtemanche *et al*. 2002). Synchrony within a population of GrCs may affect multiple PCs as each GrC contacts between 45 (Palay & Chan-Palay 1974) and 300 PCs (Eccles *et al*. 1967). Indeed the simple spike patterns of PCs have been shown to synchronise over distances of 100 μm but not further (Jaeger 2003; De Zeeuw *et al*. 1997).

Larger groups of GrCs gave stronger oscillatory signals (**Fig. 4.7**). That the relationship between oscillation score and GrC number is well described by a double exponential function implies that the higher the number of GrCs, the smaller the impact of adding further GrCs will be on signal strength. The appearance of signals in groups of GrCs receiving desynchronised inhibition is artefactual in that it arises from the perfect desynchronisation of the inhibitory input. Such perfect desynchronisation would never

occur *in vivo*. However, it may imply that single inhibitory inputs mediated across a large enough population of GrCs could impact downstream PC firing.

4.5 Conclusions

I have shown that increases in the rate of GoC firing can dramatically alter the gain of the GrC I–O function meaning that GoCs are suitable devices to regulate the gain of information transfer through the GrC layer.

Oscillations in the GoC network do not directly affect GrC gain or offset (when measured over at least one cycle) but can pattern the responses of populations of GrCs in a manner which may contribute to oscillations in the local field potential and convey a temporally variant signal to postsynaptic PCs (Courtemanche *et al*. 2002).

Chapter Five

5. The effect of phasic inhibition on burst coding in granule cells

5.1 Introduction

In **Chapter 4** I showed how synchrony in the GoC network could affect GrC processing of rate-coded MF inputs, but MF inputs don't invariably carry rate coded information. Many sensory signals are transmitted by bursts of MF activity, for example a large proportion of MF signals conveying tactile stimulation to the skin (Garwicz *et al*. 1998; Jörntell & Ekerot 2006) or the whiskers (Chadderton *et al*. 2004; Rancz *et al*. 2007) are encoded in this way. Such MFs are capable of firing at extremely high rates (up to ~ 700 Hz; Rancz *et al*. 2007) but are rapidly-adapting (Garwicz *et al*. 1998), and undergo STD (Saviane & Silver 2006) such that they reliably signal the onset of sensory stimuli.

If bursts of MF activity are conveying a timing signal then the temporal structure as well as the magnitude of the signal is likely to be important, yet it is not known how phasic inhibition or indeed synchronised oscillations in the GoC network are likely to affect GrC processing of MF burst inputs.

I have used dynamic clamp and computer simulations with an "integrate and fire" (IF) model GrC (Rothman *et al*. 2009) to investigate the interaction between inhibitory input and simulated bursts of MF activity in GrCs.

5.2 Number of MF inputs required to drive a GrC

The number of MF inputs required to make a GrC spike is a source of contention (Rancz *et al*. 2007; D'Angelo *et al*. 1995; Jorntell & Ekerot 2006; Chadderton *et al*. 2004; Gabbiani *et al*. 1994). To test how many burst type MF inputs would realistically be required to trigger at least one GrC action potential under my experimental conditions MF bursts similar to those reported in Rancz *et al*. 2007 were simulated. Poisson-distributed input times were generated using a step function (such that the probability of an input occurring at the start of the train was close to one and decayed

exponentially with a τ of 2.7 ms) to bias the highest firing rates towards the beginning of the train. Bursts were only accepted if they contained 6–7 events within a 70 ms window, had an instantaneous spike frequency between 300 and 800 Hz and a mean spike frequency between 100 and 190 Hz. The amplitude of individual simulated MF inputs was slightly larger in the simulated trains than in the MF bursts reported in Rancz *et al*. 2007.

Between one and four MF bursts were summed and injected in the presence of 420 pS tonic inhibition into an established IF GrC model (**Fig. 5.1**; Rothman *et al*. 2009). The model had a whole cell C_m set to 3.1 pF, V_m set to -75 mV and E_{GABA} set to -75 mV. The GrC model spiked twice with three MF inputs, four times with four MF inputs and failed to spike with fewer than three MF inputs (**Fig. 5.1**).

These results imply that multiple, near-simultaneous MF burst inputs are likely to be required to drive a GrC to spike therefore multiple near-simultaneous simulated MF bursts should be used in dynamic clamp experiments to ensure spiking.

5.3 The effect of GoC synchrony on GrC processing of MF burst inputs in slice

As discussed in the previous chapter neighbouring GoCs tend to fire in loose synchrony (Dugue *et al*. 2008; Verveake *et al*. 2009), however, the extent to which the synchrony of inhibition, and the relative phase thereof, can regulate the passage of MF burst signals through the GrC layer has not been studied.

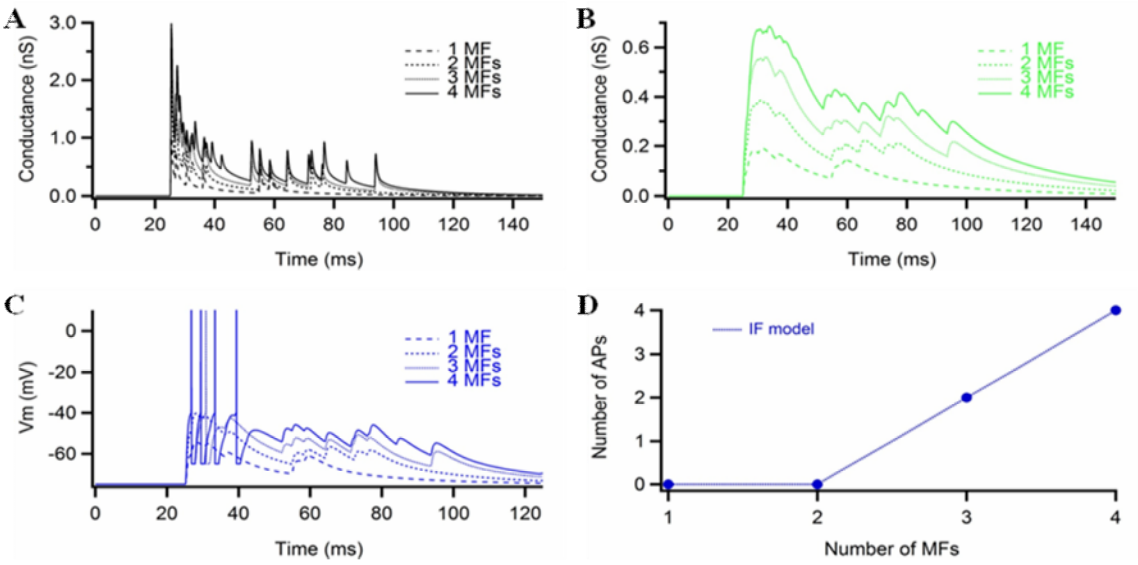

Fig. 5.1: Number of MF inputs required to elicit spiking in a model GrC. **A**. AMPA (black) and **B**. NMDA (green) conductances used to simulate bursting activity in 1–4 MFs. MF inputs were presented with 420 pS tonic inhibition (not shown). **C**. The IF model's spiking response to different numbers of MF input (Blue). **D**. Summary of data in **C**. AP = Action potential.

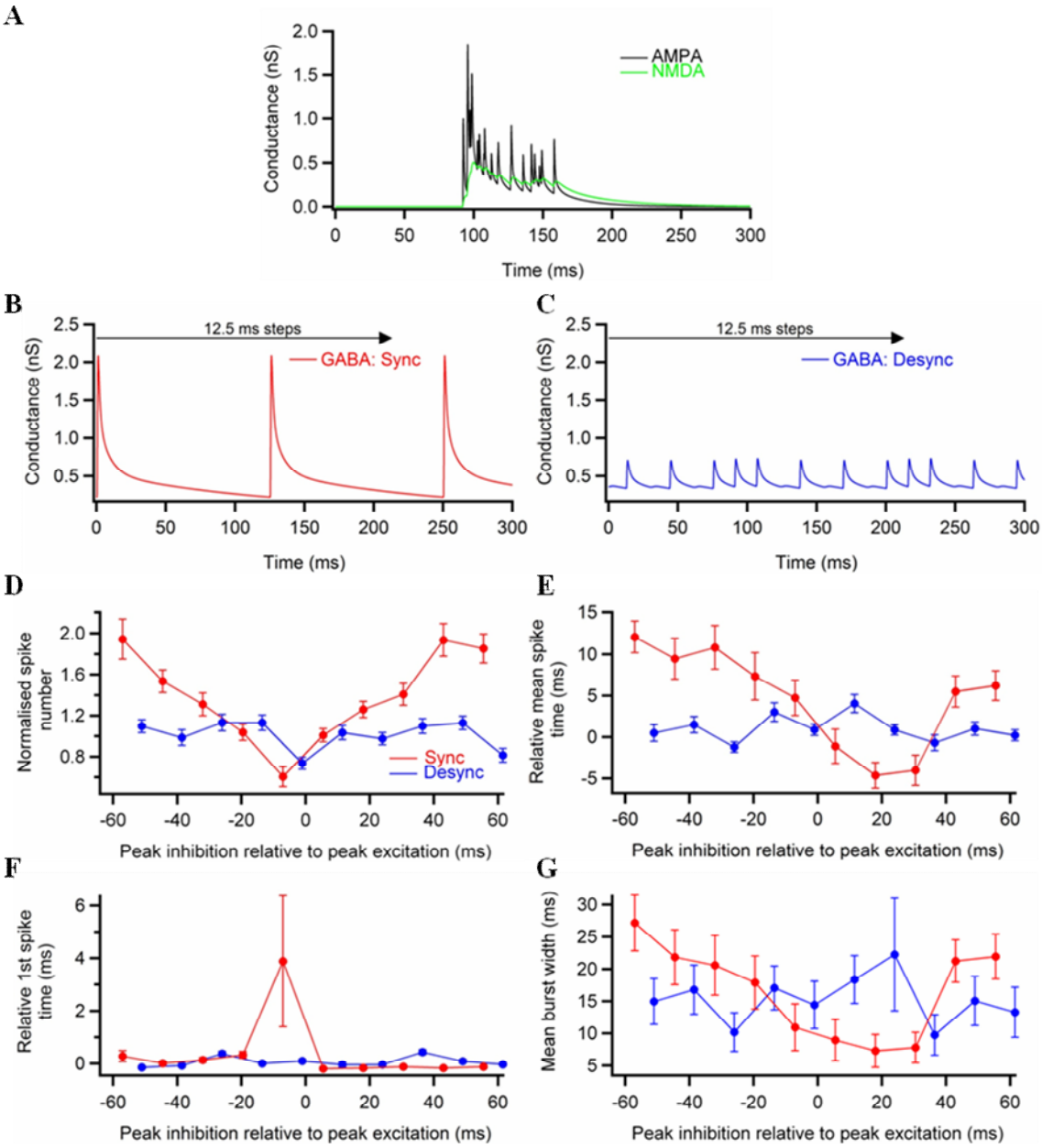
A
Conductance (nS)
AMPA
NMDA
Time (ms)
B
12.5 ms steps
GABA: Sync
Conductance (nS)
Time (ms)
C
12.5 ms steps
GABA: Desync
Conductance (nS)
Time (ms)
D
Normalised spike number
Sync
Desync
Peak inhibition relative to peak excitation (ms)
E
Relative mean spike time (ms)
Peak inhibition relative to peak excitation (ms)
F
Relative 1st spike time (ms)
Peak inhibition relative to peak excitation (ms)
G
Mean burst width (ms)
Peak inhibition relative to peak excitation (ms)

Fig. 5.2: The effect of inhibitory synchrony on GrC processing of MF burst inputs. **A**. Simulated burst input from 4 MFs was injected with inhibitory input arising from 8 GoCs (5 direct, 3 spillover) firing at 8 Hz (scaled to 0.8) either perfectly synchronised (**B**; red) or desynchronised (**C**; blue). Inhibitory waveforms were shifted by 12.5 ms steps relative to excitation over the course of 125 ms (1 inhibitory cycle). **D**. Mean number of spikes elicited with peak phasic inhibition arriving at different times relative to peak excitation (x-axis) normalised to the number of spikes elicited with tonic inhibition alone. Error bars represent SEM (N = 17). **E**. Mean spike timing (mean time of all spike in the GrC burst response) with peak phasic inhibition arriving at different times relative to peak excitation. Mean spike times are presented relative to the mean spike time with tonic inhibition alone. Only cells which spiked at all time points were included in this analysis (N = 12). **F**. First spike timing with peak phasic inhibition arriving at different times relative to peak excitation. First spike times are given relative to the first spike time with tonic inhibition alone. Again, only cells which spiked at all time points were included in this analysis (N = 12). **G**. GrC output burst width (time of final spike - time of first spike) with peak phasic inhibition arriving at different times relative to peak excitation (N = 17). Error bars represent one SEM.

To ensure reliable excitatory drive I simulated burst input arising from 4 MFs (**Fig. 5.2A**) and injected them into GrCs via dynamic clamp with either tonic inhibition alone (420 pS), perfectly synchronised phasic inhibition, or totally desynchronised phasic inhibition. Phasic inhibition constituted inhibitory conductance waveforms arising from 8 simulated GoCs; 5 making direct inputs, 3 spillover only, each firing at 8 Hz (and therefore scaled by 0.8) in conjunction with 20 pS tonic inhibition such that mean inhibition across a cycle was 420 pS. The phasic inhibitory waveforms were shifted in 12.5 ms steps across 125 ms (one inhibitory cycle; **Fig. 5.2B, C**) relative to peak excitation and GrC spiking responses were recorded. GrC responses were noisy, so experiments were repeated multiple times in each cell to accrue cell-based average responses, data presented is the average across cells (**Fig. 5.2**).

The number of spikes fired by each GrC injected with MF burst input and synchronised/desynchronised inhibitory inputs was normalised to the number of spikes recorded in the same GrCs with MF burst input and tonic inhibition (a steady state inhibitory conductance of equal magnitude; 420 pS; **Fig. 5.2D**). Spike output varied with the timing of peak inhibition relative to peak excitation with both synchronised (Kruskal-Wallis test $P < 0.001$) and desynchronised (Kruskal-Wallis test $P < 0.05$) inhibition. Normalised spiking output decreased as a function of the temporal distance between peak synchronised inhibition and peak excitation. The relationship was well approximated by two straight lines (from peak inhibition arriving at -57 ms to peak inhibition arriving at -7 ms and from peak inhibition arriving at -7 ms to 55.5 ms; r^2 = 0.99 and 0.93 respectively; F-test $P < 0.001$ and 0.005 respectively). Normalised spiking output obtained in the presence of desynchronised inhibition did not show the same clear trend (from peak inhibition arriving at -51 ms to peak inhibition arriving at -1 ms and from peak inhibition arriving at -1 ms to 61.5 ms; r^2 = 0.30 and 0.07 respectively; F-test $P = 0.34$ and 0.60 respectively). Synchronised inhibition reduced the GrC's mean spiking response by 26 % relative to tonic inhibition when arriving in phase with excitation and increased GrC spiking by up to 130 % when arriving out of phase with excitation. The desynchronised inhibitory waveform also altered the GrC's spiking response to burst input reducing spiking by a maximum of 15 % relative to tonic inhibition when arriving in phase with excitation and increasing spiking by a maximum of 32 % when out of phase with excitation. Thus the peak-to-trough spike output ratio with synchronised inhibition was 3.1:1 vs 1.6:1 with desynchronised inhibition. The coarse nature of the experiment (i.e. shifting inhibition in 12.5 ms steps) would likely

serve to underestimate the maximal spike reduction and peak to trough ratio resulting from synchronised and desynchronised inhibition.

As useful information might be contained in the exact timing of GrC spikes I looked at the mean spike times, first spike times and burst widths of GrC spiking responses to burst MF input with synchronised and desynchronised inhibition arriving at different times relative to peak excitation. Mean spike times and first spike times are presented relative to mean spike times and first spike times obtained with tonic inhibition.

The mean spike time (mean time of all spikes in the GrC response) was advanced by peak synchronised inhibition arriving during, or shortly after, peak excitation, but delayed when peak inhibition arrived out of phase with excitation (relative to mean spike time with tonic inhibition; **Fig. 5.2E**). The advance in mean spike time was maximal with peak inhibition arriving shortly (18 ms) after peak excitation. The relationship between mean GrC spike time and the timing of peak synchronised inhibition relative to peak excitation could be reasonably approximated with a straight line (from peak inhibition arriving at -57 ms to peak inhibition arriving at 18 ms; r^2 = 0.85; F-test $P < 0.001$). The relationship between mean GrC spike time and the timing of peak desynchronised inhibition relative peak excitation showed no such trend (from peak inhibition arriving at -51 ms to peak inhibition arriving at 24 ms; $r^2 = 0.33$; F-test $P = 0.23$).

The first spike in any given GrC response profile was typically more robust than other spikes (**Fig. 5.2F**). However, in some cells it was delayed by peak synchronised inhibition arriving very close to peak excitation (Friedman test $P < 0.0001$). The maximum mean delay in first spike time was a mere 3.9 ms by comparison to a maximum change in mean spike time of over 15 ms, this implies that synchronised inhibition arriving in phase with, or shortly after, peak excitation reduced mean spike time primarily by eliminating spikes occurring late in the GrC response. Conversely, increases in mean spike time arose due to a reduction in inhibition in phase with excitation resulting in an increase in probability of spikes occurring towards the end of the GrC response train. This pattern was reflected in the mean burst width (time of the last spike in the GrC response – time of the first spike; **Fig. 5.2G**) which varied by a factor of 3.7 across the inhibitory cycle. The relationship between mean GrC burst width and the timing of peak synchronised inhibition relative peak excitation could be

approximated with a straight line (from peak inhibition arriving at -57 ms to peak inhibition arriving at 18 ms; $r^2 = 0.97$; F-test $P < 0.0001$). Again, the relationship between mean GrC burst width and the timing of peak desynchronised inhibition relative peak excitation showed no clear trend (from peak inhibition arriving at -51 ms to peak inhibition arriving at 24 ms; $r^2 = 0.37$; F-test $P = 0.14$).

It seems that synchronised inhibition could selectively truncate and weaken or exaggerate the impact of MF bursts according to phase while desynchronised inhibition had an approximately consistent suppressive effect on MF signals.

5.4 The effect of single IPSPs on GrC processing of MF burst inputs

The above results show that synchronised inhibitory input can alter the way in which GrCs integrate bursts of MF activity. However, it is not known to what extent individual GoC–GrC inputs might affect GrC processing of MF burst inputs. To test if precisely-timed, single GoC–GrC inputs can reliably affect the GrC response to bursts of MF input, I injected the same MF burst inputs as described above, this time with either tonic inhibition (420 pS) or phasic input from 4 GoCs (two making direct connections two making spillover only connections) each firing at 8 Hz (and scaled by 0.8), desynchronised relative to each other (spike times were extracted from a model of the GoC network responding to sparse desynchronising input; Verveake *et al*. 2010), with 200 pS tonic inhibition (such that total inhibition was equal to 420 pS across one cycle). The inhibitory waveform was shifted in finer, 5 ms steps, relative to peak excitation (**Fig. 5.3**).

Individual direct inhibitory inputs were capable of eliminating spikes arising late in the train in some cases (**Fig. 5.3C**; Friedman test $P < 0.0001$) but this was not reflected in mean spike timing (**Fig. 5.3D**; Friedman test $P = 0.24$), burst width (**Fig. 5.3F**; Friedman test $P = 0.36$) or 1st spike timing, which varied by less than 1 ms (**Fig. 5.3E**) suggesting that individual direct IPSCs were occasionally able to knock out one or more spikes in the GrC burst response but typically did not affect overall spike timing.

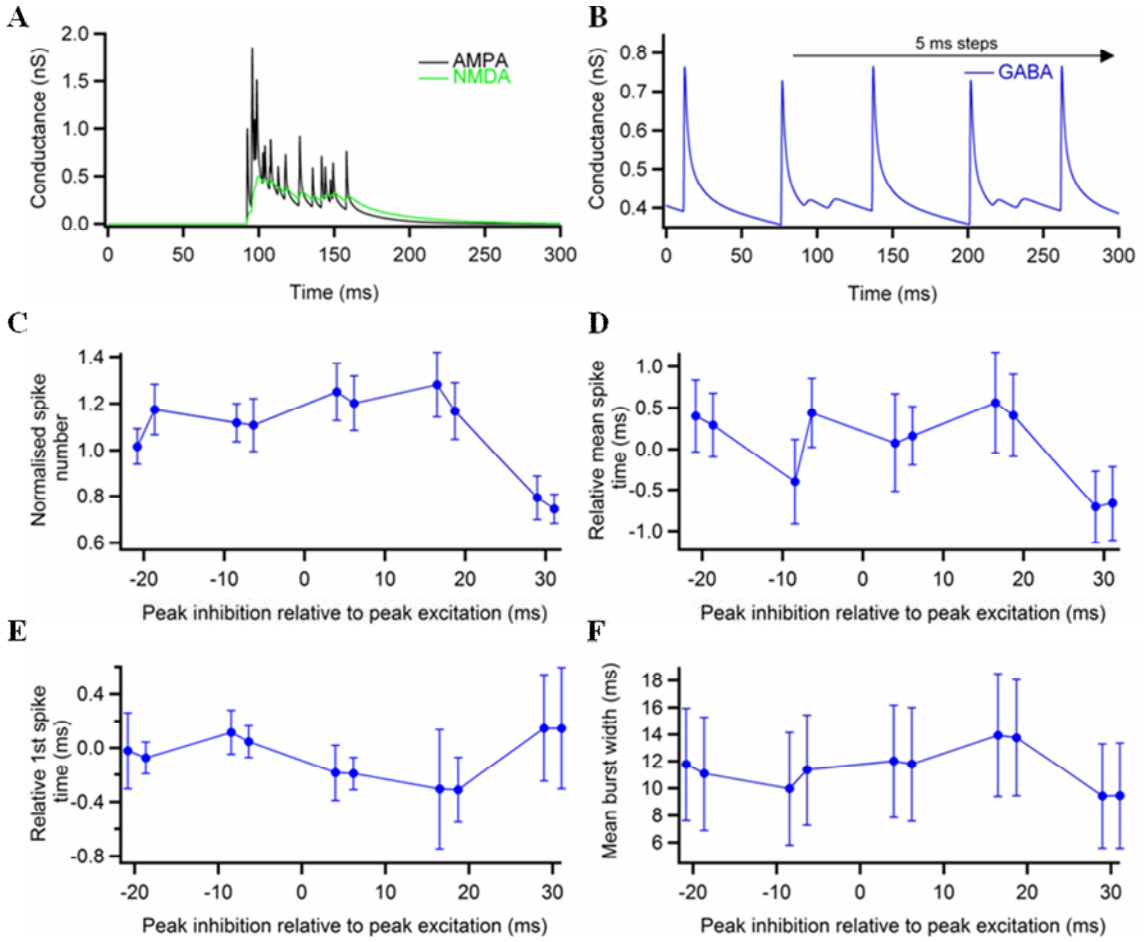

Fig. 5.3: The effect of single GoC–GrC inputs on GrC processing of MF burst inputs. **A**. Excitatory conductances emulating burst inputs from 4 MFs were injected with **B**. inhibitory input arising from 4 temporally desynchronised GoCs (two direct, two spillover; each firing at 8 Hz and scaled to 0.8). Inhibitory waveforms were shifted in 5 ms steps relative to excitation. **C**. Mean number of spikes elicited with direct phasic GoC inputs arriving at different times relative to excitation (the x-axis represents the temporal distance of the peak of the nearest direct inhibitory input to peak excitation). Spiking output was normalised to the number of spikes elicited with tonic inhibition alone (N = 23). **D**. Mean spike timing with phasic inhibition arriving at different times relative to peak excitation. Data are presented relative to the mean spike time with tonic inhibition alone. Only cells which spiked at all time points were included in this analysis (N = 21). **E**. First spike timing with phasic inhibition arriving at different times relative to excitation. Data are presented relative to the mean spike time with tonic inhibition alone (N = 21). **F**. Burst width with phasic inhibition arriving at different times relative to peak excitation (N = 23). Error bars represent SEM.

These results suggest that individual GoC–GrC inputs are unlikely to have a marked effect on a GrC's early response to MF burst input but may in some cases knock out spikes occurring later in the response. However, they are unlikely to have systematic effect on the timing of the GrCs spiking response.

5.5 The effect of a burst of GoC input on GrC processing of MF burst inputs

GoCs do not invariably fire steadily *in vivo* and can respond to sensory input with bursts, pauses or modulations of their spiking output (e.g. Van Kan *et al*. 1993; Vos *et al*. 1999b; Tahon *et al*. 2005; Holtzman *et al*. 2006; Heine *et al*. 2010). It is not clear to what extent burst of activity in GoCs would be synchronised by common MF or parallel fibre input, nor is it precisely known when their output would arrive at GrCs relative to MF input. Therefore I have investigated the effect of a burst of GoC inputs on GrC processing of a burst of MF inputs (from 3 MFs in this case). I injected 8 GoC–GrC synaptic waveforms (5 direct, 3 spillover only, scaled by 0.8), either tightly synchronised or loosely-synchronised on top of a resting tonic inhibition of 420 pS (**Fig. 5.4**) and shifted the inhibitory waveform in 5 ms steps relative to peak excitation.

Both loosely-, and tightly-synchronised inhibitory input were most effective at knocking out GrC spikes when arriving with, or shortly after, peak excitation (**Fig. 5.4D**; N = 8; Freidman test $P < 0.0001$ in both cases). Closely-synchronised GoC inputs caused a greater peak reduction in GrC output, however desynchronised inhibition caused a slightly larger mean reduction in spiking across the time points measured (30 ± 11 % vs 24 ± 24 %). Both synchronised and desynchronised inhibition advanced mean spike time by preferentially knocking out spikes occurring later in the train however neither had a detectable affect on the timing of the first spike or burst width (**Fig. 5.4F** & **G**). It is, however, difficult to ascertain much information on spike timing due to the small sample size.

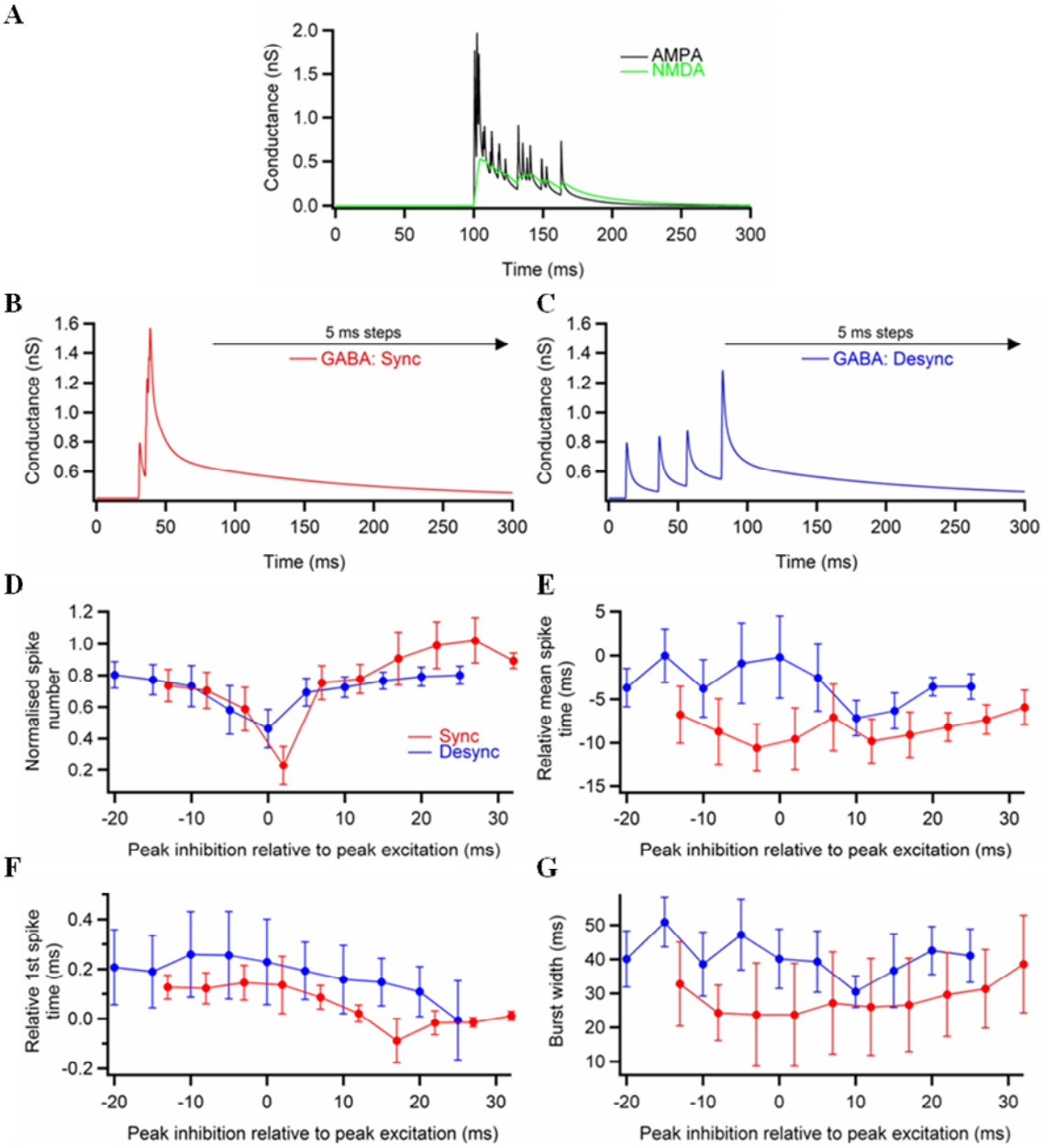
A
Conductance (nS)
AMPA
NMDA
Time (ms)
B
5 ms steps
GABA: Sync
Conductance (nS)
Time (ms)
C
5 ms steps
GABA: Desync
Conductance (nS)
Time (ms)
D
Normalised spike number
Sync
Desync
Peak inhibition relative to peak excitation (ms)
E
Relative mean spike time (ms)
Peak inhibition relative to peak excitation (ms)
F
Relative 1st spike time (ms)
Peak inhibition relative to peak excitation (ms)
G
Burst width (ms)
Peak inhibition relative to peak excitation (ms)

Fig. 5.4 The effect of a burst of GoC inputs on GrC processing of a burst of MF inputs. **A**. Excitatory conductances used to investigate the effect of a burst of GoC activity on GrC processing of burst MF inputs. Simulated burst inputs from 3 MFs were injected with 8 inhibitory inputs (5 direct, 3 spillover only) either tightly (**B**; red) or loosely (**C**; blue) synchronised on top of tonic inhibition (420 pS). Inhibitory waveforms were shifted in 5 ms steps relative to excitation. **D**. Mean number of spikes elicited with peak phasic inhibition arriving at different times relative to peak excitation normalised to the number of spikes elicited with tonic inhibition alone (N = 8). **E**. Mean spike timing with peak phasic inhibition arriving at different times relative to peak excitation. Data presented relative to mean spike timing with tonic inhibition alone. Only cells which spiked at all time points were included in this analysis (N = 4). **F**. First spike timing with peak phasic inhibition arriving at different times relative to peak excitation. Data presented relative to first spike time with tonic inhibition alone (N = 4). **G**. Burst width with peak phasic inhibition arriving at different times relative to peak excitation (N = 8). Error bars represent SEM.

5.6 The effect of GoC synchrony on GrC processing of MF burst inputs *in silico*

Dynamic clamp probably represents the best means of studying synaptic integration in simple cells like the GrC. However, a drawback of this method and of slice patch-clamp physiology in general is that experiments are necessarily limited in duration so there is a finite limit on the amount of parameter space that can be conceivably investigated within an experiment. (Ideally much smaller shifts in the timing of the inhibitory waveforms would have been used in the above experiments). Further, biological noise and variability often necessitates the use of large sample numbers and statistical methods or unphysiological stimuli in order to obtain observable effects. In this regard computational models can prove useful. I used the IF GrC model to perform a more detailed analysis of the effect of the synchrony and phase of inhibition on GrC processing of MF burst inputs.

5.6.1 The effect of GoC synchrony on GrC processing of MF burst inputs *in silico* – default experimental settings

Simulated input from 4 MFs was used to provide excitatory drive. The excitatory input was injected into the GrC model with inhibitory input from 4 GoCs (three making direct contacts, one spillover only, all scaled by 0.8 to represent STD from ongoing GoC activity at 8 Hz). GoC inputs were either perfectly synchronised or totally desynchronised and were injected with sufficient tonic inhibition to make total inhibition over the course of one cycle equal to 420 pS. The phase of the inhibitory inputs was shifted in 1 ms steps relative to the excitatory input to investigate the effect of phase of inhibition on GrC processing of MF burst inputs (**Fig. 5.5A**). The model had a cell capacitance set to 3.1 pF, V_m set to -75 mV and E_{GABA} set to -75 mV.

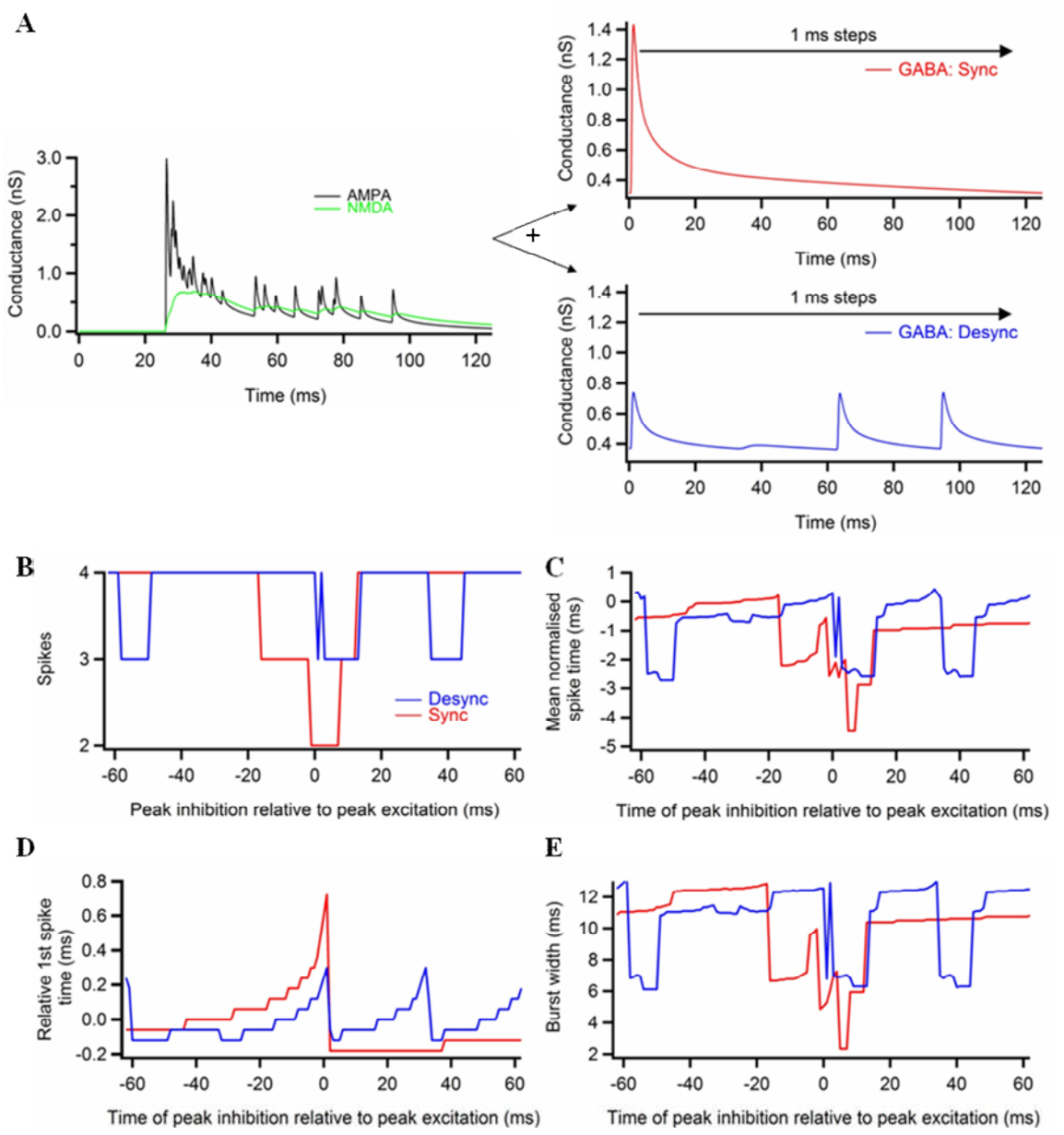
A
Conductance (nS)
AMPA
NMDA
Time (ms)
1 ms steps
GABA: Sync
GABA: Desync
B
Spikes
Desync
Sync
Peak inhibition relative to peak excitation (ms)
C
Mean normalised spike time (ms)
Time of peak inhibition relative to peak excitation (ms)
D
Relative 1st spike time (ms)
Time of peak inhibition relative to peak excitation (ms)
E
Burst width (ms)
Time of peak inhibition relative to peak excitation (ms)

Fig. 5.5: The effect of inhibitory synchrony on processing of MF burst inputs in a model GrC. **A**. Conductances used to investigate the effect of GoC network synchrony on GrC processing of burst inputs. Excitatory input; burst input from 4 simulated MFs (left), was injected with inhibitory input arising from 4 GoCs either perfectly synchronised (red) or desynchronised (blue). Inhibitory waveforms were shifted in 1 ms steps relative to peak excitation over the course of 1 cycle (125 ms). Mean inhibitory conductance across 1 cycle was 420 pS. **B**. Number of spikes generated when peak synchronised (red) or desynchronised (blue) inhibition arrives at different times relative to peak excitation. **C**. Mean spike timing with peak inhibition arriving at different times relative to peak excitation. Mean spike timing data is presented relative to the mean spike time with tonic inhibition alone. **D**. First spike timing with peak phasic inhibition arriving at different times relative to peak excitation. First spike times are presented relative to the first spike time with tonic inhibition alone. **E**. Burst width with peak phasic inhibition arriving at different times relative to peak excitation.

The synchrony and phase of inhibition altered the model's spiking response to burst MF input. Synchronised inhibition was effective at reducing the number of spikes in the GrC response when arriving during or a few ms after peak excitation but could still knock out spikes when arriving shortly before peak excitation. Single direct desynchronised inhibitory inputs were most effective at eliminating spikes when arriving shortly after peak excitation (coincident with the later spikes in the train that were triggered by weaker excitatory conductance). The spillover input was not effective at reducing spike output alone but slightly boosted the effectiveness of the following direct IPSC (**Fig. 5.5B**).

The mean output spike number over the 125 ms cycle was similar for synchronised and desynchronised inhibition (paired T-test; P = 0.3). However, as in the dynamic clamp experiments (**Fig. 5.2D**), the maximal change in spike output across a cycle was greater when inhibition was synchronised, the peak-to-trough output ratio for synchronised inhibition was 2:1 vs 4:3 for desynchronised inhibition. Synchronised inhibition also caused a greater maximal reduction in spike output than desynchronised inhibition (**Fig. 5.5B**).

The timing of the first spike (relative to the first spike obtained with tonic inhibition), which would signal the onset of the stimulus, was robust and shifted by less than 1 ms in the face of synchronised inhibition and by less than 0.4 ms in response to desynchronised inhibition (**Fig. 5.5D**). The timing of the mean spike envelope was more susceptible to change than the first spike. Changes in mean spike timing were largely dictated by the elimination of spikes. Indeed the maximum shift in mean spike time without eliminating a spike was 1.2 ms. The change in mean spike timing was closely reflected by the pattern of change in burst width (**Fig. 5.5E**) suggesting that inhibition primarily affected the late spikes in the GrC output train serving to truncate the GrC spiking response.

In accordance with dynamic clamp data the results above show that synchronised inhibition can alter the width and magnitude of a GrC response to MF burst input relative to phase, however they also imply that single GoC inputs could be effective at knocking out GrC spikes and regulating spike timing.

These results are predicated on very specific parameters, the model has fixed V_m, E_{GABA} and capacitance values. In reality the V_m, E_{GABA} and capacitance vary between GrCs and V_m and E_{GABA} vary with animal age. For this reason I have repeated the above experiments for a range of V_m, E_{GABA} and capacitance values to see to what extent these parameters might alter the effectiveness of temporally specific GoC mediated inhibitory input on GrC processing of MF burst inputs.

5.6.2 The effect of GoC synchrony on GrC processing of MF burst inputs – V_m dependence

The V_m of GrCs shows some intrinsic variability. Under the recording conditions utilised in this study GrCs exhibited a mean V_m close to -75 mV (and varied between -68 and -85 mV), however, mean resting membrane potential has been reported *in vitro* to be as low as -80 mV (Rothman *et al*. 2009) and may be higher *in vivo* (Chadderton *et al*. 2004). GrC V_m depends on age (Cathala *et al*. 2003) and recording conditions, and is sensitive to ongoing synaptic input. In order to test the effect of V_m on the inhibitory regulation of GrC responses to MF burst inputs I repeated the experiment outlined above with resting membrane potential values ranging from -65 to -85 mV (**Fig. 5.6**).

In the IF GrC model, depolarising the resting membrane potential tended to increase spiking in response to simulated MF input (**Fig. 5.6**). As before, synchronised inhibition arriving close to the time of peak excitation reduced spiking, desynchronised direct inhibitory inputs arriving shortly after peak excitation also reduced spiking (though to a lesser extent) except at a V_m of -70 where desynchronised inhibition had no effect on the IF model's spiking output. The window over which inhibition was effective at knocking out spikes varied with V_m (**Fig. 5.6**).

The synchronisation of inhibition had no significant effect on the mean spike output (average across all phases) across V_m values (F-Test $P > 0.5$; **Fig. 5.7A**). Synchronised inhibition consistently produced a greater maximum to minimum spiking ratio across the inhibitory cycle than desynchronised inhibition, however, the ratio varied with voltage by more than two-fold (**Fig. 5.7B**).

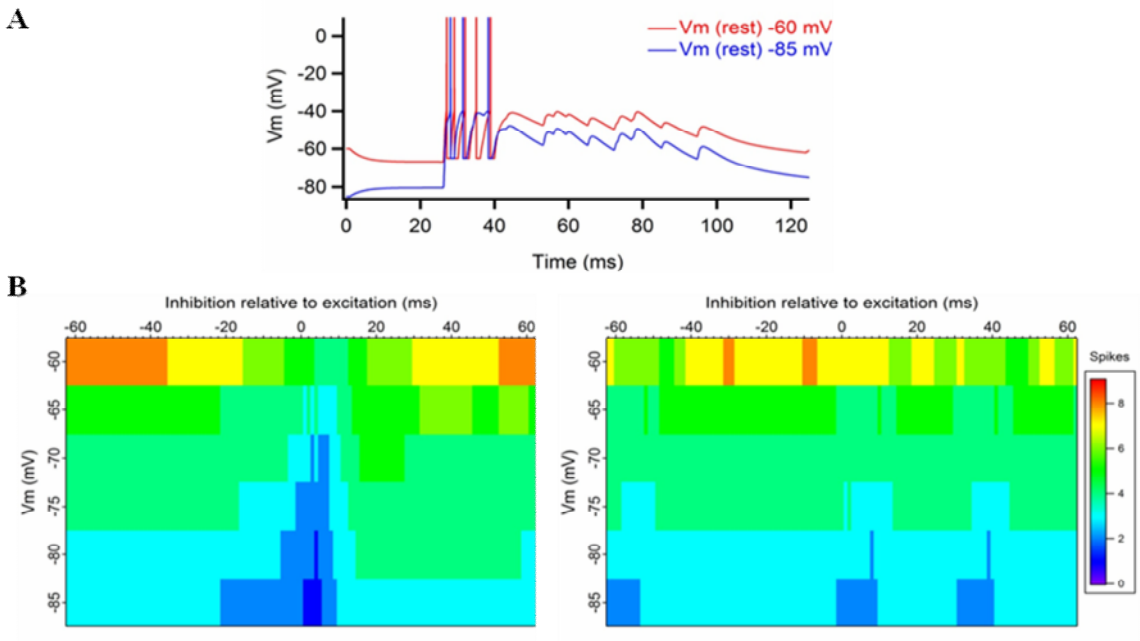

Fig. 5.6: The effect of V_m on GrC integration of simulated GoC inhibition and MF burst inputs. **A**. Example outputs from the IF model with resting V_m set to -60 (red) and -85 mV (blue). **B**. 2-D plots showing spike output (indicated by colour) in response to the same MF burst inputs in the presence of synchronised (left) and desynchronised (right) inhibitory input (as shown in **Fig. 5.5A**) with peak inhibition shifted in 1 ms steps relative to peak excitation (x-axis) at a range of resting membrane potentials (y-axis).

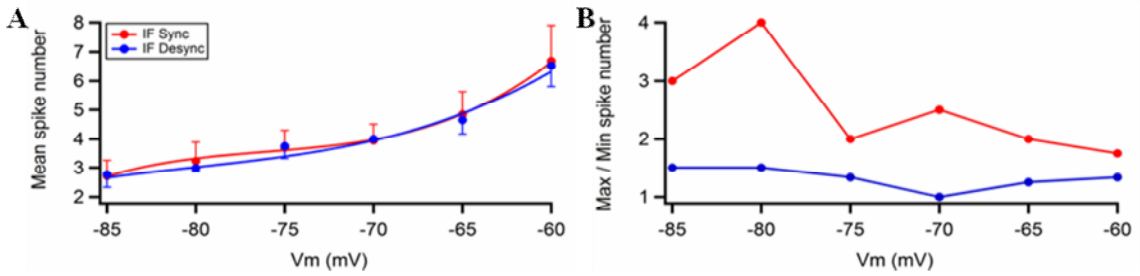

Fig. 5.7: Summary of data presented in **Fig. 5.6**. **A**. Mean spike number (average across cycle) for a range of resting membrane potentials with synchronised inhibition (red) and desynchronised inhibition (blue) in the IF GrC model. Fits represent a polynomial function error bars represent SEM. **B**. Ratio between the largest spiking response and smallest spiking response across the inhibitory cycle in the IF GrC models with synchronised (red) and desynchronised inhibition (blue).

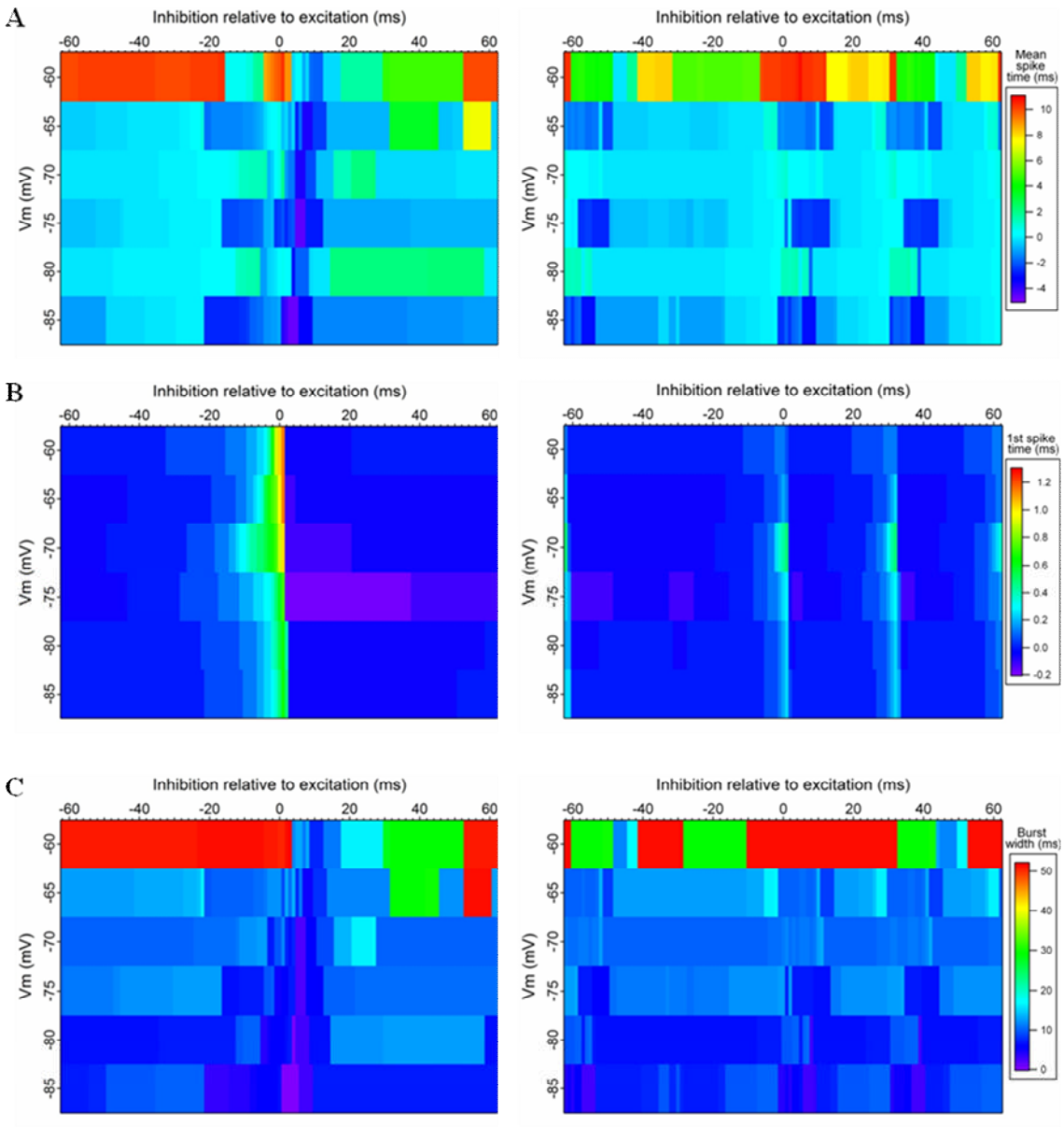

Fig. 5.8: Voltage dependence of the effect of inhibition on the timing of an IF GrC model's response to burst MF input. 2-D plots showing the effect of V_m (y-axis), phase of inhibition (x-axis) and synchrony of inhibition (left – synchronised vs right – desynchronised) on **A**. the mean spike timing (relative to mean spike timing with tonic inhibition; indicated by colour) **B**. the timing of the first spike (relative to first spike timing with tonic inhibition; indicated by colour) and **C**. the width (indicated by colour) of the GrC burst response to burst input from 4 MFs.

To investigate the more subtle effects that inhibitory synchrony might have on output spike timing at different V_m values, I analysed the mean spike times, first spike times and burst widths obtained in the above simulations (**Fig. 5.8**).

In the IF GrC model, changes in V_m did not affect the susceptibility of the first GrC action potential to phasic inhibition which shifted by little more than 1 ms (relative to 1st spike time with tonic inhibition; **Fig. 5.8B**). For all V_m values the mean spike time of the burst tended to advance when synchronised inhibition arrived shortly before, during or shortly after peak excitation, mean spike time was delayed when inhibition arrived out of phase with excitation. Desynchronised inhibition was most effective at advancing mean spike time when arriving shortly after peak excitation (**Fig 5.8A**). Synchronised inhibition arriving shortly before, during or after peak excitation was able to shorten the GrC output burst width, desynchronised inhibition arriving shortly after peak excitation could also shorten burst width but the effect was very mild (**Fig. 5.8C**). In general increasing V_m tended to increase burst width. The greatest reductions in burst width produced by inhibition occurred at depolarised V_m values.

These results suggest that the qualitative effects of synchronised and desynchronised inhibition on GrC processing of MF burst inputs do not vary significantly with V_m. Synchronised inhibition arriving close to peak excitation reduced the GrC response and shortened burst width relative to synchronised inhibition arriving out of phase with peak excitation (**Fig. 5.6**, **5.8C**). The average spike output did not vary significantly between synchronised and desynchronised inhibition, however, the ratio between peak GrC spiking output and minimal GrC spiking output was much larger with synchronised inhibition than desynchronised inhibition. The peak to trough spiking ratio recorded with synchronised inhibition was somewhat voltage dependent and tended to be larger at more hyperpolerised values of V_m.

5.6.3 The effect of GoC synchrony on GrC processing of MF burst inputs – E_{GABA} dependence

The effect of any synaptic input is determined to a large extent by the reversal potential for that input. Under my recording conditions GoC–GrC IPSCs reversed at -75 mV in close agreement with Jörntell & Ekerot 2006. Rothman *et al*. 2009 estimated an E_{GABA} value of -75 mV for rats from P25–P35, a value I have adopted for the experiments

presented in this thesis. However, the true reversal potential for GABAergic inputs in the cerebellar GrCs of young adult rats has thus far not been published (though preliminary perforated patch experiments suggest the figure is approximately accurate). E_{GABA} varies with age; Brickley *et al*. 1996 found a value for E_{GABA} of -62.9 ± 4.8 mV in P18-21 rats using the perforated patch technique. It is known that E_{GABA} becomes more negative with maturation in these cells and may be subject to change depending on ongoing activity (e.g. Pathak *et al*. 2007; Jedlicka *et al*. 2011). As a consequence I have investigated the effect of E_{GABA} on the inhibitory regulation of GrC firing responses to MF burst stimuli (**Fig. 5.9**).

Increasing E_{GABA} tended to increase spiking in response to MF input. Peak synchronised inhibition arriving close to the time of peak excitation or desynchronised inhibitory inputs (except at E_{GABA} values of -60 mV and -70 mV) arriving shortly after peak excitation reduced spiking. The window over which inhibition was effective varied with E_{GABA} (**Fig. 5.9**). Synchronised inhibition consistently produced a greater peak-to-trough spiking ratio than desynchronised inhibition. The peak to trough spiking ratio was largest at -80 mV (**Fig. 5.10B**), however the synchronisation of inhibition had no significant effect on mean spike output across E_{GABA} values (F-test $P < 0.8$; **Fig. 5.10A**).

The effect of E_{GABA} on GrC output timing was investigated as before (**Fig. 5.11**). Changes in E_{GABA} produced analogous effects on spike timing to changes in resting V_m. The first spike remained robust in the face of inhibition while mean spike time and burst width were advanced and reduced respectively by synchronised inhibition arriving around the time of peak excitation across the E_{GABA} values tested (**Fig. 5.11**). The impact of inhibition on spike timing varied with E_{GABA}.

These results suggest that the qualitative effects of synchronised and desynchronised inhibition on GrC processing of MF burst inputs are robust to changes in E_{GABA}. Synchronised inhibition arriving close to peak excitation reduced the GrC response and shortened burst width relative to synchronised inhibition arriving out of phase with peak excitation (**Fig. 5.9B**, **5.11C**). The average spike output did not vary significantly with synchronised vs desynchronised inhibition, however, the ratio between peak GrC output and minimal GrC output was larger with synchronised inhibition than desynchronised inhibition and varied with E_{GABA} (**Fig. 5.10B**).

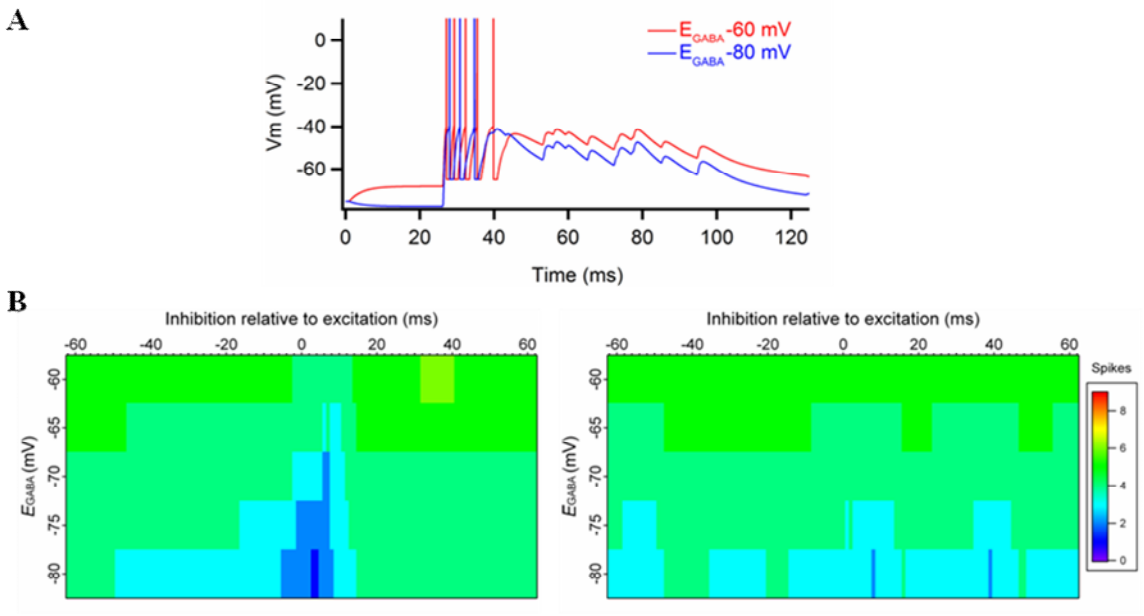

Fig. 5.9: Effect of E_{GABA} on GrC integration of simulated GoC inhibition and MF burst inputs. **A**. Example outputs from the IF GrC model with E_{GABA} set to -60 (red) and -80 mV (blue) in response to 4 MF burst inputs in the presence of 420 pS tonic inhibition. **B**. 2-D plots showing spike output (indicated by colour) in response to MF burst inputs in the presence of synchronised (left) and desynchronised (right) inhibition shifted in 1 ms steps relative to peak excitation (x-axis) at a range of E_{GABA} values (y-axis).

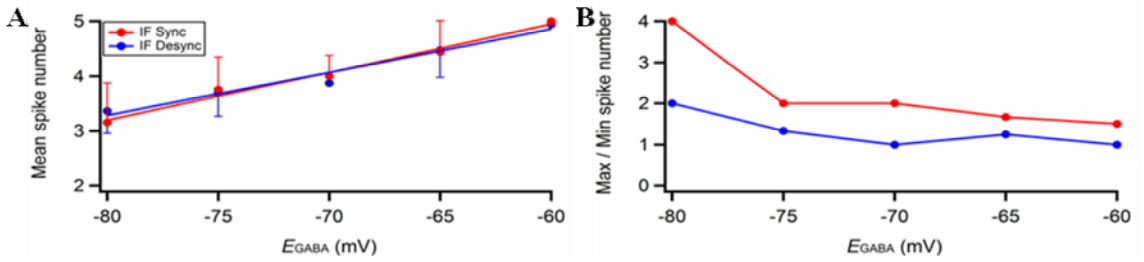

Fig. 5.10: Summary of data presented in **Fig. 5.9**. **A**. Mean spike number across 1 cycle for a range of E_{GABA} values with synchronised inhibition (red) and desynchronised inhibition (blue). Fits represent a linear function, error bars represent SEM. **B**. Ratio between largest spiking response and smallest spiking response across the inhibitory cycle with synchronised (red) and desynchronised inhibition (blue) for a range of E_{GABA} values.

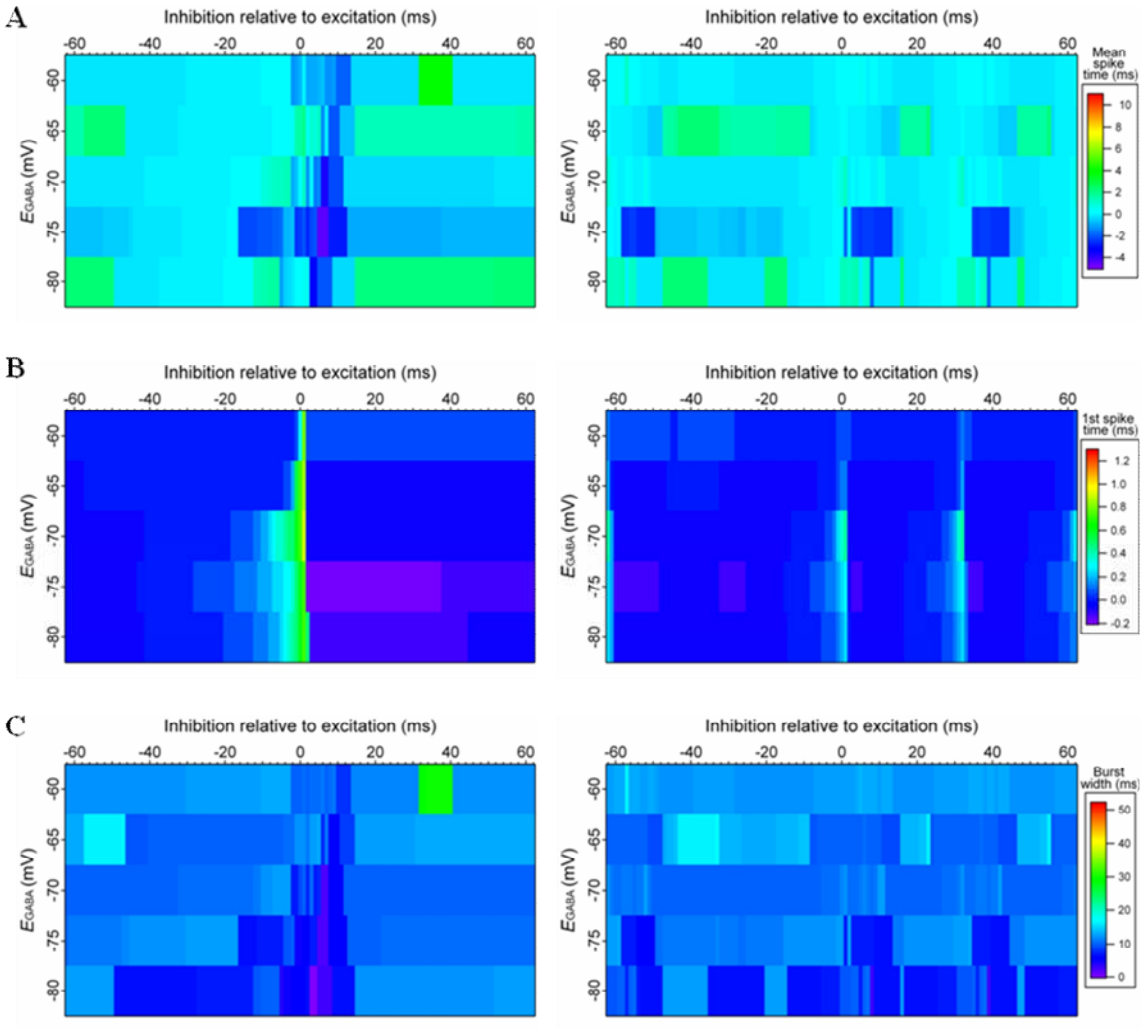

Fig. 5.11: E_{GABA} dependence of the effect of inhibition on the timing of an IF GrC model's response to burst MF input. 2-D plots showing the effect of E_{GABA} (y-axis), phase of inhibition (x-axis) and synchrony of inhibition (left – synchronised vs right – desynchronised) on **A**. the mean spike time (relative to mean spike time with tonic inhibition; indicated by colour) **B**. the timing of the first spike (relative to first spike timing with tonic inhibition; indicated by colour) and **C**. the width (indicated by colour) of the GrC burst response.

5.6.4 The effect of GoC synchrony on GrC processing of MF burst inputs – GrC C_m dependence

GrCs exhibit a variable whole cell C_m but have been reported to exhibit mean values of around 3.2 pF (e.g. Rothman *et al*. 2009) in this study GrCs (N = 340) had a slightly higher mean whole cell C_m of 3.8 ± 1.0 pF, values ranged between 2.1 and 5.9 pF. This represents a sizeable disparity in the synaptic input required to charge different GrCs. However, the amplitude of inhibitory inputs does not appear to be scaled according to cell C_m. Indeed IPSC amplitude (as measured in my paired recording experiments) does not correlate significantly with C_m (Pearson's rank; r = 0.27; P = 0.2; **Fig. 5.12**). To test how GrCs of different capacitances would handle burst MF input with either synchronised or desynchronised inhibition I repeated the modelling experiments outlined above with V_m and E_{GABA} set to -75 mV and whole cell C_m values ranging from 2 to 4 pF (**Fig. 5.13**).

Increasing cell C_m decreased the GrC spiking response to MF burst input. Peak synchronised inhibition arriving close to the time of peak excitation reduced spiking across C_m values. Desynchronised direct inhibitory inputs arriving shortly after peak excitation reduced spiking to a lesser extent, except at capacitance values of 2.5 and 4 pF where they had no effect on spike output. The window over which inhibition was effective varied with C_m (**Fig. 5.13**); however the synchronisation of inhibition had no significant effect on mean spike output across C_m values (**Fig. 5.14A**; F-test; P < 0.9). Synchronised inhibition consistently produced a greater peak-to-trough spiking ratio than desynchronised inhibition: This effect was greatest at C_m values above 3 (**Fig. 5.14B**).

To investigate the effect that inhibitory synchrony might have on output spike timing in cells with different C_m values I analysed the mean spike times, first spike times and average GrC burst lengths for the above simulations (**Fig. 5.15**).

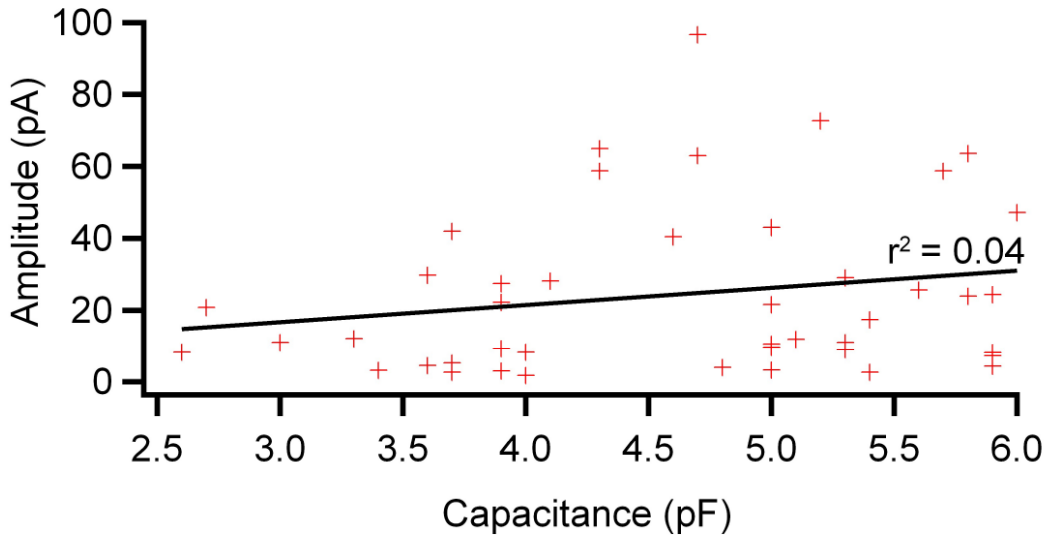

Fig. 5.12: Relationship between GrC C_m and GoC–GrC IPSC amplitude. Correlation between GrC C_m and direct IPSC amplitude measured in GoC–GrC paired recordings (N = 44). Only IPSCs exhibiting a direct component were included. The black line represents a linear fit to the data. IPSC amplitude was poorly correlated with GrC C_m; Pearson's rank; r = 0.27.

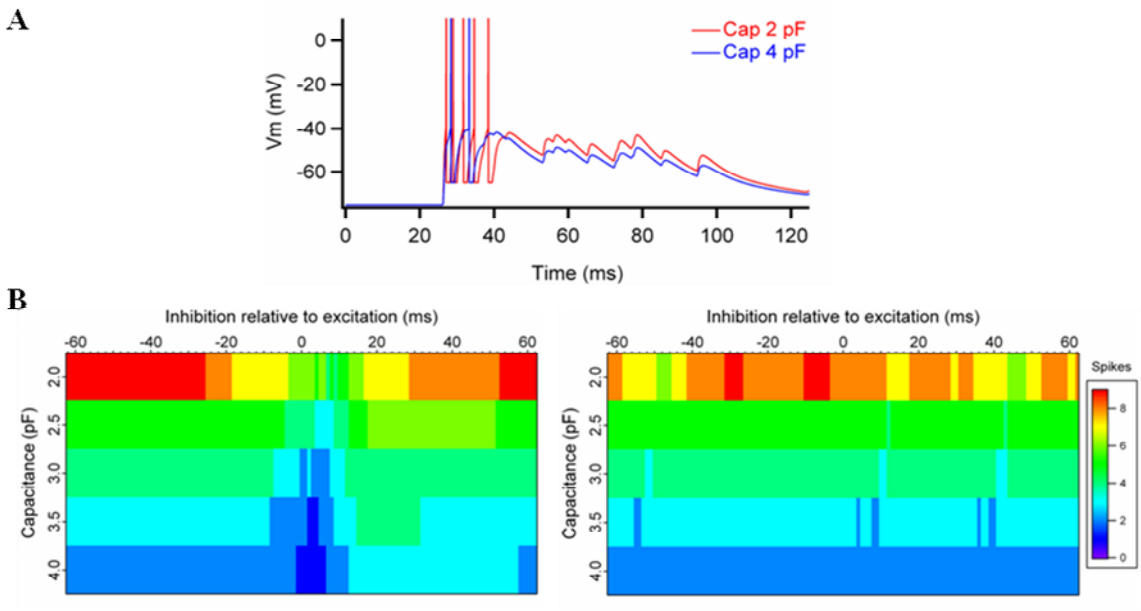

Fig. 5.13: The effect of C_m on GrC integration of simulated GoC inhibition and MF burst inputs. **A**. Example outputs from the IF GrC model with whole cell C_m set to 2 (red) and 4 pF (blue) in response to 4 MF burst inputs in the presence of 420 pS tonic inhibition. **B**. 2-D plots showing spike output (indicated by colour) in response to MF burst input in the presence of synchronised (left) and desynchronised (right) inhibition shifted in 1 ms steps relative to peak excitation (x-axis) at a range of whole cell capacitance values (y-axis).

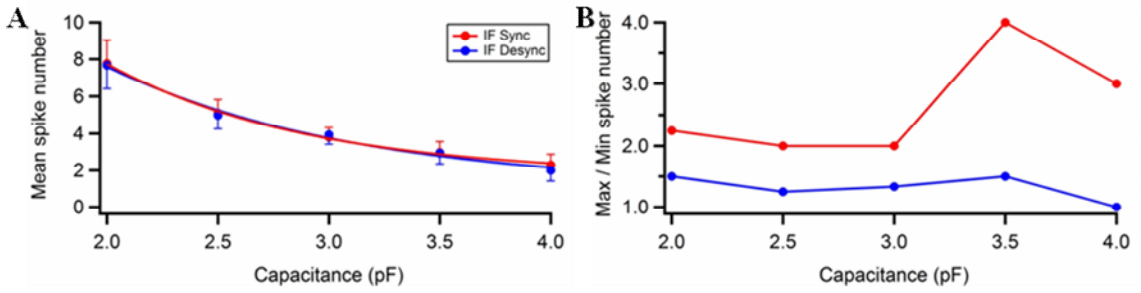

Fig. 5.14: Summary of data presented in **Fig. 5.13**. **A**. Mean spike number across 1 cycle for a range of capacitance values with synchronised inhibition (red) and desynchronised inhibition (blue). Fits represent an exponential function error bars give SEM. **B**. Ratio between largest spiking response and smallest spiking response across the inhibitory cycle with synchronised (red) and desynchronised inhibition (blue).

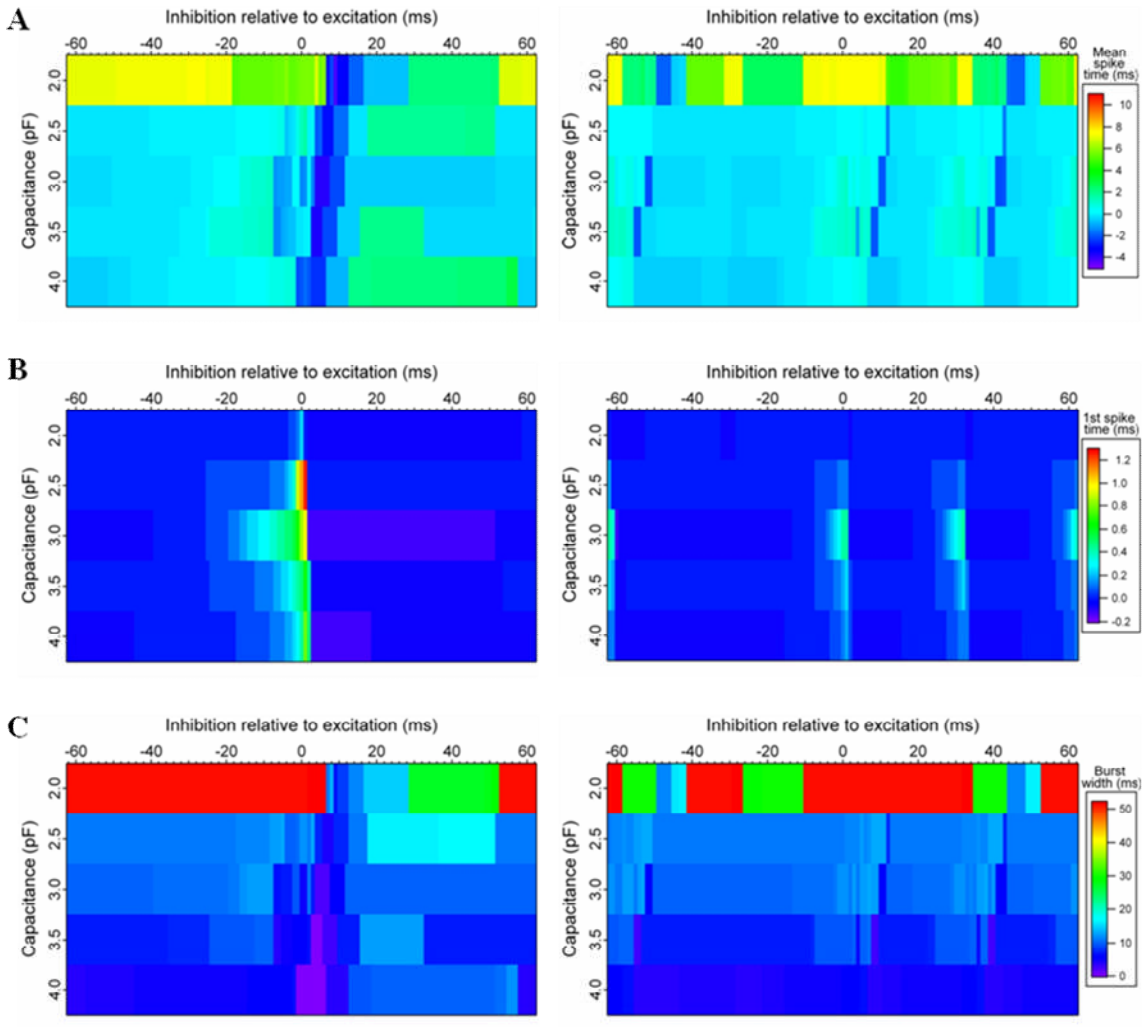

Fig. 5.15: C_m dependence of the effect of inhibition on the timing of the IF GrC model's response to burst MF input. 2-D plots showing the effect of C_m (y-axis), phase of inhibition (x-axis) and synchrony of inhibition (left – synchronised vs right – desynchronised) on **A**. the mean spike timing (relative to mean spike timing with tonic inhibition; indicated by colour) **B**. the timing of the first spike (relative to first spike timing with tonic inhibition; indicated by colour) and **C**. the width (indicated by colour) of the GrC burst response.

The first spike in the GrC response remained robust in the face of inhibition while mean spike time and burst width were advanced and reduced respectively by synchronised inhibition arriving around the time of peak excitation in the IF model across C_m values. Desynchronised inhibitory inputs could also advance and reduce while mean spike time and burst width (though to a lesser extent) by arriving shortly after peak excitation. Burst width was greater in model GrCs with small C_m values.

These results suggest that the qualitative effects of synchronised and desynchronised inhibition on GrC processing of MF burst inputs are robust to changes in capacitance, but the quantitative effects vary considerably across the limited range of C_m values tested. Synchronised inhibition arriving close to peak excitation reduced the GrC response and shortened burst width relative to synchronised inhibition arriving out of phase with peak excitation (**Fig. 5.13** & **5.15C**). The average spike output did not vary significantly between synchronised and desynchronised inhibition, however, the ratio between peak GrC output and minimal GrC output was much larger with synchronised inhibition than desynchronised inhibition and varied with C_m (**Fig. 5.16**). The changes in the model's responses with C_m may explain some of the variability observed among GrCs in slice.

5.7 Discussion

5.7.1 The number of MF burst inputs required to trigger spiking in a GrC

In order to gauge an appropriate level of excitation to use in my investigation of the effect of GoC mediated inhibition on GrC processing of MF burst inputs I used computer modelling to determine how many simultaneous MF bursts would likely be required to evoke spiking in a GrC. The MF burst inputs I used were constrained to the parameters of those reported in Rancz *et al*. 2007 in response to whisker stimulation, having very high instantaneous spike frequencies followed by rapid adaptation. Individual excitatory inputs, based on data from Rothman *et al*. 2009, within the bursts had a larger amplitude than those recorded in Rancz *et al*. 2007, perhaps due to the use of ketamine/xylazine anaesthesia in the latter study (e.g. Wang *et al*. 2011)

The IF GrC model required input from 3 simulated MFs in order to spike (**Fig. 5.1**). A few preliminary experiments indicated that in slice GrCs generally require two or 3 simulated inputs to spike (not shown). This conflicts with Rancz *et al*. 2007 who report that single MFs triggered to fire rapid bursts will elicit firing in GrCs.

The argument as to whether single or multiple MFs are required to trigger GrC firing is a point of some contention in the field with other studies claiming that activation of multiple MFs is required to trigger GrC firing (D'Angelo *et al*. 1995; Jorntell & Ekerot 2006; Chadderton *et al*. 2004; Gabbiani *et al*. 1994; Rancz *et al*. 2007). Notably, Rancz *et al*. 2007 evoked firing using focal stimulation which is a fairly nonspecific technique (as discussed in **3.5**). It is possible that stimulation triggered firing in multiple MFs or caused local K^+ release resulting in an increase in excitation, indeed; preliminary experiments have shown that stimulating in the locality of a GrC even in the absence of a direct connection can increase excitability (not shown).

Notably, Rancz *et al*. 2007 found that whisker stimulation is typically conveyed to GrCs by input from only one MF, which brings into question the validity of utilising excitatory input from multiple simultaneous bursts in the above experiments. However, only a small number of GrCs were recorded in Rancz *et al*. 2007 and it has been shown elsewhere that GrCs typically receive multiple MF inputs of the same modality and even sub-modality (Jörntell & Ekerot 2006). It is unlikely that all whiskers were stimulated by the air puff utilised for whisker stimulation in Rancz *et al*. 2007, so the remaining MF inputs may convey input from other whiskers or respond to different forms of whisker movement (whisking is a complicated activity). Alternatively, the other MFs may convey different forms of sensory input, many of which might also be encoded by MF bursts, all be it with different dynamics (Garwicz *et al*. 1998).

5.7.2 The effect of synchrony and phase of inhibition on GrC of processing MF burst inputs

I have used dynamic clamp and computer modelling to investigate how the phase and synchrony of GoC–GrC inhibition will affect GrC processing of MF burst inputs. In dynamic clamp experiments shifting a synchronised inhibitory waveform (comprised of input from 8 GoCs, 5 direct, 3 spill) relative to peak excitation had a large effect on spike output; GrC spike output was roughly three times greater when synchronised

inhibition arrived out of phase with peak excitation than when it arrived approximately in phase. By contrast, shifting the desynchronised inhibitory waveform relative to peak excitation had only a modest effect on spike output (**Fig 5.2D**). The IF GrC model also exhibited a larger peak-to-trough ratio for GrC firing output with synchronised inhibition than with desynchronised inhibition across the cycle (**Fig. 5.5B**). This suggests that synchronised inhibition may serve to diminish or augment the volume of MF burst signals passing through the GrC layer relative to the phase of the GoC cycle.

Average model GrC spike output across the full 125 ms cycle was similar for desynchronised and synchronised inhibition in a GrC model implying that net GrC excitability does not (directly) change with inhibitory synchrony and supporting the findings of the previous chapter suggesting that synchrony has little effect on GrC gain (over a sufficiently large time scale).

Inhibition also had effects on the timing of spikes in the GrC response to MF burst input. Mean spike time and burst width were reduced by the arrival of synchronised inhibition close to, or shortly after, peak excitation and increased when synchronised inhibition arrived out of phase with excitation, while desynchronised inhibition had little clear effect on spike timing (**Fig. 5.2**). The GrC model likewise showed a reduction in mean spike time and burst width when synchronised inhibition arrived close to the time of peak excitation, but also showed a reduction in mean spike time and burst width when desynchronised direct inhibitory inputs arrived shortly after peak excitation (**Fig. 5.5B**). The reductions in mean spike time and burst width were largely mediated through the elimination of spikes occurring late in the GrC response, early spikes were quite robust to inhibition (**Fig. 5.2** & **5.5**). Given that MF burst inputs typically convey information regarding the onset of sensory stimuli which might be required to trigger a rapid and appropriate motor response, it seems to make sense that inhibition should be able to sharpen a signal without delaying it. Burst inputs arriving out of phase with synchronised inhibition appear to be augmented, perhaps enhancing their salience to downstream PCs in accordance with the phase of inhibition.

These results were obtained using perfectly synchronised or desynchronised inhibitory inputs. As discussed in the previous chapter this was done for convenience. In reality GoCs tend to be only loosely synchronised (Dugue *et al*. 2009; Verveake *et al*. 2010). Subsequent experiments should utilise more realistic inhibitory waveforms, however it

is unlikely that looser synchronisation in the inhibitory input would have dramatically different qualitative effects (i.e. the first spikes in the GrC response would likely remain quite robust while later spikes could be knocked out by approximate coincidence with the peak of the inhibitory waveform).

It is also not clear that oscillations in the GoC network would persist in the presence of burst MF input. Tactile inputs such as skin or hair stimulation typically elicit bursts or pauses in GoC firing over large receptive fields (Vos *et al*. 1999b; Tahon *et al*. 2005; Holtzman *et al*. 2006a; Holtzman *et al*. 2006b) and the termination of oscillations in the local field potential in the GrC layer has been correlated with multiple sensorimotor behaviours (Hartmann & Bower 1998). However, the stimuli used in these studies were typically quite gross and as previously discussed GoC activity may not correlate well with the activity of surrounding GrCs (Van Kan 1993; Barmack & Yakhnitsa 2008; Heine *et al*. 2010). Further, oscillations in the GrC layer have been shown to persist during active whisking (Hartmann & Bower 1998). So GoC synchrony may not be appreciably altered in the face of subtle tactile inputs received during whisking.

Several cell parameters in these experiments were fixed; V_m was set to -75 mV with current injection and E_{GABA} was set to -75 mV. In modeling experiments capacitance was also fixed at 3.1 pF. In reality these parameters are by no means fixed. Indeed in the dynamic clamp experiments there was not only dramatic cell to cell variability, but in many cases trial to trial variability. Data were averaged to give a population trend but in doing this valuable information may have been lost. That responses in some cells were reliably altered by inhibitory input and not in others might serve a functional purpose, diversifying GrC activity and therefore increasing the number of patterns a PC population could learn. In order to test how changes in different cellular parameters might affect a GrC's sensitivity to inhibition I repeated the modelling experiments at different V_m, E_{GABA}, and C_m values.

5.7.3 Stability of the effect of synchrony and phase of inhibition on GrC burst processing

Across values of V_m and E_{GABA} the ratio between peak firing (when inhibition was out of phase with excitation) and minimal firing (when inhibition was in phase with excitation) was far greater for synchronised inhibition than desynchronised inhibition in

the GrC model, though the magnitude of the difference varied with these parameters (**Fig. 5.7B** & **5.10B**), conversely, average spiking output (across a cycle) was similar for synchronised and desynchronised inhibition (**Fig. 5.7A** & **5.10A**). This would suggest that the qualitative observations regarding mean spike output made in the previous section are robust to moderate changes in V_m and E_{GABA} such as may occur between GrCs.

V_m and E_{GABA} vary with animal age (Brickley *et al*. 1998; Cathala *et al*. 2003). That the qualitative effects of inhibition are resistant to changes in V_m and E_{GABA} suggests that inhibition is performing similar functions during the developmental stages and young adulthood.

The reduction in spike number elicited by inhibition arriving close to, or shortly after, peak excitation (**Fig. 5.5B**) was reflected in a reduction of mean spike time and mean burst width across V_m and E_{GABA} values investigated. As with dynamic clamp experiments changes in spike number and timing tended to arise from the elimination of spikes occurring later in the GrC burst response, the first spike was robust to inhibition across the values of V_m and E_{GABA} investigated (**Fig. 5.6**, **5.8**, **5.9** & **5.11**).

GrCs have quite varied whole cell capacitance levels (between 2.1 and 5.9 pF in this study). The spiking output of a model GrC receiving common excitatory and inhibitory conductance varied dramatically with C_m (**Fig. 5.15**), it is perhaps surprising then that the amplitude of inhibitory synaptic inputs does not appear to be matched to cell C_m (**Fig. 5.14**), as such a population of GrCs *in vivo* receiving common excitatory and inhibitory inputs might give dramatically different responses. Feasibly, however, MF inputs might be scaled to cell C_m in a way that GoC inputs are not. It is also possible that smaller cells express a greater concentration of compensatory active conductances, though based on my observations from dynamic clamp experiments this is unlikely to be the case (smaller cells spike more frequently than larger ones). Increasing C_m reduced spiking output in the model GrC. The ratio between peak firing and minimal firing was far greater with synchronised inhibition than desynchronised inhibition, though the size of the gap did vary with C_m, peaking close to the mean GrC capacitance value recorded from cells in this study. It is interesting that cell C_m confers these computational properties on GrCs and raises the possibility that GrCs of different

capacitances could convey differing signals to an upstream PC despite receiving common MF input.

In the IF model there was parameter space in which desynchronised inhibitory inputs were not effective at reducing GrC spike output and burst width but for the majority of V_m, E_{GABA} and C_m values tested they had a detectable effect.

5.7.4 The potential impact of individual GoC–GrC IPSCs

To test whether single direct inhibitory inputs could have an effect on GrC processing of MF burst inputs I utilised dynamic clamp to deliver simulated burst input from 4 MFs in conjunction with a desynchronised inhibitory input. Direct inhibitory inputs arriving a little after (~30 ms) peak excitation were capable of reducing the occurrence of spikes late in the GrC burst response but had no appreciable effect on spike timing (**Fig. 5.3**). The potential impact of individual GoC–GrC inputs will likely depend on individual GrC parameters and the nature of the excitation it coincides with but in general the efficacy is likely to be limited.

In the IF model single IPSCs were capable of knocking out spikes and affecting spike timing across the majority of the parameter space examined, however these results were obtained in the absence of realistic biological noise. The model GrC utilised was quite simple and not designed to mimic the minutiae of GrC behaviour thus all results obtained there from should be treated with caution.

It seems that individual GoC inputs are unlikely to reliably negate the occurrence of specific spikes, particularly if one takes into account the high failure rate at the GoC–GrC synapse (~ 20 %). As such individual GoC–GrC inputs are poorly suited to provide a temporally precise “and not” signal. This is particularly true of spillover only inputs which failed to knock out spikes in both the dynamic clamp and modelling experiments. To have a reliable effect it appears that inhibition needs to be synchronised or delivered at rate.

5.7.5 The potential impact of bursts of GoC–GrC IPSCs

Steady state firing may not persist in the presence of burst MF input. The majority of GoCs respond to tactile inputs with bursts or pauses in firing (e.g. Vos *et al*. 1999b; Holtzman *et al*. 2006b) and bursts of inhibitory input have been recorded in GrCs in response to tactile stimulation (Jörntell & Ekerot 2006). To model the occurrence of a burst of GoC activity 8 GoC inputs were delivered, either tightly synchronised or loosely synchronised (it is not known how well synchronised evoked bursts of GoC activity would typically be) on top of a resting tonic inhibition of 420 pS. The inhibitory waveform was shifted relative to MF burst input. Both the tightly- and loosely-synchronised bursts reduced the GrC spike output (in some cases to zero). The tightly-timed GoC burst caused a larger reduction in the GrC's spike output when delivered in phase with peak excitation but the loosely-timed GoC burst was effective over a broader time range. Effects on the timing of the GrC burst response where unclear due to the small number of cells available for analysis.

The effectiveness of a burst of GoC inputs will depend on its magnitude and timing. Vos *et al*. 1999b showed that GoCs respond to stimulation of the trigeminal nerve with bursts of firing typically occurring early (5–10 ms) or late (13–26 ms) relative to the stimuli, or both early and late. The early response is presumed to convey a direct spinocerebellar MF signal while the late response may arise from either parallel fibre input and/or cerebrocerebellar MFs (Vos *et al*. 1999b; De Schutter *et al*. 2000; Tahon *et al*. 2005). If the first response is conveyed by MFs that carry a similar signal to GrCs and the GoCs that innervate them then inhibition would be expected to arrive very shortly after peak excitation (typically around 2 ms for the feed forward signal to arrive via the GoCs; Kanichay 2008) limiting the time window for integration (Pouille & Scanziani 2001) and eliminating all but the first (or first few spikes). The late response would likely curtail spiking towards the end of the GrC burst response. If, however, GoC provide lateral rather than feedforward inhibition then inhibition may arrive at almost any point relative to peak excitation and may perform quite different functions.

5.8 Conclusions

Desynchronised inhibitory input elicits a generalised reduction in the GrC spiking response to MF burst inputs. By contrast synchronised inhibition can diminish or augment the GrC response depending on the phase of its arrival relative to the MF input. Early spikes in the GrC response tend to be quite robust while later spikes are

easily blocked by the near coincident arrival of synchronised inhibitory input, serving to sharpen the GrC response and thus more reliably signal the onset of a given stimulus. Modelling suggests that the qualitative effects of synchronised inhibition are likely to be robust across a range of physiological values for V_m, E_{GABA} and C_m.

Individual GoC–GrC inputs have a questionable efficacy *in silico* and *in vitro*, thus it seems unlikely that individual GoC inputs are suitable to convey a temporally precise signal.

It is not clear whether GoC synchrony persists in the presence of tactile input. The most typical GoC responses to tactile input are a burst or pause in firing. Bursts of GoC activity (on top of a typical resting level of inhibition) were very effective at reducing the GrC spiking response when arriving close to or shortly after peak MF excitation as they might be expected to *in vivo* (Vos *et al*. 1999).

Chapter Six

6. Modulation of inhibition in the GrC layer

6.1 Introduction

The previous chapters have shown how changes in the rate and timing of inhibitory input can affect GrC processing of MF derived input. However, the rate and timing of inhibitory input may not be the only parameters that are subject to change. The magnitude of inhibition may also be regulated by neuromodulatory inputs.

ACh has been shown to increase the GABAergic inhibitory conductance received by GrCs (in slice) approximately four fold over a time course lasting several minutes via the activation of nicotinic acetylcholine receptors (nAChRs). The increase in GABA is mediated by Ca^{2+}-dependent vesicular release but is action potential independent (Rossi *et al*. 2003). Cholinergic modulation of inhibition in the GrC layer could represent a potent means of regulating MF throughput, however, the specific nAChR and cell type responsible for the ACh mediated GABA release are unknown. I have attempted to address these questions using a combination of pharmacological, electrophysiological and imaging techniques. I also attempted to investigate the potential physiological relevance of ACh-evoked GABA release through the focal stimulation of sparse endogenous cholinergic inputs to the cerebellum (Jaarsma *et al*. 1997).

The magnitude of GoC-mediated inhibition has been shown to be subject to modulation via the activation of $GABA_B$Rs (Mapelli *et al*. 2009) and mGluRs (group II & III) both of which reduce release probability at GoC synapses (Mitchell & Silver 2000). The activation of $GABA_B$Rs is likely to arise from the presence of ambient GABA in the GrC layer and has only a minor effect on GoC release probability (Mapelli *et al*. 2009). In contrast the activation of mGluRs is thought to result from glutamate spillover from active MF terminals onto GoC presynapses and has a potent effect on GoC mediated inhibition (Mitchell & Silver 2000). To date, however, this mGluR mediated disinhibition has only been demonstrated in juvenile animals (P12–13), wherein the glomerulus is immature, so it is not clear to what extent the effect is relevant in the adult cerebellum. Furthermore, the study utilised focal stimulation in the GrC layer to trigger

mGluR activation so the synaptic specificity of the disinhibition is unclear. If GoC-mediated inhibition is sensitive to the level of MF activity a post synaptic GrC receives then the GrC I–O function may be dramatically altered. As such I have investigated the potency and synaptic specificity of mGluR mediated disinhibition in young adult rats using paired GoC–GrC recordings.

6.2 Augmentation of GrC inhibition via activation of nicotinic ACh receptors

6.2.1 Pharmacology of nicotine evoked GABA release in the GrC layer

Nicotine (100 µM) was puff-applied via a patch pipette to the surface of the GrC layer while recording from GrCs using the GrC E_{Cl} = 0 mV intracellular solution (**Table 2.3**). At a holding potential of -60 mV 10 second puff application of nicotine evoked a strong, long lasting inward current (**Fig. 6.1A**) peaking at 116 ± 60 pA (1800 ± 940 pS; N = 71), 4.3 times the charge carried by tonic inhibition alone. The effect on the rate of sIPSCs was variable, sometimes eliciting a reduction and other times an increase. Repeat application following a 5 minute recovery period produced a response of similar magnitude (paired T-test P = 0.81; N = 7; **Fig. 6.1A**). To investigate the pharmacological profile of nicotine-induced GABA release, secondary responses were elicited in the presence of various pharmacological manipulations; the evoked charge was measured and expressed as a percentage of the initial (control) response (Kruskal-Wallis test P = 0.001). In accordance with Rossi *et al*. 2003, secondary responses were completely blocked by bath application of the $GABA_AR$ antagonist GBZ (10 µM; N = 5; Dunn test P < 0.001; **Fig. 6.1A, B**) but not by application of the Na^+ channel blocker TTX (1 µM; N = 5; Dunn test P > 0.05; **Fig. 6.1B**).

To investigate the receptor subtype responsible for mediating the nicotine induced GABA release I elicited secondary responses in the presence of a range of nAChR antagonists. The most common nAChR found in the mammalian central nervous system is the α4β2 subtype. In order to determine whether this subtype mediates ACh induced GABA release I applied dihydro-β-erythroidine (DβE 4 µM), an inhibitor of α4 and α6 containing and α3β2 type nAChRs (Harvey & Luetje 1996), which had no significant effect on the nicotine-evoked response (Dunn test P > 0.05; N = 6; **Fig.**

6.1B). Another nAChR expressed widely in the central nervous system, and the only subtype to date specifically localised to GoCs (Wang *et al*. 2002) is the α7 subtype. However the selective α7 nAChR blocker methyl-caconitine (40 nM) also failed to block the nicotine-induced release of GABA (Dunn test $P > 0.05$; N = 4; **Fig. 6.1B**). To confirm this finding the α7 specific agonist Choline (1 mM) was bath applied 5 minutes subsequent to a confirmed nicotine response and accordingly failed to yield a detectable response (N = 3; not shown). The cerebellum contains many non-classical nAChRs (Turner & Kellar 2005) including nAChRs of the type found at neuromuscular junctions (de la Garza *et al*. 1987), the neuromuscular nicotinic receptor antagonist pancuronium (Pan 10 μM) was therefore tested and found to produce an ~ 75% reduction in nicotine evoked GABA release (N = 5; Dunn test $P < 0.05$; **Fig. 6.1B, C**).

These findings confirm that nicotine-evoked GABA release is action potential independent and suggest that it may be mediated by an atypical nAChR subtype.

6.2.2 GoCs as a mediator of nicotine evoked GABA release

The only known means of changing the level of GrC inhibition over a rapid timescale is through an increase in the activity of the GoC network. To see if GoCs respond to nicotine and thus represent a potential locus for the nicotine-induced GABA release I made patch clamp recordings from individual GoCs with simultaneous Ca^{2+} imaging of the cell body (using Fluo 5F). GoCs were visualised through the inclusion of Alexa 594 in the patch pipette (**Fig. 6.2A**). These experiments were carried out at room temperature to maximise the probability of success. In all cells tested (N = 4) puff application of nicotine (100 μm) to the surface of the slice induced a large Ca^{2+} response ($\Delta F/F = 1.3 \pm 1.9$; **Fig. 6.2B, C**), in 3 of the 4 cells this was accompanied by an increase in firing rate (5.5 ± 2.3 fold; **Fig. 6.2C**). In the remaining cell nicotine elicited a cessation of spiking accompanied by a large depolarisation followed by a hyperpolarisation and gradual recovery (**Fig. 6.2D**).

Nicotine-evoked GABA release was insensitive to TTX and thus action potential independent. To check if GoCs would respond to nicotine in the absence of the ability to fire action potentials I repeated the above experiments in the presence of TTX (1 μM). In all cells (N = 5) puff application of nicotine caused rapid depolarisation (37.3 ± 5.9 mV) coupled with a large Ca^{2+} response (mean $\Delta F/F = 2.9 \pm 1.8$; **Fig. 6.2E**).

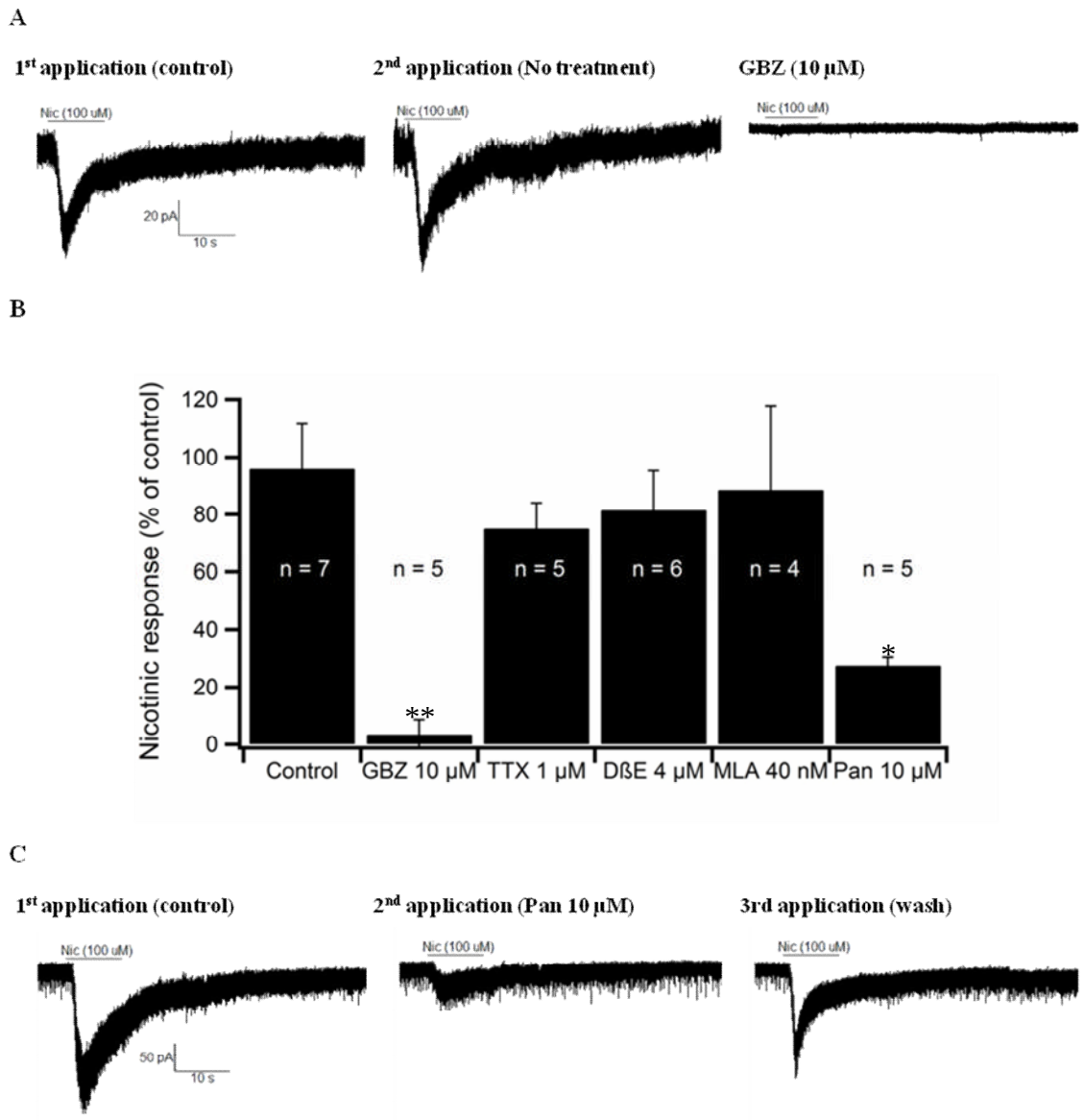

Fig. 6.1: The pharmacology of nicotine-evoked GABA release. **A**. Example voltage clamp recordings from a GrC (held at -60 mV, E_{Cl} set to 0 mV) upon (10 second) puff application of 100 µM nicotine (left), a second puff of 100 µM nicotine (centre), and a third puff of 100 µM nicotine in the presence of 10 µM gabazine (GBZ). **B**. Chart shows charge elicited by a 2nd puff application of 100 µM nicotine in the presence of the indicated pharmacological manipulation expressed as a percentage of the charge evoked by an initial control puff application of 100 µM nicotine. Error bars represent SEM. GrCs were subjected to either: no treatment (Control; N = 5), GBZ (10 µM; N = 5; ** Dunn test $P < 0.001$), tetrodotoxin (TTX 1 µM; N = 5), Dihydro-β-erythroidine (DβE 4 µM; N = 6), methyl-caconitine (MLA 40 nM; N = 4) or pancuronium (Pan 10 µM; * Dunn test $P < 0.05$). **C**. Recording conditions as in **A**, example traces showing a GrC response to 100 µM nicotine (left), in the presence of 10 µM pancuronium (centre) and following washout (right).

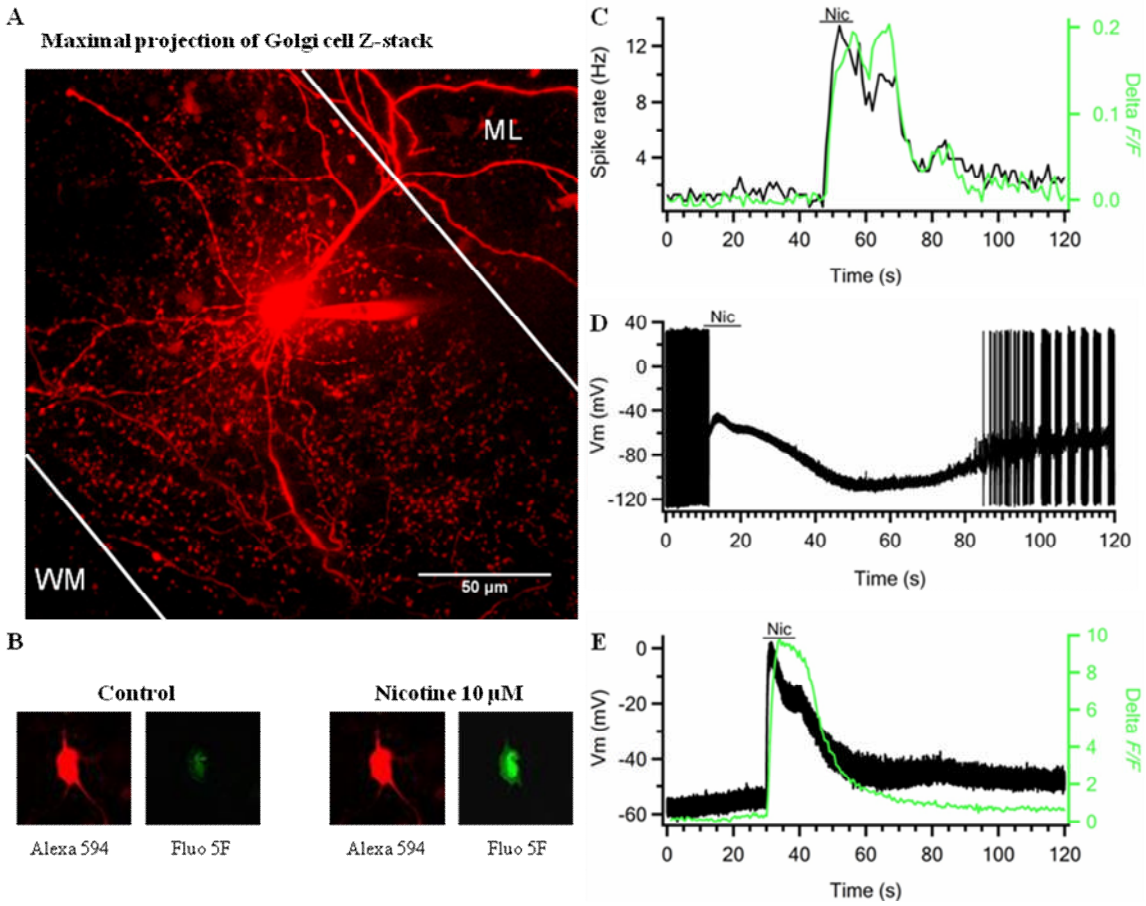

Fig. 6.2: GoC response to nicotine. **A**. Maximal projection of a Z-stack showing a GoC (labelled with Alexa 594) with descending dendrites and axon confined to the GrC layer and ascending dendrites reaching into the molecular layer. **B**. The same GoC labelled with Alexa 594 (red) and Fluo 5F (green) under control conditions (left) and during puff application of 100 µM nicotine (right). **C**. Example data showing the change in spiking rate and Ca^{2+} response induced by puff application of 100 µM nicotine in one GoC. **D**. Spiking output from another GoC in response to puff application 100 µM nicotine. **E**. Example data showing the V_m and Ca^{2+} response induced by puff-application of 100 µM nicotine in a GoC in the presence of 1 µM TTX.

It is not known whether GoCs can release GABA in an action potential independent fashion. To test if somatic depolarisation alone might be sufficient to elicit GABA release I made paired GoC–GrC recordings and once a connection had been established (**Fig. 6.3A**) the presynaptic GoC was depolarised from a V_m of -80 mV (with a 1 nA step for 5 s) to an average V_m of -26 ± 20 mV and the postsynaptic response recorded (N = 4). Presynaptic depolarisation had no effect on GrC I_{hold} (0.28 ± 0.36 pA; Mann-Whitney U test P = 0.22; **Fig. 6.3B**).

If nicotine mediates its effects by augmenting GABA release from GoCs then one might expect that at low concentrations it would have an observable effect on direct GoC–GrC transmission. In order to test this hypothesis I evoked GoC–GrCs inputs using a stimulating electrode and investigated the effect of bath application of 10 µM nicotine on synaptic transmission. In all cells (N = 6) nicotine induced in an inward current shift (35.5 ± 9.2 pA averaged over the duration of nicotine application reflecting an increase in inhibitory conductance of 554.7 pS). Conversely the amplitude of evoked synaptic potentials decreased by 57% in the same period (a reduction of 36.3 ± 6.6 pA; paired T-test P = 0.003; **Fig. 6.4**). To determine whether this reduction in amplitude reflected a pre- or postsynaptic change in synaptic efficacy the coefficient of variation (CV; a measure of variability in input size) of the synaptic input was determined in the presence and absence of nicotine. The CV was unchanged by 10 µM nicotine (0.31 vs 0.32; paired T-test P = 0.64) indicating that the reduction in amplitude is likely to be the result of a post synaptic effect; a decrease in the number or efficacy of post synaptic $GABA_A$Rs resulting from the dramatically increased GABA exposure.

These results suggest that if nicotine-evoked GABA release is mediated by GoCs then it may be released by an as yet unidentified action potential-independent mechanism.

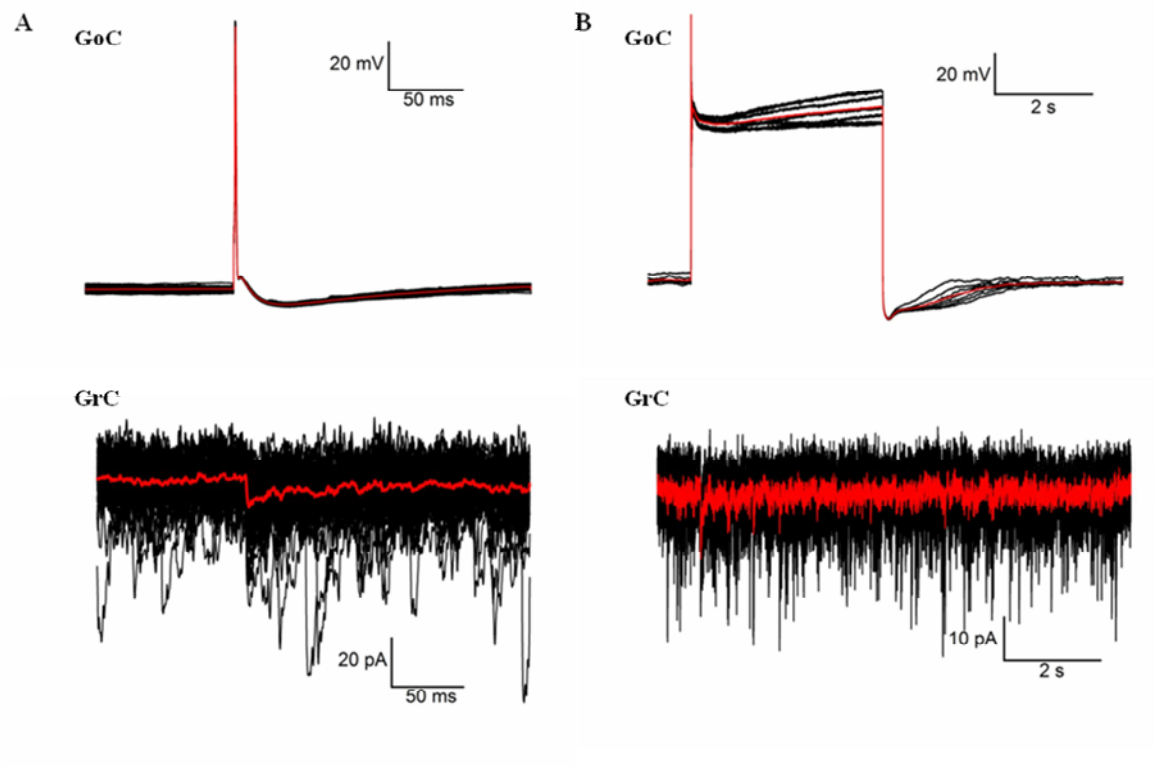

Fig. 6.3: The effect of GoC V_m on GrC inhibition. **A**. Paired GoC–GrC recording showing a presynaptic GoC action potential evoked with a 1 ms 1 nA current injection (top) and the post synaptic IPSC (bottom) individual trials (50) in black, average in red. **B**. Presynaptic GoC depolarisation evoked with a 3 s 1 nA current injection (top) and the postsynaptic response (bottom) individual trials (6) in black, average in red. A 10 s recovery was allowed between stimulus presentations.

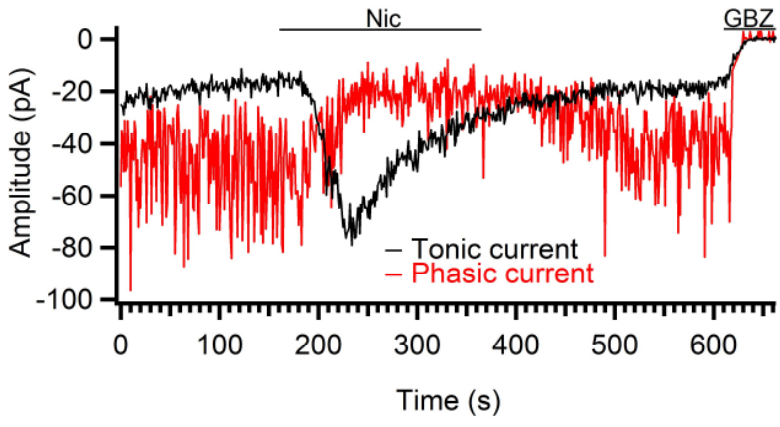

Fig. 6.4: The effect of nicotine on GoC–GrC synaptic transmission. Example voltage clamp recording from a GrC held at -60 mV with E_{GABA} set to 0 mV showing the effect of nicotine on the resting inhibitory conductance (black) and the amplitude of evoked IPSCs triggered at 1 Hz (red). Nic = nicotine (10 µM), GBZ = gabazine (10 µM).

6.2.3 Activation of endogenous cholinergic inputs to the GoC

To investigate whether cholinergic inputs to GoCs (Jaarmsa *et al*. 1997) could represent a physiological means of modulating inhibition in the GrC layer I made whole cell recordings from GoCs under conditions of ionotrophic glutamatergic block (50 µM GYKI & 50 µM AP5) and attempted to evoke cholinergic inputs through focal stimulation in the surrounding tissue. Recordings were carried out at room temperature and GoCs were held at -70 mV. The most common evoked responses were inhibitory and were either sensitive to strychnine (0.3 µM) and presumed to be inputs from Lugaro cells or were preceded by a brief depolarisation, insensitive to strychnine and presumed to be gap junction potentials (not shown). Despite searching for cholinergic inputs in a total of 88 GoCs in all layers of all lobules of cerebellar slices cut in different planes, putative cholinergic inputs were only detected in 3 cells. In two cells the inputs had a large amplitude (205.1 ± 7.6 pA and 173.8 ± 8.4 pA) fast 20–80 % rise time (0.28 ± 0.02 ms and 0.27 ± 0.04 ms) and fast weighted decay (1.1 and 1.2 ms; **Fig. 6.5A**). Both were blocked by bath application of the nAChR antagonist mecamylamine (25 µM) in one case the recording lasted long enough to demonstrate a recovery upon washout of the drug (**Fig. 6.5B**). Given the large amplitude, fast timecourse and high reliability of these inputs it is possible that they represent some form of ACh evoked regenerative event rather than a direct synaptic input. In a third cell the cholinergic input was not detectable as a post synaptic current upon stimulation at 1 Hz, however rapid stimulation (150 Hz) while recording in current clamp elicited a dramatic increase in firing rate which was followed by a period of silence and finally recovery, the increase in firing rate was blocked by bath application of mecamylamine (25 µM; **Fig. 6.5C**).

Cholinergic inputs to GoCs appear to be rare, but may be potent modulators of GoC activity.

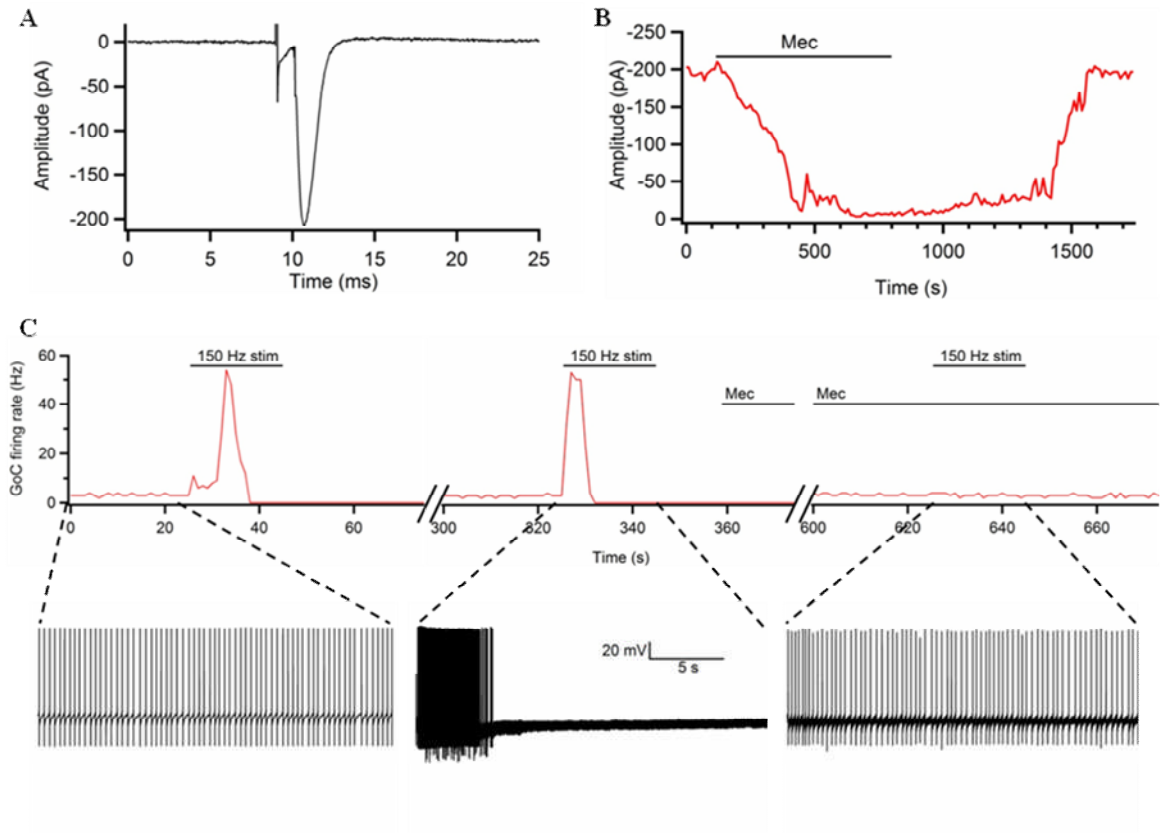

Fig. 6.5: Cholinergic inputs to GoCs. **A**. Example of a putative ACh-mediated EPSC recorded in a GoC voltage clamped at -70 mV. **B**. Effect of 25 µM mecamylamine (Mec) on the amplitude of the same putative ACh-mediated EPSC, data points represent the average of 5 IPSCs acquired at 1 Hz. **C**. Spiking rate of a GoC at rest and in response to rapid stimulation of a putative cholinergic input (which failed to elicit a detectable EPSC), stimulation of the input resulted in rapid GoC firing followed by a period of quiescence and recovery. This effect was blocked by 25 µM mecamylamine. Example spiking traces are shown below at rest (left) during 150 Hz stimulation (centre) and during stimulation with 25 µM mecamylamine (right). These experiments were carried out at room temperature.

6.3 Relief of GrC inhibition via activation of mGluRs

6.3.1 Effect of mGluR agonism on GoC–GrC IPSCs

In juvenile rats mGluR agonism can reduce GoC-mediated GABA release. To see if this mGluR-mediated disinihibition persists in adult animals I tested the effect of the mGluR group I & II agonist 1-Amino-1,3-dicarboxycyclopentane (ACPD; 100 µM) on GoC-mediated IPSCs recorded from GrCs in the paired patch configuration in slices prepared from P25 rats (**Fig. 6.6**).

ACPD (100 µM) reduced the amplitude of single IPSCs by 95 ± 10 % (N = 8; paired T-test P = 0.008; **Fig. 6.6A, C**) and the spillover conductance (measured as in **3.4.2**) induced by a train of 12 IPSCs delivered at 50 Hz by 89 ± 6 % (N = 6; paired T-test P = 0.003; **Fig. 6.6B, C**). Additionally it elicited an outward current shift of 12.0 ± 6.7 pA (**Fig. 6.6B**), the outward current shift was not observed when GBZ (10 µM) was applied prior to the application of ACPD (N = 3; not shown) as such it is assumed to reflect a suppression of resting inhibitory GABAergic conductance of 187 ± 57 pS (almost half the resting amount of inhibition; N = 8). ACPD increased the gain and offset of the GrC I–O function (measured as described in **chapter 4**) however in these experiments ACPD was bath-applied and as such it was difficult to disentangle the direct effects of ACPD from the time- and activity-dependent increase in excitability observed in all GrCs (data not shown; Armano *et al*. 2000).

This data suggests that mGluR mediated disinhibition is not only present in the adult rat but may be more pronounced than in the juvenile rat.

6.3.2 Specificity of mGluR mediated effects

It has been reported that glutamate released from MFs can suppress GABA release from GoCs (Mitchell & Silver 2000). I made recordings from GoC–GrC pairs and used careful minimal stimulation in the white matter tract to selectively trigger single MF inputs to the postsynaptic GrC, once identified ionotrophic glutametergic input was blocked with 50 µM NBQX and 10 µM AP5. The MF was then stimulated at a rate of 100 Hz while the effect on the GoC–GrC IPSC was observed.

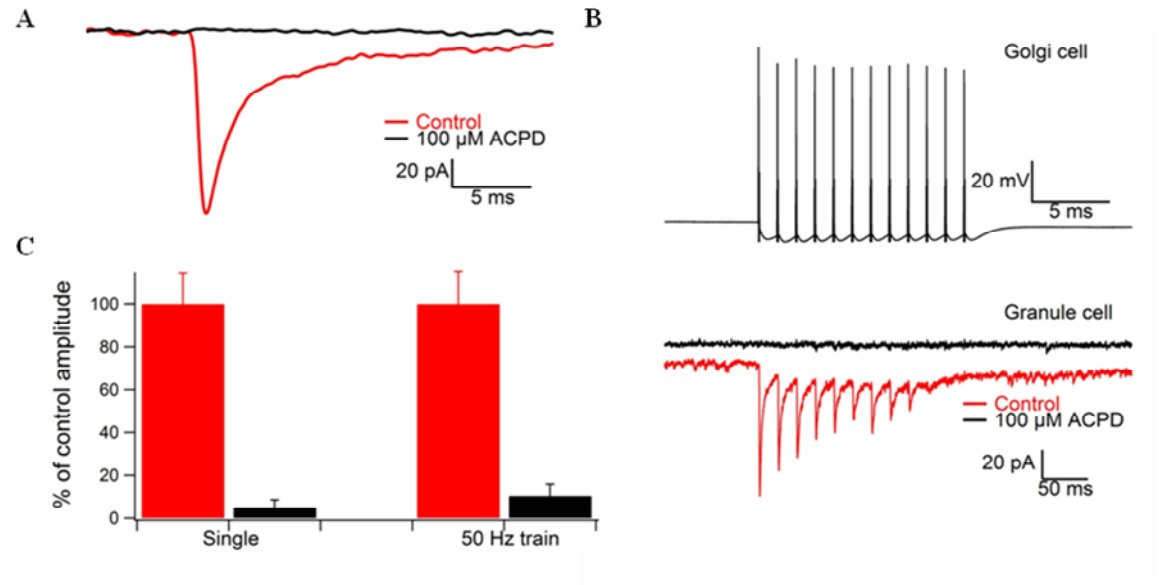

Fig. 6.6: The effect of mGluR agonism on GrC inhibition. **A**. Averaged GrC IPSC recorded from a GoC–GrC pair under control conditions (red) and in the presence of ACPD (black), recordings were baseline subtracted for comparison. Traces represent average of 100 trials. **B**. Presynaptic GoC action potentials triggered at 50 Hz with 1 ms 1 nA current injections (top) and post-synaptic GrC response under control conditions (red) and in the presence of ACPD (black). Traces represent the average of 50 trials. **C**. Quantification of the reduction in GrC IPSC amplitude and the amplitude of spillover generated by a 50 Hz train (measured 50 ms after the final IPSC).

MF stimulation did not affect the GoC mediated IPSC amplitude (N = 7). It is not clear whether my failure to elicit an mGluR mediated reduction in IPSC amplitude with MF stimulation results from not activating the right glomerulus (i.e. the glomerulus containing the presynaptic GoC axon terminal), not activating enough glomeruli or whether mGluR mediated disinhibition is not in fact MF mediated.

6.4 Discussion

6.4.1 Cholinergic regulation of inhibition in the GrC layer

In accordance with Rossi *et al*. 2003 I found that application of nicotine to the surface of the GrC layer produced an increase in the level of GABAergic inhibition roughly 4 times greater than the resting inhibitory conductance to which GrCs are exposed. This suggests that cholinergic signals could represent a potent means of regulating inhibition in the GrC layer. The increase in inhibition was insensitive to TTX and is thus action potential-independent.

Nicotine-induced GABA release was not significantly blocked by antagonists of typical α4β2 or α7 type nAChRs, nor could it be elicited by choline, a selective agonist of α7 type nAChRs. By contrast, Wall 2003 found a significant reduction (62.5 ± 5 %) in ACh mediated GABA release in the presence of the α4β2 nAChR antagonist DβE. This discrepancy is puzzling especially as a four fold greater concentration of DβE was used in the present study. Both studies used a small sample number (N = 6 above vs N = 4 in Wall 2003).

That a significant proportion of the nicotine induced GABA release was blocked by pancuronium, a blocker of neuromuscular type nAChRs implies that at least part of the effect is likely to be mediated by non-classical central nervous system nAChRs. The cerebellum contains many non-classical nAChRs; Turner and Kellar (2005) reported six, structurally-distinct, heteromeric nAChR populations in the rat cerebellum, including several subtypes that had not been previously encountered. Interestingly nicotine has been shown to induce high-frequency oscillations in the molecular layer of the cerebellar cortex that are partially blocked by pancuronium but not by blockers of α4β2 or α7 type nAChRs (Middleton *et al*. 2008) implying that the two effects might be mediated by a common receptor subtype. Further pharmacological and

immunohistochemical analysis is required to define the receptor subtype involved more specifically.

The GoC is the major inhibitory interneuron in the GrC layer. That nicotine is capable of inducing rapid firing, or dramatic depolarisation coupled with a strong Ca^{2+} signal (under conditions in which action potential firing is blocked; **Fig. 6.2**) in these cells suggests that ACh/nicotine induces GABA release primarily via GoCs. Further, ACh-mediated GABA release is shown to be Ca^{2+}- and vesicle-dependent (Rossi *et a*l. 2003) supporting this assumption, as the only other identified source of GABA in the GrC layer is glial cells which release GABA via Best1 channels, a mechanism that does not involve vesicular release (Lee *et al*. 2010). However, if GoCs are the locus of ACh mediated GABA release it is surprising that bath application of 10 µM nicotine did not affect the CV of GoC–GrC eIPSCs. Nicotine might have been expected to reduce release probability by exhausting the supply of readily releasable vesicles or increase it by increasing the concentration of Ca^{2+} at the presynapse, it is possible that these two effects counteracted each other or that ACh-evoked release is mediated by a different mechanism.

Interestingly, a class of perisomatic-targeting interneurons in the hippocampus have recently been shown to respond to ACh with GABA release in a manner which is action potential-independent but requires the activation of presynaptic T-type Ca^{2+} channels and α3β4 (ganglionic) type nAChRs, further, ACh-evoked synaptic transmission in these cells is regulated differently to typical action potential-dependent transmission (Tang *et al*. 2011). It is possible that GoCs employ a similar mechanism, indeed both α3 and β4 nAChR subunits are expressed in the cerebellum and at the concentrations used (10 µM) pancuronium would be expected to inhibit α3β4 type nAChRs (the IC50 is in the micromolar range; Jonsson *et al*. 2006). This could explain the ability of the ganglionic nAChR blocker hexamethonium to block nicotine-induced inhibition of PC simple spike firing *in vivo* (de la Garza *et al*. 1987). It is possible, therefore, that the ACh evoked GABA release identified in GoCs may represent a more generalised mechanism. It would be interesting to observe if ACh-evoked GABA release from GoCs is specifically dependent on the activation of α3β4 type nAChRs and presynaptic T-type Ca^{2+} channels.

Given the magnitude of the GABA release in response to a relatively modest puff application of nicotine it is possible that the nicotine is activating a large portion of the GoC network via gap junctions. Indeed, gap junctions have been shown to transmit Ca^{2+} signals (Harris 2007). It would be interesting to test this possibility by observing the effect of gap junction blockers on nicotine-evoked GABA release.

Cholinergic inputs to the cerebellum are known to be scarce (Jaarsma *et al*. 1997). Two types of cholinergic input have been identified: Cholinergic MFs arising from the vestibular nuclei and innervating the nodulus and ventral uvula (Barmack *et al*. 1992a, Barmack *et al*. 1992b) which have been shown to innervate both GrCs and unipolar brush cells. And beaded choline acetyltransferase-immunoreactive fibers which originate in the pedunculopontine tegmental nucleus, the lateral paragigantocellular nucleus, and to a lesser extent the various raphe nuclei. In both the cerebellar cortex and the cerebellar nuclei these fibers run an irregular course and make asymmetric synaptic junctions with small and medium-sized dendritic profiles including those of GoCs (Jaarsma *et al*. 1997). It has also been suggested that a subpopulation of GoCs exist that use ACh as a cotransmitter (Illing 1990; De Lacalle *et al*. 1993).

In accordance with the evidence for a sparse distribution of cholinergic inputs to the cerebellum I had difficulty evoking cholinergic inputs to GoCs. This difficulty may have been compounded by the fact that beaded choline acetyltransferase-immunoreactive fibers run an irregular course in the cerebellar cortex and so are likely to be severed in the slicing procedure.

Two types of putative cholinergic input were identified. The first (N = 2) elicited a large rapid inward current in voltage clamp, the second (N = 1) did not elicit a clear inward current, but rapid stimulation was sufficient to drive a GoC to firing rates of over 50 Hz. Both inputs were blocked by the nicotinic antagonist mecamylamine. It is feasible that the first type of cholinergic input represents the result of a direct cholinergic synaptic input to the GoC while the second type results from spillover of ACh from a cholinergic bouton onto non-synaptic targets on the GoC. Further, the two inputs might arise from different types of cholinergic axons (MF, beaded or GoC). Of course extreme caution must be applied when trying to interpret results from very small data sets.

The apparent rarity of cholinergic inputs to GoCs could feasibly limit their relevance to cerebellar processing; alternatively my inability to detect inputs in significant numbers could be an artefact of my experimental procedure. To date no study has determined the proportion of GoCs that receive cholinergic innervation, if the proportion is truly small it seems surprising that all GoCs tested express nAChRs (as judged by their response to nicotine). Further immunocytochemical analysis would be needed to give a good indication of the true proportion of GoCs contacted by cholinergic fibres. However, as GoCs are networked through gap junction coupling (Dugue *et al*. 2009; Verveake *et al*. 2010) cholinergic inputs may be capable of driving groups of GoCs through a very limited number of inputs.

6.4.2 mGluR mediated regulation of inhibition in the GrC layer

It has been shown that mGluR agonism reduces GABA release from GoCs in juvenile rats. My results show that this mechanism is not a developmental feature and is indeed more pronounced in the young adult rat: 100 µM ACPD elicited a 95 ± 10 % reduction in IPSC amplitude vs 75 ± 5 % in the juvenile rat (Mitchell & Silver 2000). In my hands, 100 µM ACPD also elicited a reduction in the resting GABAergic conductance 187 ± 57 pS, though this effect was not detected in other studies (Rossi *et al*. 2003). ACPD agonises group I and II mGluRs, however agonism of group III mGluRs has also been shown to elicit a modest reduction in GoC-mediated GABA release in the juvenile animal (Mitchell & Silver 2000). These results suggest that mGluRs could play a potent role in modulating inhibition in the GrC layer.

Just as nicotine may increase GABA release from GoCs by enhancing the concentration of Ca^{2+} at the GoC axon terminal, ACPD may reduce GABA release by reducing the concentration of Ca^{2+} at the GoC axon terminal, indeed activation of mGluRs inhibits somatically measured Ca^{2+} influx in dissociated GoCs (Knoflach *et al*. 2001).

It was shown that focal stimulation of MFs in the GrC layer could reduce GABA release (also elicited by focal stimulation in the GrC layer) via the activation of mGluRs (Mitchell & Silver 2000). I tried to replicate this effect using paired recording with careful stimulation of single MFs in the white matter tract but was unable to do so (N = 7). This result could have several explanations: It is possible that the mGluR effect is synapse specific and requires the activation of the MF rosette specifically invaded by

the axon pertaining to the patched presynaptic GoC, in which case the probability of observing an effect in each experiment would be ~ one in four (each GrC having approximately four dendrites), leaving a probability of detecting no effect in seven experiments at ~ 0.13. Alternatively, it is possible that the effect is non-specific and requires the activation of several MFs pertaining to an individual GoC to generate sufficient glutamate spillover. It is also possible that mGluR-mediated disinhibition requires the release of a cofactor which can be elicited through stimulation in the GrC layer, but not the white matter tract. Finally, it is possible that mGluR-mediated disinhibition, rather than being mediated via MFs may, in fact, result from parallel fibre activation which would be triggered by stimulation in the GrC layer but not the white matter tract. Indeed, stimulation of parallel fibres has been shown to hyperpolarise GoCs via the activation of mGluR2 (Watanabe *et al*. 2003). These possibilities could perhaps be disentangled through further paired recordings in conjunction with focal stimulation in different regions of the cerebellar cortex.

The conditions under which mGluR-mediated disinhibition occurs will determine its effect on GrC computation. If the effect is synapse specific then it could serve to exaggerate the impact of high frequency inputs by selectively shutting down inhibition at active MF terminals in a frequency dependent fashion. If this is the case, then the output of a GrC would not be a direct function of the mean MF input rate but would instead depend upon the distribution of activity across its synapses. Alternatively, if the disinhibition is mediated by generalised MF or parallel fibre activity the result would be a non-specific activity dependent disinhibition in the GrC layer. This would be counterintuitive as GoCs have been presumed to constrain excitation in the GrC layer to within a useful dynamic range relative to net MF input (Marr 1969). However, in accord with this possibility increased parallel fibre activity has been shown to reduce GoC firing via an mGluR2 dependent mechanism (Watanabe *et al*. 2003; Holtzman *et al*. 2011). Conversely, if mGluR mediated disinhibition requires the activity of a cofactor, the effect could be quite specific and carefully regulated.

6.5 Conclusions

Inhibition in the GrC layer is subject to modulation and can be increased through the activation of nAChRs and reduced through the activation of mGluRs. Both of these effects appear likely to be mediated by regulating GABA release from the GoC,

however, the exact mechanisms and physiological relevance of these effects requires further study. While the timing of individual GoC–GrC inputs may have precise functional relevance, changes in the level of inhibition induced by modulatory inputs may be quite coarse (both temporally and spatially) and may serve to modify GrC gain, offset and threshold.

Chapter Seven

7. General discussion

I have studied GoC mediated inhibition in the GrC layer of the cerebellar cortex. GrCs integrate sensorimotor (Fine *et al*. 2002) and other types of information (Katz & Steinmetz 2002; Ito 2008; Moulton *et al*. 2010) which they receive via MF inputs. GoCs are the only inhibitory interneuron shown to directly contact GrCs and as such are uniquely placed to regulate the passage of MF information through the GrC layer. I have characterised the GoC–GrC synapse using a combination of focal stimulation and GoC–GrC paired recordings and investigated how different patterns of activity at this synapse can affect synaptic integration in the GrC. I have also investigated how this relationship might be further complicated by the action of neuromodulatory inputs.

7.1 The GoC–GrC synapse

7.1.1 Methodological considerations in characterising a synapse

In **Chapter 3** I investigated the GoC – GrC synapse by looking at spontaneous IPSCs, IPSCs evoked with a stimulating electrode and through paired GoC – GrC recordings. The three methods reveal average IPSCs of markedly different character (**Table 7.1**).

Table 7.1: GoC – GrC IPSCs

	Spontaneous	Evoked	Paired
Amplitude (pS)	948 ± 371	1031 ± 859	270 ± 325
Rise time (ms)	0.21 ± 0.09	0.41 ± 0.27	2.1 ± 3.2
Weighted decay (ms)	8.1 ± 4.3	13 ± 8.6	23 ± 16

Paired recordings gave significantly smaller and slower IPSC waveforms than spontaneously occurring or evoked IPSCs. This is probably because the paired technique allows the controlled sampling of true unitary GoC–GrC inputs (many of which proved to be small spillover inputs) in a way that the other techniques do not.

The frequency-dependence of the synapse also varied between eIPSCs and paired IPSCs. That characterisation of the GoC–GrC synapse using a stimulating electrode produced such different results to paired recordings brings into question the suitability of focal stimulation for synaptic characterisation. The error associated with focal stimulation is likely to be greatest when multiple presynaptic cells contact a single postsynaptic cell, the presynaptic cells of interest have dense overlapping axonal plexuses and/or are connected via gap junctions and unitary input size is small, as is the case for the GoC–GrC input. By contrast only a small number of MFs contact a GrC, the MFs may be reasonably well separated and the unitary MF input size is relatively large (DiGregorio *et al*. 2002) meaning that a stimulating electrode might be a more suitable tool to study activity at this synapse. However, results may still be confounded by an unphysiological depolarisation of the stimulated axon, activation of the surrounding cellular milieu (possibly leading to the release of modulatory transmitters) and increased extracellular K^+ resulting from the depolarisation of neighbouring cells. With regard to the latter two possibilities; pilot experiments have shown that stimulation of the cellular milieu can increase GrC excitability even in the absence of a direct MF input (not shown).

7.1.2 Properties of the GoC–GrC synapse

Paired recordings revealed that individual direct GoC – GrC IPSCs are small, rapidly rising and contain a significant, slow spillover component (**Table 7.1**). An unexpectedly high proportion of connections (36%) were purely spillover-mediated. The prevalence of spillover inputs suggests relevance for cerebellar processing.

The slow nature of the spillover inputs implies that they are poorly suited to conveying temporally precise signals and thus probably act almost purely to set the gain of the GrC response (Crowley *et al*. 2009) in accordance with Marr's initial assertions as to the role of GoC (Marr 1969). The direct component of the IPSC may be more suited to temporally precise tasks. It is interesting to note then that there were examples of post synaptic GrCs receiving different types of input (direct and spillover) from the same presynaptic GoC, feasibly the GoC was conveying precise timing signals to one and a general reflection of network excitability to the other.

That IPSCs undergo marked STD while spillover summates in a rate-dependent fashion implies that when GoC firing is sustained at higher rates the precise timing of IPSCs has decreased relevance; that it is the level and not the timing of inhibition that is significant under conditions of high network activity.

Spillover seems to summate in a linear fashion at individual GoC–GrC synapses but may undergo some form of supralinear boosting if multiple inputs are activated simultaneously. Such a supralinearity may curtail GrC activity more effectively in states of high network activity.

7.2 The effect of activity at the GoC–GrC synapse

The cerebellar cortex has a relatively uniform structure and therefore is likely to have a uniform complement of computational properties throughout (the vestibular cerebellar cortex, which has an enrichment of UBCs, may have slightly different computational properties to the rest of the cerebellar cortex). Differences in the inputs and downstream targets of the cerebellar cortex are therefore likely be responsible for the great number of differing functions ascribed to different regions of the cerebellar cortex (e.g. eyeblink conditioning, the VOR and regulation of balance).

In **Chapters 4** & **5** I investigated how different patterns of GoC activity can affect GrC processing of two extreme types of MF input. Rate-coded MF inputs which give a reliable modulation in their firing relative to some continuous variable (e.g. head velocity in a preferred direction; Arenz *et al*. 2008) and burst-coded MF inputs; rapidly-adapting responses which typically signal the onset of a sensory input (e.g. a whisker deflection; Rancz *et al*. 2007).

I used dynamic clamp and modelling to investigate the effect of different patterns of activity at the GoC synapse on GrC processing of MF input. In these experiments the MF input and GoC input presented to a given GrC were decoupled (one did not affect the other). However, it is not clear that this would be the case *in vivo*, a generalised increase in MF activity might be expected to increase and/or alter the synchrony of GoC activity, indeed most GoCs have been reported to show broad functional tuning (Van Kan *et al*. 1993; Holtzman *et al*. 2006), though some show more narrow response

patterns to only a single modality and/or activity that is not well correlated with that of most surrounding MFs (Van Kan *et al*. 1993; Heine *et al*. 2010). Conversely in the vestibular cerebellum, increased GoC activity might reduce MF input by inhibiting unipolar brush cells (Dugue *et al*. 2005). Without knowing more about the functional connectivity of the GrC layer it is difficult to predict the exact relationship between excitation and inhibition in GrCs (which likely constitutes a spectrum). Nevertheless, decoupling the two elements and testing the effect of different rates and levels of synchrony of GoC activity has allowed me to construct a framework that can be applied when the functional anatomy of the GrC layer is understood in better detail.

7.2.1 The effect of changes in GoC firing rate on GrC computation

As suggested by previous studies (Mitchell & Silver 2003; Crowley *et al*. 2009) altering the rate of GoC firing has a powerful effect on the gain of the GrC I–O function suggesting that GoCs are well suited to maintain GrC activity to within a set dynamic range in the face of widely varying MF input, consistent with Marr's hypothesis (Marr 1969). Though this effect was only demonstrated using rate coded MF input (**Chapter 4.2**) it has been shown elsewhere that increases in GoC firing would have a similar suppressive effect on GrC processing of MF burst inputs (Rothman *et al*. 2010).

Notably, in addition to altering the slope of the GrC I–O function, increased inhibition appeared to reduce the GrC's maximal firing rate. The mechanism responsible for this effect is unclear; however it may be due to a reduction in voltage fluctuations at depolarised potentials (Mitchell & Silver 2003). The shunt of the inhibition could serve to low pass filter (smooth) the excitatory input resulting in less sharp depolarisation and repolarisation (sharp voltage fluctuations are known to facilitate spiking by releasing Na^+ channels from use dependent block). This would reduce spiking under conditions of increased MF input/GrC firing rate where action potential related conductances have a particularly marked control over spiking behaviour. It is not immediately obvious how scaling a GrCs maximal output could be useful to cerebellar processing but it may prevent over excitation when the GrC network is in a highly active state.

7.2.2 The effect of the timing of GoC firing on GrC computation

If GoC inputs serve purely to regulate gain in the face of varying levels of network excitability, then it is not clear why the GoC–GrC input waveform can contain a fast component, indeed spillover alone is quite adequate for this role (as are changes in the level of tonic inhibition; Mitchell & Silver 2003; Crowley *et al*. 2009). That the GoC–GrC input can contain a fast component implies that it must be performing some temporally precise task. However, individual simulated GoC–GrC inputs were not particularly effective at reducing the number or timing of spikes triggered in GrCs by bursts of MF activity (**Chapter 5.4**).

In contrast, bursts of GoC inputs were highly effective at reducing the number of spikes triggered in GrCs by bursts of MF activity (**Chapter 5.5**). Such precisely timed bursts of GoC activity can be triggered by bursts of MF input (Kanichay *et al*. 2008). If cerebellar circuitry is arranged such that the GoC provides feedforward (rather than lateral) inhibition, bursts of MF activity arriving at a GrC would be expected to be shortly followed by a burst of inhibitory input. Previous work in hippocampal pyramidal cells shows that this arrangement can enhance the temporal precision of neuronal spiking (Pouille & Scanziani 2001). I have shown that inhibition arising from near-simultaneous activation of a group of GoCs arriving shortly after an excitatory input would indeed sharpen the GrC response by limiting the window for integration. By contrast if cerebellar circuitry is arranged such that GoCs are providing lateral inhibition to GrCs then bursts of GoC input may come at a variety of times relative to MF input. When arriving in phase with MF input bursts of GoC activity were quite effective at blocking the MF signal and as such could provide an “and not” signal. Feasibly, the relief of inhibition via the silencing of GoCs might play an equally important role in gating MF signals however this question was not directly addressed.

7.2.3 The effect of GoC synchrony on GrC computation

The impact of GoC–GrC inputs may be augmented by synchronisation of the GoC network (Vos *et al*. 1999a; Dugue *et al*. 2009; Verveake *et al*. 2010). I investigated how GrC processing of MF inputs is affected by GoC synchrony.

Interestingly, the level of GoC synchrony does not affect the gain of the GrC I–O function (when measured over at least one inhibitory cycle; **Chapter 4.3**). This implies that the cerebellum may be able to perform rate-coded operations over a slow timescale

without being appreciably perturbed by the level of GoC synchrony. AMPAR/NMDAR excitatory conductances at the parallel fibre-PC synapse vary over a relatively rapid timecourse and as such would be expected to reliably convey rapid oscillations in GrC layer activity, however mGluR conductances at parallel fibre-PC synapse occur over a much slower timescale and as such may not reflect oscillations in the GrC layer occurring in the beta or theta band (Tempia *et al*. 1998).

Inhibitory synchrony can pattern the response of a population of GrCs without need for any inherent synchrony in the MF input (**Chapter 4.3**). This would provide a time variant, feed-forward signal to PCs.

To date there has been limited direct study of how oscillations in the GrC layer might affect overlying PC activity, perhaps in part because of the limited stability of GrC layer oscillations and the complication of other oscillatory elements in the circuit (e.g. the climbing fibre input; Llinás 2011). However, in general PC activity correlates well with that of the underlying GrC layer (Lu *et al*. 2005) as underlying GrCs are favoured with higher connection probability, synaptic weights and lower susceptibility to certain forms of LTD; (Isope & Barbour 2002; Sims & Hartell 2005; Sims & Hartell 2006). Further, it has been shown in the paramedian lobule of the cerebellar cortex in monkeys that during active and passive expectancy the negative phase of the oscillatory local field potential (which is associated with bursts of GrC multiunit activity; Courtemanche *et al*. 2002; Hartmann and Bower 1998) is also associated with an increase in PC simple spike output (though PC activity increases slightly ahead of peak local field potential; Courtemanche *et al*. 2002). Simulations in large network models would be useful to determine the extent to which GrC synchrony can affect PC and in turn DCN output (Gleeson *et al*. 2007).

Oscillatory activity in the GrC layer, if reliably signalled to PCs, may self-perpetuate by triggering oscillations in the DCN which could instigate oscillations in MF and climbing fibre input via excitatory and inhibitory projection neurons, respectively.

7.3 The role of GoC–GrC inhibition in cerebellar processing

GoCs determine the gain and timing of GrC firing in response to MF inputs. The importance of GoC function has been demonstrated by the pharmacological ablation of the majority of the GoC population, which results in severe motor defects. Though these deficits recover to some extent with time, animals lacking GoCs remain impaired at sophisticated motor tasks (Watanabe *et al*. 1998). It is not clear to what extent the deficits resulted from disruption of the gain or timing of inhibition, however, the recovery from severe motor defects was associated with a reduction in the GrC NMDA conductance that may offset overexcitability in the GrC layer associated with GoC loss. Further, mutations that affect the timing of PC simple spike firing without affecting the average rate also result in motor deficits (Hoebeek *et al*. 2005; De Zeeuw *et al*. 2011) implying that the role of the GoC in regulating the timing of simple spikes is likely to be relevant to motor behaviour. Thus the GoC may have multiple computational functions.

7.3.1 GoCs as gain regulators

The Marr-Albus framework specifies that the optimum amount of GrC (and therefore parallel fibre) activity for pattern storage and retrieval is ~ 1% and proposed that GoCs could maintain this level of excitability in the face of widely-varying levels of MF excitation (Marr 1969; Albus 1971). Assuming that GoCs receive feedforward (rather than lateral) MF input, my results show that GoCs are well-suited to adaptively regulate GrC excitability in this way. If however GoCs are providing predominantly lateral inhibition (Kanichay 2008; Jörntell & Ekerot 2006; Heine *et al*. 2010) then they would likely serve to regulate GrC gain relative to context, effectively scaling MF throughput.

Changes in gain have been shown to underlie a range of neuronal computations (Silver 2010). Visual responses in the monkey parietal cortex are scaled relative to head and eye position (Andersen *et al*. 1985; Brotchie *et al*. 1995) allowing a distributed representation of space relative to body-centred coordinates. Such coordinate transforms are necessary for visually-guided reaching (Silver 2010). Gain control could also enable coordinated bimanual action by scaling commands sent to one limb relative to the predicted effect of motor commands to the other limb (Yokoi *et al*. 2011). It is possible that GoCs are mediating complex operations similar to these by scaling GrC activity in the cerebellar cortex.

7.3.2 GoCs as signal decomposers

Adaptive filter models of the cerebellar cortex (e.g. Fujita *et al*. 1982; Medina & Mauk 2000; Lepora *et al*. 2010) typically require that GrCs decompose sensory input to give a complex array of outputs with different characteristic patterns. Although individual GoC–GrC IPSCs do not reliably affect (and therefore reliably complicate the array of) GrC spiking patterns my results suggest that synchronised GoC activity or bursts of GoC activity could act in this regard. GrC responses to fixed excitatory and inhibitory input show great variability (in part due simply to variability in cell capacitance; **Chapter 5.6**) and individual inhibitory inputs vary greatly in magnitude (**Chapter 3**). Even with fixed inhibitory and excitatory input this would generate some variability in GrC responses to a common MF input. However if we consider a population of MFs conveying a noisy signal with varying rates of adaption it is likely that there would be a great deal of variety in GrC responses. GrCs would spike or not depending on the level of GoC-mediated inhibition relative to excitation. As MFs adapt to the stimulus GrCs and GoCs would receive less MF excitation, however the reduction in GoC-mediated inhibition might push other GrCs receiving more slowly-adapting inputs over threshold, thus the GoCs could allow GrCs to respond with variable levels of delay to a sensory input. This picture could be further complicated when we consider that GoCs may be activated via parallel fibre inputs or inhibited via mGluR activation leading to a complex evolving pattern of activity across the GrC layer. Such patterning of GrC responses could explain how the cerebellar cortex is able to learn to give an appropriately delayed response to a MF encoded conditioned stimulus in eyeblink conditioning (Medina & Mauk 2000). In this regard it would be interesting to test if GoC activity patterns triggered in response to sensory stimuli are reliable on a trial-to-trial basis.

7.3.3 GoCs as oscillators

The cerebellum shows a remarkable array of oscillatory activity (e.g. Isope *et al*. 2002; Middleton *et al*. 2008; D'Angelo *et al*. 2009; Ros *et al*. 2009; Llinás 2011), my data show that oscillations in the GoC network (Vos *et al*. 1999; Dugue *et al*. 2009; Verveake *et al*. 2010) could impose oscillatory behaviour on the GrC population which may in turn underlie oscillations in the GrC layer field potential that have been observed *in vivo* (Hartmann & Bower 1998; Courtemanche *et al*. 2002; Courtemanche & Lamarre

2005; Dugue *et al*. 2009). The presence of such oscillatory activity is not easily explained by either the Marr-Albus (Marr 1969; Albus 1971) or adaptive filter frameworks (Fujita *et al*. 1982), however, they do not preclude these models from explaining cerebellar behaviours firstly because, as shown (**Chapter 4.3**), the presence of oscillations in the GrC layer does not affect GrC gain and therefore may not interfere with rate-coded tasks and secondly because it is not clear that synchrony persists in the presence of the active motor behaviours to which these models have been applied (Pellerin & Lamarre 1997; Hartmann & Bower 1998).

Oscillations in the GrC layer have been proposed to reflect a baseline clocking system important for the temporal segmentation of incoming data (Hartmann & Bower 1998) and/or to promote communication with other brain regions entrained to similar frequencies such as the sensorimotor cortex (O'Connor *et al*. 2002). With regard to the latter possibility, I have shown that bursts of MF activity are more effectively transmitted when arriving out of phase with synchronised inhibition, but more reliably convey information about the timing of stimulus onset when arriving approximately in phase with or shortly before synchronised inhibition. This is achieved by GoC inhibition selectively eliminating later spikes in the GrC response to MF burst input and thus reducing the GrC burst width and advancing the mean spike time (**Chapter 5.3**).

To date synchrony in the GrC layer has not been shown to persist during the majority of active motor behaviours. Indeed, it has been suggested that desynchronization of oscillations reflects a process of active uncoupling of neural ensembles to allow the emergence of new ensembles, which may be necessary to proceed from one cognitive state or behaviour to another (Rodriguez *et al*. 1999). However it is interesting to note that many voluntary motor behaviours, such as reaching, are characterized by large discontinuities (i.e. steps) in the tremor frequency range (approximately 10 Hz). These discontinuities are coherent with activity in the primary motor cortex (M1) and single unit activity within the DCN (Soteropoulos & Baker 2006). It is possible that these DCN oscillations find their source in the cerebellar cortex and that they exist to synchronise cerebellar output with motor output from other regions to optimise motor timing and coordination.

If GrC layer oscillations do not have an active role in dictating specific motor outputs (or at least the timing thereof) then it is probable that they perform some sensory

function. It is interesting to note that oscillations in the GrC layer persist during whisking in rodents which itself occurs at ~ 10 Hz (though not necessarily in phase with the oscillations; Hartmann & Bower 1998; O'Connor *et al*. 2002; Kleinfeld *et al*. 2006). Oscillations in the GrC layer of the paramedian lobe in monkey were strongest when the animal was actively expecting a stimulus that would signal the initiation of some motor activity (Courtemanche *et al*. 2002). It is possible that the oscillations exist to increase the sensitivity of the cerebellar cortex to sensory input (Singer & Gray 1995). Oscillations in the cerebellar cortex are well correlated with oscillations in the sensory cortex and most strongly when the animal is preparing for a motor output in response to some signal (O'Connor *et al*. 2002; Courtemanche *et al*. 2005). My results show that the timing of a burst of MF activty relative to the phase of inhibition can serve to diminish or augment a GrC's output. Oscillatory activity in the GrC layer may serve to sensitise the cerebellar cortex to appropriately timed direct sensory and cortical input.

7.4 Modulation of inhibition in the cerebellar GrC layer

Neuromodulatory inputs can alter the relationship between excitation, inhibition and GrC activity and may alter the functional state of cerebellar microzones (Schweighofer *et al*. 2004). I have investigated two types of input in the cerebellar cortex that may modulate GoC mediated inhibition.

7.4.1 Cholinergic regulation of inhibition

My data suggests that activation of an atypical population of nAChRs on GoCs can dramatically augment their inhibitory output via an action potential independent mechanism (**Chapter 6.2**). This is an interesting pharmacological observation, however, it is not clear what role cholinergic inputs could play in the cerebellar cortex *in vivo*. Cholinergic inputs to the cerebellar cortex are sparse (Jaarsma *et al*. 1997) and if they reliably activate GoCs, may do so in a fashion that is different from the GoC response to puff application of nicotine. If these inputs elicit strong activation of GoCs then their scarcity may not be problematic as excitation may propagate via gap junctions. However, to date there has been no observation of physiological effects akin to those mediated by nicotine application *in vivo* either by way of a very dramatic GoC depolarisation or a slow and substantial increase in the inhibitory conductance experienced by GrCs.

If ACh-evoked enhancement of inhibition does occur *in vivo* it may be linked to very specific behavioural states. Choline acetlytransferase-immunoreactive fibers originate from the pedunculopontine tegmental nucleus, the lateral paragigantocellular nucleus, and to a lesser extent in various raphe nuclei all of which have been linked to attention and sleep (Kobayashi & Isa 2002; Dergacheva *et al*. 2010; Smythies 1997).

Increased cholinergic input to the GrC layer during attention would likely cause a dramatic increase in inhibitory conductance in the GrC layer that would restrict the passage of MF information. It is possible that this increase in inhibition may reduce noise and help sparsify the MF input (both of which may be important to cerebellar function; Marr 1969). This could be particularly useful as attention may elicit an increase in input to the cerebellar cortex much of which may be non task related.

It is feasible that ACh-mediated inhibition could shut down cerebellar activity during sleep to conserve energy. However, slow wave oscillations persist in the GrC layer during sleep and are phase locked to activity in the DCN and the cerebral cortex (Ros *et al*. 2009; Rowland *et al*. 2010). Further, the pedunculopontine tegmental nucleus and lateral paragigantocellular nucleus are most heavily active during paradoxical sleep (characterised by rapid eye movement; Verret *et al*. 2005) during which activity in the cerebellar cortex is increased (Andre & Arrighi 2003). Thus again it seems likely that they would be acting to sparsify input and decrease noise during paradoxical sleep.

The function of paradoxical sleep is not well understood, but it has been linked to the consolidation of memory (Diekelmann & Born 2010). Sleep has also been shown to improve motor learning in the cerebellum (Walker *et al*. 2005; Maquet *et al*. 2003). Feasibly cholinergic inputs could play some role in the consolidation of motor learning during sleep.

Cholinergic inputs to the cerebellum do not exclusively target GoCs; cholinergic MFs are thought to also target GrCs and unipolar brush cells while diffuse, beaded, choline acetlytransferase-immunoreactive fibres run an irregular course traversing all layers of the cerebellar cortex and have been shown to contact molecular layer interneurons (Jaarsma *et al*. 1997). ACh has been shown to enhance the activity and synchrony of molecular layer interneurons (de la Garza *et al*. 1987; Middleton *et al*. 2008) decrease

simple spike firing in PCs (via a mixed nicotinic and muscarinic mechanism; de la Garza *et al*. 1987) and enhance PC responses to glutamate via a muscarinic mechanism (Andre *et al*. 1993). Taken together these findings further imply that cholinergic inputs to the cerebellum serve to increase the filtering of MF inputs, but may enhance the impact of signals which are sufficiently potent to pass the GrC layer filter, thereby enhancing pattern selectivity.

7.4.2 mGluR mediated regulation of inhibition

Activation of mGluRs by glutamate spillover represents a very different type of modulatory signal to that conveyed by cholinergic inputs in that it is likely to be inextricably linked to the dominant form of signalling in the cerebellar cortex, i.e. it is dependent on the level of MF activity, rather than some extraneous input.

I have built on previous results published in our lab (Mitchell & Silver 2000) showing that activation of mGluRs can reduce the magnitude of GoC–GrC inputs in the juvenile rat. I show that mGluR-mediated disinhibition persists and is more pronounced in the young adult and that mGluR activation can also reduce the level of tonic inhibition to which GrCs are subject. The level of disinhibition achieved by application of the group I and II mGluR agonist ACPD suggests that mGluR activity could have a dramatic impact on GrC computation. In the juvenile synapse, endogenously released glutamate had only a slightly smaller magnitude of effect than ACPD application and there is no reason to believe that this would not be the case in the adult.

A clear computational consequence of mGluR mediated disinhibition is to confer high pass filtering characteristics on the GrC layer, as an increase in excitation above a certain threshold will suppress inhibition further increasing the chance of the excitatory signal to evoke firing. The GrC layer has been proposed to act as a high pass filter by others (Solinas *et al*. 2010). Interestingly, however, mGluR mediated disinhibition occurs over a timecourse of several hundred milliseconds (Mitchell & Silver 2000) meaning that, were disinhibition evoked by a burst of MF activity, the maximal suppression of inhibition would occur after the burst had finish. This raises the possibility that disinhbition serves as a means of sensitising GrCs to subsequent inputs and may act to increase the impact of persistent or repetitive stimuli.

The specific computational consequences of mGluR mediated disinhibition are likely to depend on the precise locus of and activity dependence/timecourse of the effect, none of which could be ascertained in my experiments.

If disinhibition occurs in a synapse specific fashion, i.e. rapid firing of a MF shuts down inhibition at all of its glomeruli then it would confer additional non-linear properties on GrC computation. GrC firing would not represent a clear function relating to the amount of excitatory conductance arriving from each of its MF synapses, as double the amount of charge arriving through half the number of MFs would result in a higher rate of firing due to the reduction in inhibitory conductance at those synapses. If, by contrast, mGluR mediated disinhibition requires the activation of multiple MFs or is parallel fibre mediated then it is likely to exert an effect on all of the GoC–GrC connections made by a given GoC resulting in a much less specific decrease in network inhibition similar to the effect of decreases in GoC excitability that have been reported in response to mGluR activation at parallel fibre synapses (Watanabe *et al*. 2003; Holtzmann *et al*. 2011).

7.5 Summary

I have characterised the GoC–GrC synapse and show that individual GoC–GrC inputs are smaller and more frequently mediated purely by spillover than previously realised. Previous overestimates of GoC–GrC input magnitude are likely to arise from the non – specific activation of GoC axons with focal stimulation.

The GoC is a suitable device to regulate the gain of the GrC I–O function in accordance with predictions of the Marr-Albus framework, however synchronised GoC activity and/or bursts of GoC activity may also provide precise temporal signals that may be useful to cerebellar processing. Individual GoC–GrC inputs may convey temporal signals though with very poor efficacy/reliability.

Cholinergic inputs to the cerebellum may sparsify MF signals by activating nAChRs expressed on GoCs and eliciting an increase in the level of inhibition in the GrC layer. By contrast, rapid MF input may activate mGluRs on GoCs leading to a reduction in the level of inhibition and conferring high pass filtering characteristics on the GrC layer, however, the specificity of this high pass filter remains to be determined.

Bibliography

Albus JS. (1971) A theory of cerebellar function. Math. Biosci. **10**: 25-61.

Andersen RA, Essick GK, Siegel RM. (1985) Encoding of spatial location by posterior parietal neurons. Science **230**, 456-458.

Andre P, Arrighi P. (2003) Hipnic modulation of cerebellar information processing: implications for the cerebro-cerebellar dialogue. Cerebellum. **2**: 84-95.

Andre P, Pompeiano O, White SR. (1993) Activation of muscarinic receptors induces a long-lasting enhancement of Purkinje cell responses to glutamate. Brain Res. **617**: 28-36.

Apps R, Garwicz M. (2005) Anatomical and physiological foundations of cerebellar information processing. Nat Rev Neurosci. **6**: 297-311.

Apps R, Hawkes R. (2009) Cerebellar cortical organization: a one-map hypothesis. Nat Rev Neurosci. **10**: 670-81.

Arenz A, Bracey EF, Margrie TW. (2009) Sensory representations in cerebellar granule cells. Curr Opin Neurobiol. **19**: 445-51.

Arenz A, Silver RA, Schaefer AT, Margrie TW. (2008) The contribution of single synapses to sensory representation in vivo. Science. **321**: 977-80.

Armano S, Rossi P, Taglietti V, D'Angelo E. (2000) Long-term potentiation of intrinsic excitability at the mossy fiber-granule cell synapse of rat cerebellum. J Neurosci. **20**: 5208-16.

Baca SM, Marin-Burgin A, Wagenaar DA, Kristan WB Jr. (2008) Widespread inhibition proportional to excitation controls the gain of a leech behavioral circuit. Neuron. **57**: 276-89.

Barmack NH. (2003) Central vestibular system: vestibular nuclei and posterior cerebellum. Brain Res Bull. **60**: 511-41

Barmack NH, Baughman RW, Eckenstein FP, Shojaku H. (1992a) Secondary vestibular cholinergic projection to the cerebellum of rabbit and rat as revealed by choline acetyltransferase immunohistochemistry, retrograde and orthograde tracers. J Comp Neurol. **317**: 250-70.

Barmack NH, Baughman RW, Eckenstein FP. (1992b) Cholinergic innervation of the cerebellum of the rat by secondary vestibular afferents. Ann N Y Acad Sci. **656**: 566-79.

Barmack NH, Yakhnitsa V. (2008) Functions of interneurons in mouse cerebellum. J Neurosci. **28**: 1140-52.

Bell CC. (2002) Evolution of cerebellum-like structures. Brain Behav Evol. **59**: 312-26.

Bengtsson F, Jörntell H. (2009) Sensory transmission in cerebellar granule cells relies on similarly coded mossy fiber inputs. Proc Natl Acad Sci U S A. **106**: 2389-94.

Bower JM. (2002) The organization of cerebellar cortical circuitry revisited: implications for function. Ann N Y Acad Sci. **978**: 135-55.

Braitenberg V, Atwood RP. (1958) Morphological observations on the cerebellar cortex. J Comp Neurol. **109**: 1-33.

Brickley SG, Cull-Candy SG, Farrant M. (1996) Development of a tonic form of synaptic inhibition in rat cerebellar granule cells resulting from persistent activation of GABAA receptors. J Physiol. **497**: 753-9.

Brickley SG, Farrant M, Swanson GT, Cull-Candy SG. (2001) CNQX increases GABA-mediated synaptic transmission in the cerebellum by an AMPA/kainate receptor-independent mechanism. Neuropharmacology. **41**: 730-6.

Bright DP, Renzi M, Bartram J, McGee TP, MacKenzie G, Hosie AM, Farrant M, Brickley SG. (2011) Profound desensitization by ambient GABA limits activation of δ-containing GABAA receptors during spillover. J Neurosci. **31**: 753-63.

Brotchie PR, AndersenRA, Snyder LH, Goodman SJ. (1995) Head position signals used by parietal neurons to encode locations of visual stimuli. Nature **375**: 232-235.

Bureau I, Dieudonné S, Coussen F, Mulle C. (2000) Kainate receptor-mediated synaptic currents in cerebellar Golgi cells are not shaped by diffusion of glutamate. Proc Natl Acad Sci U S A. **97**: 6838-43.

Cajal S. (1894) The Croonian Lecture. La fine structure des centres nerveux. Proc R Soc Lond. B. **55**: 444-68.

Cajal S. (1911) Histologie du sistéme nerveux de l'homme et des vertebras (transl, Azoulay L). vol 2: Maloine, Paris.

Carta M, Mameli M, Valenzuela CF. (2004) Alcohol enhances GABAergic transmission to cerebellar granule cells via an increase in Golgi cell excitability. J Neurosci. **24**: 3746-51.

Cathala L, Misra C, Cull-Candy S. (2000) Developmental profile of the changing properties of NMDA receptors at cerebellar mossy fiber-granule cell synapses. J Neurosci. **20**: 5899-905.

Cathala L, Brickley S, Cull-Candy S, Farrant M. (2003) Maturation of EPSCs and intrinsic membrane properties enhances precision at a cerebellar synapse. J Neurosci. **23**: 6074-85.

Chadderton P, Margrie TW, Häusser M. (2004) Integration of quanta in cerebellar granule cells during sensory processing. Nature. **428**: 856-60.

Chiu CS, Brickley S, Jensen K, Southwell A, Mckinney S, Cull-Candy S, Mody I, Lester HA. (2005) GABA transporter deficiency causes tremor, ataxia, nervousness, and increased GABA-induced tonic conductance in cerebellum. J Neurosci. **25**: 3234-45.

Courtemanche R, Chabaud P, Lamarre Y. (2009) Synchronization in primate cerebellar granule cell layer local field potentials: basic anisotropy and dynamic changes during active expectancy. Front Cell Neurosci. **3**: Article 6.

Courtemanche R, Lamarre Y. (2005) Local field potential oscillations in primate cerebellar cortex: synchronization with cerebral cortex during active and passive expectancy. J Neurophysiol. **93**: 2039-52.

Courtemanche R, Pellerin JP, Lamarre Y. (2002) Local field potential oscillations in primate cerebellar cortex: modulation during active and passive expectancy. J Neurophysiol. **88**: 771-82.

Crowley JJ, Fioravante D, Regehr WG. (2009) Dynamics of fast and slow inhibition from cerebellar golgi cells allow flexible control of synaptic integration. Neuron. **63**: 843-53.

D'Angelo E, De Filippi G, Rossi P, Taglietti V. (1995) Synaptic excitation of individual rat cerebellar granule cells in situ: evidence for the role of NMDA receptors. J Physiol. **484**: 397-413.

D'Angelo E, Nieus T, Maffei A, Armano S, Rossi P, Taglietti V, Fontana A, Naldi G. (2001) Theta-frequency bursting and resonance in cerebellar granule cells: experimental evidence and modeling of a slow k+-dependent mechanism. J Neurosci. **21**: 759-70.

D'Angelo E, Rossi P, Armano S, Taglietti V. (1999) Evidence for NMDA and mGlu receptor-dependent long-term potentiation of mossy fiber-granule cell transmission in rat cerebellum. J Neurophysiol. **81**: 277-87.

D'Errico A, Prestori F, D'Angelo E. (2009) Differential induction of bidirectional long-term changes in neurotransmitter release by frequency-coded patterns at the cerebellar input. J Physiol. **587**: 5843-57

De Camilli P, Miller PE, Levitt P, Walter U, Greengard P. (1984) Anatomy of cerebellar Purkinje cells in the rat determined by a specific immunohistochemical marker. Neuroscience. **11**: 761-817.

de la Garza R, Bickford-Wimer PC, Hoffer BJ, Freedman R. (1987) Heterogeneity of nicotine actions in the rat cerebellum: an in vivo electrophysiologic study. J Pharmacol Exp Ther. **240**: 689-95.

de Lacalle S, Hersh LB, Saper CB. (1993) Cholinergic innervation of the human cerebellum. J Comp Neurol. **328**: 364-76.

De Schutter E, Steuber V. (2009) Patterns and pauses in Purkinje cell simple spike trains: experiments, modeling and theory. Neuroscience. **162**: 816-26.

De Zeeuw CI, Hoebeek FE, Bosman LW, Schonewille M, Witter L, Koekkoek SK. (2011) Spatiotemporal firing patterns in the cerebellum. Nat Rev Neurosci. **12**: 327-44.

De Zeeuw CI, Yeo CH. (2005) Time and tide in cerebellar memory formation. Curr Opin Neurobiol. **15**: 667-74.

Dean P, Porrill J. (2011) Evaluating the adaptive-filter model of the cerebellum. J Physiol. **589**: 3459-70.

Dean P, Porrill J, Ekerot CF, Jörntell H. (2010) The cerebellar microcircuit as an adaptive filter: experimental and computational evidence. Nat Rev Neurosci. **11**: 30-43.

Dean I, Robertson SJ, Edwards FA. (2003) Serotonin drives a novel GABAergic synaptic current recorded in rat cerebellar purkinje cells: a Lugaro cell to Purkinje cell synapse. J Neurosci. **23**: 4457-69.

Dergacheva O, Wang X, Lovett-Barr MR, Jameson H, Mendelowitz D. (2010) The lateral paragigantocellular nucleus modulates parasympathetic cardiac neurons: a mechanism for rapid eye movement sleep-dependent changes in heart rate. J Neurophysiol. **104**: 685-94.

Diekelmann S, Born J. (2010) The memory function of sleep. Nat Rev Neurosci. **11**: 114-26.

Dieudonné S. (1998) Submillisecond kinetics and low efficacy of parallel fibre-Golgi cell synaptic currents in the rat cerebellum. J Physiol. **510**: 845-66.

Dieudonné S, Dumoulin A. (2000) Serotonin-driven long-range inhibitory connections in the cerebellar cortex. J Neurosci. **20**: 1837-48.

DiGregorio DA, Nusser Z, Silver RA. (2002) Spillover of glutamate onto synaptic AMPA receptors enhances fast transmission at a cerebellar synapse. Neuron. **35**: 521-33

Diño MR, Nunzi MG, Anelli R, Mugnaini E. (2000) Unipolar brush cells of the vestibulocerebellum: afferents and targets. Prog Brain Res. **124**: 123-37.

Diño MR, Willard FH, Mugnaini E. (1999) Distribution of unipolar brush cells and other calretinin immunoreactive components in the mammalian cerebellar cortex. J Neurocytol. **28**: 99-123.

Dugué GP, Brunel N, Hakim V, Schwartz E, Chat M, Lévesque M, Courtemanche R, Léna C, Dieudonné S. (2009) Electrical coupling mediates tunable low-frequency oscillations and resonance in the cerebellar Golgi cell network. Neuron. **61**: 126-39.

Dugué GP, Dumoulin A, Triller A, Dieudonné S. (2005) Target-dependent use of co-released inhibitory transmitters at central synapses. J Neurosci. **25**: 6490-8.

Dumoulin A, Triller A, Dieudonné S. (2001) IPSC kinetics at identified GABAergic and mixed GABAergic and glycinergic synapses onto cerebellar Golgi cells. J Neurosci. **21**: 6045-57.

Eccles J, Llinas R, Sasaki K. (1964) Golgi cell inhibition in the cerebellar cortex. Nature. **204**: 1265-6.

Eccles JC, Ito M, Szentagothai J. (1967) The Cerebellum as a Neuronal Machine. Springer - Verlag.

Economo MN, Fernandez FR, White JA. (2010) Dynamic clamp: alteration of response properties and creation of virtual realities in neurophysiology. J Neurosci. **30**: 2407-13.

Edgley SA, Lidierth M. (1987) The discharges of cerebellar Golgi cells during locomotion in the cat. J Physiol. **392**: 315-32.

Ekerot CF, Jörntell H. (2008) Synaptic integration in cerebellar granule cells. Cerebellum. **7**: 539-41.

Farrant M, Nusser Z. (2005) Variations on an inhibitory theme: phasic and tonic activation of GABA(A) receptors. Nat Rev Neurosci. **6**: 215-29.

Fine EJ, Ionita CC, Lohr L. (2002) The history of the development of the cerebellar examination. Semin Neurol. **22**: 375-84.

Fitzgerald MJT, Folan-Curran J. (2002) Clinical neuroanatomy and related neuroscience. W. B. Saunders.

Forti L, Cesana E, Mapelli J, D'Angelo E. (2006) Ionic mechanisms of autorhythmic firing in rat cerebellar Golgi cells. J Physiol. **574**: 711-29.

Fredette BJ, Mugnaini E. (1991) The GABAergic cerebello-olivary projection in the rat. Anat Embryol (Berl). **184**: 225-43.

Fujita M. (1982) Adaptive filter model of the cerebellum. Biol Cybern. **45**: 195-206.

Gabbiani F, Midtgaard J, Knöpfel T. (1994) Synaptic integration in a model of cerebellar granule cells. J Neurophysiol. **72**: 999-1009

Gad YP, Anastasio TJ. (2010) Simulating the shaping of the fastigial deep nuclear saccade command by cerebellar Purkinje cells. Neural Netw. **23**: 789-804.

Galliano E, Mazzarello P, D'Angelo E. (2010) Discovery and rediscoveries of Golgi cells. J Physiol. **588**: 3639-55.

Garwicz M, Jorntell H, Ekerot CF. (1998) Cutaneous receptive fields and topography of mossy fibres and climbing fibres projecting to cat cerebellar C3 zone. J Physiol. **512**: 277-93.

Gleeson P, Steuber V, Silver RA. (2007) neuroConstruct: a tool for modeling networks of neurons in 3D space. Neuron. **54**: 219-35.

Glickstein M, Doron K. (2008) Cerebellum: connections and functions. Cerebellum. **7**: 589-94.

Golgi C. (1874) Sulla fina anatomia del cervelletto umano. Archivio Italiano per le Malattie Nervose **2**: 90-107.

Golgi C. (1883) Sulla fina anatomia degli organi centrali del sistema nervoso IV. Sulla fina anatomia delle circonvoluzioni cerebellari. Riv Sper Freniatr Med Leg Alien Ment. **9**: 1-17.

Hamann M, Rossi DJ, Attwell D. (2002) Tonic and spillover inhibition of granule cells control information flow through cerebellar cortex. Neuron. **33**: 625-33.

Hámori J, Szentágothai J. (1966) Identification under the electron microscope of climbing fibers and their synaptic contacts. Exp Brain Res. **1**: 65-81.

Hámori J, Szentágothai J. (1968) Identification of synapses formed in the cerebellar cortex by Purkinje axon collaterals: an electron microscope study. Exp Brain Res. **5**: 118-28.

Hámori J, Takács J. (1989) Two types of GABA-containing axon terminals in cerebellar glomeruli of cat: an immunogold-EM study. Exp Brain Res. **74**: 471-9.

Hámori J, Takács J, Petrusz P. (1990) Immunogold electron microscopic demonstration of glutamate and GABA in normal and deafferented cerebellar cortex: correlation between transmitter content and synaptic vesicle size. J Histochem Cytochem. **38**: 1767-77.

Harris AL. (2007) Connexin channel permeability to cytoplasmic molecules. Prog Biophys Mol Biol. **94**: 120-43.

Hartell NA. (2002) Parallel fiber plasticity. Cerebellum. **1**: 3-18.

Hartmann MJ, Bower JM. (1998) Oscillatory activity in the cerebellar hemispheres of unrestrained rats. J Neurophysiol. **80**: 1598-604.

Harvey SC, Maddox FN, Luetje CW. (1996) Multiple determinants of dihydro-beta-erythroidine sensitivity on rat neuronal nicotinic receptor alpha subunits. J Neurochem. **67**: 1953-9.

Harvey RJ, Napper RM. (1991) Quantitative studies on the mammalian cerebellum. Prog Neurobiol. **36**: 437-63.

Heck D, Borst A, Antkowiak B. (2003) Passive spatial and temporal integration of excitatory synaptic inputs in cerebellar Purkinje cells of young rats. Neurosci Lett. **341**: 79-83.

Heine SA, Highstein SM, Blazquez PM. (2010) Golgi cells operate as state-specific temporal filters at the input stage of the cerebellar cortex. J Neurosci. **30**: 17004-14.

Herold S, Hecker C, Deitmer JW, Brockhaus J. (2005) alpha1-Adrenergic modulation of synaptic input to Purkinje neurons in rat cerebellar brain slices. J Neurosci Res. **82**: 571-9.

Hirono M, Obata K. (2006) Alpha-adrenoceptive dual modulation of inhibitory GABAergic inputs to Purkinje cells in the mouse cerebellum. J Neurophysiol. **95**: 700-8.

Hoebeek FE, Stahl JS, van Alphen AM, Schonewille M, Luo C, Rutteman M, van den Maagdenberg AM, Molenaar PC, Goossens HH, Frens MA, De Zeeuw CI. (2005) Increased noise level of purkinje cell activities minimizes impact of their modulation during sensorimotor control. Neuron. **45**: 953-65.

Holtzman T, Sivam V, Zhao T, Frey O, van der Wal PD, de Rooij NF, Dalley JW, Edgley SA. (2011) Multiple extra-synaptic spillover mechanisms regulate prolonged activity in cerebellar Golgi cell-granule cell loops. J Physiol. **589**: 3837-54.

Holtzman T, Mostofi A, Phuah CL, Edgley SA. (2006b) Cerebellar Golgi cells in the rat receive multimodal convergent peripheral inputs via the lateral funiculus of the spinal cord. J Physiol. **577**: 69-80.

Holtzman T, Rajapaksa T, Mostofi A, Edgley SA. (2006a) Different responses of rat cerebellar Purkinje cells and Golgi cells evoked by widespread convergent sensory inputs. J Physiol. **574**: 491-507.

Houston CM, Bright DP, Sivilotti LG, Beato M, Smart TG. (2009) Intracellular chloride ions regulate the time course of GABA-mediated inhibitory synaptic transmission. J Neurosci. **29**: 10416-23.

Huang CM, Huang RH. (1998) Measuring parallel fiber length in the rat cerebellum. Brain Res. **801**: 211-5.

Illing RB. (1990) A subtype of cerebellar Golgi cells may be cholinergic. Brain Res. **522**: 267-74.

Isope P, Barbour B. (2002) Properties of unitary granule cell-->Purkinje cell synapses in adult rat cerebellar slices. J Neurosci. **22**: 9668-78.

Isope P, Dieudonné S, Barbour B. (2002) Temporal organization of activity in the cerebellar cortex: a manifesto for synchrony. Ann N Y Acad Sci. **978**: 164-74.

Ito M. (2001) Cerebellar long-term depression: characterization, signal transduction, and functional roles. Physiol Rev. **81**: 1143-95.

Ito M. (2006) Cerebellar circuitry as a neuronal machine. Prog Neurobiol. **78**: 272-303.

Ito M. (2008) Control of mental activities by internal models in the cerebellum. Nat Rev Neurosci. **9**: 304-13.

Ito M. (2009) Functional roles of neuropeptides in cerebellar circuits. Neuroscience. **162**: 666-72

Ito M, Sakurai M, Tongroach P. (1982) Climbing fibre induced depression of both mossy fibre responsiveness and glutamate sensitivity of cerebellar Purkinje cells. J Physiol. **324**: 113-34.

Jaarsma D, Diño MR, Cozzari C, Mugnaini E. (1996) Cerebellar choline acetyltransferase positive mossy fibres and their granule and unipolar brush cell targets: a model for central cholinergic nicotinic neurotransmission. J Neurocytol. **25**: 829-42.

Jaarsma D, Ruigrok TJ, Caffé R, Cozzari C, Levey AI, Mugnaini E, Voogd J. (1997) Cholinergic innervation and receptors in the cerebellum. Prog Brain Res. **114**: 67-96.

Jacobson GA, Rokni D, Yarom Y. (2008) A model of the olivo-cerebellar system as a temporal pattern generator. Trends Neurosci. **31**: 617-25.

Jakab RL, Hámori J. (1988) Quantitative morphology and synaptology of cerebellar glomeruli in the rat. Anat Embryol (Berl). **179**: 81-8.

Jarvis MR, Mitra PP. (2001) Sampling properties of the spectrum and coherency of sequences of action potentials. Neural Comput. **13**: 717-49.

Jedlicka P, Deller T, Gutkin BS, Backus KH. (2011) Activity-dependent intracellular chloride accumulation and diffusion controls GABA(A) receptor-mediated synaptic transmission. Hippocampus. **21**: 885-98.

Jonsson M, Gurley D, Dabrowski M, Larsson O, Johnson EC, Eriksson LI. (2006) Distinct pharmacologic properties of neuromuscular blocking agents on human neuronal nicotinic acetylcholine receptors: a possible explanation for the train-of-four fade. Anesthesiology. **105**: 521-33.

Jörntell H, Bengtsson F, Schonewille M, De Zeeuw CI. (2010) Cerebellar molecular layer interneurons - computational properties and roles in learning. Trends Neurosci. **33**: 524-32.

Jörntell H, Ekerot CF. (2002) Reciprocal bidirectional plasticity of parallel fiber receptive fields in cerebellar Purkinje cells and their afferent interneurons. Neuron. **34**: 797-806.

Jörntell H, Ekerot CF. (2006) Properties of somatosensory synaptic integration in cerebellar granule cells in vivo. J Neurosci. **26**: 11786-97.

Kanichay R. (2008) Feed-forward excitation of interneurons in the cerebellar granule cell layer. Unpublished thesis (PhD), University of London.

Kanichay RT, Silver RA. (2008) Synaptic and cellular properties of the feedforward inhibitory circuit within the input layer of the cerebellar cortex. J Neurosci. **28**: 8955-67.

Kaneda M, Farrant M, Cull-Candy SG. (1995) Whole-cell and single-channel currents activated by GABA and glycine in granule cells of the rat cerebellum. J Physiol. **485**: 419-35.

Katz DB, Steinmetz JE. (2002) Psychological functions of the cerebellum. Behav Cogn Neurosci Rev. **1**: 229-41.

Kelly RM, Strick PL. (2003) Cerebellar loops with motor cortex and prefrontal cortex of a nonhuman primate. J Neurosci. **23**: 8432-44

Kim YS, Shin JH, Hall FS, Linden DJ. (2009) Dopamine signaling is required for depolarization-induced slow current in cerebellar Purkinje cells. J Neurosci. **29**: 8530-8.

Kleinfeld D, Ahissar E, Diamond ME. (2006) Active sensation: insights from the rodent vibrissa sensorimotor system. Curr Opin Neurobiol. **16**: 435-44.

Knoflach F, Woltering T, Adam G, Mutel V, Kemp JA. (2001) Pharmacological properties of native metabotropic glutamate receptors in freshly dissociated Golgi cells of the rat cerebellum. Neuropharmacology. **40**: 163-9.

Kobayashi Y, Isa T. (2002) Sensory-motor gating and cognitive control by the brainstem cholinergic system. Neural Netw. **15**: 731-41.

Kondo S, Marty A. (1998) Synaptic currents at individual connections among stellate cells in rat cerebellar slices. J Physiol. **509**: 221-32.

König P. (1994) A method for the quantification of synchrony and oscillatory properties of neuronal activity. J Neurosci Methods **54**: 31-7.

Lainé J, Axelrad H. Lugaro cells target basket and stellate cells in the cerebellar cortex. Neuroreport. **9**: 2399-403.

Lang EJ, Sugihara I, Llinás R. (2006) Olivocerebellar modulation of motor cortex ability to generate vibrissal movements in rat. J Physiol. **571**: 101-20.

Langer T, Fuchs AF, Scudder CA, Chubb MC. (1985) Afferents to the flocculus of the cerebellum in the rhesus macaque as revealed by retrograde transport of horseradish peroxidase. J Comp Neurol. **235**: 1-25.

Larramendi LM, Lemkey-Johnston N. (1970) The distribution of recurrent Purkinje collateral synapses in the mouse cerebellar cortex: an electron microscopic study. J Comp Neurol. **138**: 451-9.

Latham A, Paul DH. (1971) Spontaneous activity of cerebellar Purkinje cells and their responses to impulses in climbing fibres. J Physiol. **213**: 135-56.

Le Guen MC, De Zeeuw CI. (2010) Presynaptic plasticity at cerebellar parallel fiber terminals. Funct Neurol. **25**: 141-51.

Lee S, Yoon BE, Berglund K, Oh SJ, Park H, Shin HS, Augustine GJ, Lee CJ. (2010) Channel-mediated tonic GABA release from glia. Science. **330**: 790-6.

Lepora NF, Porrill J, Yeo CH, Dean P. (2010) Sensory prediction or motor control? Application of marr-albus type models of cerebellar function to classical conditioning. Front Comput Neurosci. **4**: Article 140.

Llinás RR. (2011) Cerebellar motor learning versus cerebellar motor timing: the climbing fibre story. J Physiol. **589**: 3423-32.

Lugaro, E. (1894) Sulle connessioni tra gli elementi nervosi della corteccia cerebellare con considerazioni generali sul significato fisiologico dei rapporti tra gli elementi nervosi. Riv Sper Fren Med Leg. **20**: 297-331.

Ma WJ, Beck JM, Latham PE, Pouget A. (2006) Bayesian inference with probabilistic population codes. Nature Neurosci. **9**: 1432-1438.

Maex R, Vos BP, De Schutter E. (2000) Weak common parallel fibre synapses explain the loose synchrony observed between rat cerebellar golgi cells. J Physiol. **523**: 175-92.

Mameli M, Botta P, Zamudio PA, Zucca S, Valenzuela CF. (2008) Ethanol decreases Purkinje neuron excitability by increasing GABA release in rat cerebellar slices. J Pharmacol Exp Ther. **327**: 910-7.

Mapelli L, Rossi P, Nieus T, D'Angelo E. (2009) Tonic activation of GABAB receptors reduces release probability at inhibitory connections in the cerebellar glomerulus. J Neurophysiol. **101**: 3089-99.

Maquet P, Peigneux P, Laureys S, Boly M, Dang-Vu T, Desseilles M, Cleeremans A. (2003) Memory processing during human sleep as assessed by functional neuroimaging. Rev Neurol (Paris). **159**: 6S27-9.

Marr D. (1969) A theory of cerebellar cortex. J Physiol. **202**: 437-70.

Medina JF, Mauk MD. (2000) Computer simulation of cerebellar information processing. **3** Suppl: 1205-11.

Middleton SJ, Racca C, Cunningham MO, Traub RD, Monyer H, Knöpfel T, Schofield IS, Jenkins A, Whittington MA. (2008) High-frequency network oscillations in cerebellar cortex. Neuron. **58**: 763-74.

Middleton FA, Strick PL. (1997) Dentate output channels: motor and cognitive components. Prog Brain Res. **114**: 553-66.

Miles FA, Fuller JH, Braitman DJ, Dow BM (1980) Long-term adaptive changes in primate vestibuloocular reflex. III. Electrophysiological observations in flocculus of normal monkeys. J Neurophysiol **43**: 1437-1476.

Misra C, Brickley SG, Farrant M, Cull-Candy SG. (2000) Identification of subunits contributing to synaptic and extrasynaptic NMDA receptors in Golgi cells of the rat cerebellum. J Physiol. **524**: 147-62.

Mitchell SJ, Silver RA. (2000) Glutamate spillover suppresses inhibition by activating presynaptic mGluRs. Nature. **404**: 498-502.

Mitchell SJ, Silver RA. (2003) Shunting inhibition modulates neuronal gain during synaptic excitation. Neuron. **38**: 433-45.

Miyata M, Okada D, Hashimoto K, Kano M, Ito M. (1999) Corticotropin-releasing factor plays a permissive role in cerebellar long-term depression. Neuron. **22**: 763-75.

Moulton EA, Elman I, Pendse G, Schmahmann J, Becerra L, Borsook D. (2011) Aversion-related circuitry in the cerebellum: responses to noxious heat and unpleasant images. J Neurosci. **31**: 3795-804.

Mureşan RC, Jurjuţ OF, Moca VV, Singer W, Nikolić D. (2008) The oscillation score: an efficient method for estimating oscillation strength in neuronal activity. J Neurophysiol. **99**: 1333-53.

Nielsen TA, DiGregorio DA, Silver RA. (2004) Modulation of glutamate mobility reveals the mechanism underlying slow-rising AMPAR EPSCs and the diffusion coefficient in the synaptic cleft. Neuron. **42**: 757-71.

O'Connor SM, Berg RW, Kleinfeld D. (2002) Coherent electrical activity between vibrissa sensory areas of cerebellum and neocortex is enhanced during free whisking. J Neurophysiol. **87**: 2137-48.

O'Keefe J, Recce ML. (1993) Phase relationship between hippocampal place units and the EEG theta rhythm. Hippocampus. **3**: 317-30.

Onodera S. (1984) Olivary projections from the mesodiencephalic structures in the cat studied by means of axonal transport of horseradish peroxidase and tritiated amino acids. J Comp Neurol. **227**: 37-49.

Palay SL, Chan-Palay V. (1974) Cerebellar Cortex: Cortex and organisation. Springer-Verlag.

Pathak HR, Weissinger F, Terunuma M, Carlson GC, Hsu FC, Moss SJ, Coulter DA. (2007) Disrupted dentate granule cell chloride regulation enhances synaptic excitability during development of temporal lobe epilepsy. J Neurosci. **27**: 14012-22.

Pellerin JP, Lamarre Y. (1997) Local field potential oscillations in primate cerebellar cortex during voluntary movement. J Neurophysiol. **78**: 3502-7.

Phoka E, Cuntz H, Roth A, Häusser M. (2010) A new approach for determining phase response curves reveals that Purkinje cells can act as perfect integrators. PLoS Comput Biol. **6**: e1000768.

Pouille F, Scanziani M. (2001) Enforcement of temporal fidelity in pyramidal cells by somatic feed-forward inhibition. Science. **293**: 1159-63.

Prsa M, Dash S, Catz N, Dicke PW, Thier P. (2009) Characteristics of responses of Golgi cells and mossy fibers to eye saccades and saccadic adaptation recorded from the posterior vermis of the cerebellum. J Neurosci. **29**: 250-62.

Puia G, Costa E, Vicini S. (1994) Functional diversity of GABA-activated Cl- currents in Purkinje versus granule neurons in rat cerebellar slices. Neuron. **12**: 117-26.

Rancz EA, Ishikawa T, Duguid I, Chadderton P, Mahon S, Häusser M. (2007) High-fidelity transmission of sensory information by single cerebellar mossy fibre boutons. Nature. **450**: 1245-8.

Rochefort C, Arabo A, André M, Poucet B, Save E, Rondi-Reig L. (2011) Cerebellum shapes hippocampal spatial code. Science. **334**: 385-9.

Rodriguez E, George N, Lachaux JP, Martinerie J, Renault B, Varela FJ. (1999) Perception's shadow: long-distance synchronization of human brain activity. Nature. **397**: 430-3.

Ros H, Sachdev RN, Yu Y, Sestan N, McCormick DA. (2009) Neocortical networks entrain neuronal circuits in cerebellar cortex. J Neurosci. **29**: 10309-20.

Rossi DJ, Alford S, Mugnaini E, Slater NT. (1995) Properties of transmission at a giant glutamatergic synapse in cerebellum: the mossy fiber-unipolar brush cell synapse. J Neurophysiol. **74**: 24-42.

Rossi DJ, Hamann M. (1998) Spillover-mediated transmission at inhibitory synapses promoted by high affinity alpha6 subunit GABA(A) receptors and glomerular geometry. Neuron. **20**:783-95.

Rossi DJ, Hamann M, Attwell D. (2003) Multiple modes of GABAergic inhibition of rat cerebellar granule cells. J Physiol. **548**: 97-110.

Rothman JS, Cathala L, Steuber V, Silver RA. (2009) Synaptic depression enables neuronal gain control. Nature. **457**: 1015-8.

Rowland NC, Goldberg JA, Jaeger D. (2010) Cortico-cerebellar coherence and causal connectivity during slow-wave activity. Neuroscience. **166**: 698-711.

Ruigrok TJ. (1997) Cerebellar nuclei: the olivary connection. Prog Brain Res. **114**: 167-92.

Ruigrok TJ, Hensbroek RA, Simpson JI. (2011) Spontaneous activity signatures of morphologically identified interneurons in the vestibulocerebellum. J Neurosci. **31**: 712-24.

Saitow F, Murano M, Suzuki H. (2009) Modulatory effects of serotonin on GABAergic synaptic transmission and membrane properties in the deep cerebellar nuclei. J Neurophysiol. **101**: 1361-74

Saitow F, Suzuki H, Konishi S. (2005) beta-Adrenoceptor-mediated long-term up-regulation of the release machinery at rat cerebellar GABAergic synapses. J Physiol. **565**: 487-502.

Samonds JM, Bonds AB. (2005) Gamma oscillation maintains stimulus structure-dependent synchronization in cat visual cortex. J Neurophysiol. **93**: 223-36.

Sargent PB, Saviane C, Nielsen TA, DiGregorio DA, Silver RA. (2005) Rapid vesicular release, quantal variability, and spillover contribute to the precision and reliability of transmission at a glomerular synapse. J Neurosci. **25**: 8173-87.

Saviane C, Silver RA. (2006) Fast vesicle reloading and a large pool sustain high bandwidth transmission at a central synapse. Nature. **439**: 983-7.

Sawtell NB. (2010) Multimodal integration in granule cells as a basis for associative plasticity and sensory prediction in a cerebellum-like circuit. Neuron. **66**: 573-84.

Schonewille M, Gao Z, Boele HJ, Veloz MF, Amerika WE, Simek AA, De Jeu MT, Steinberg JP, Takamiya K, Hoebeek FE, Linden DJ, Huganir RL, De Zeeuw CI. (2011) Reevaluating the role of LTD in cerebellar motor learning. Neuron. **70**: 43-50.

Schweighofer N, Arbib MA, Dominey PF. (1996) A model of the cerebellum in adaptive control of saccadic gain. II. Simulation results. Biol Cybern. **75**: 29-36.

Schweighofer N, Doya K, Kuroda S. (2004) Cerebellar aminergic neuromodulation: towards a functional understanding. Brain Res Brain Res Rev. **44**: 103-16.

Sejnowski TJ. (1977) Storing covariance with nonlinearly interacting neurons. J Math Biol. **4**: 303-21.

Shin SL, De Schutter E. (2006) Dynamic synchronization of Purkinje cell simple spikes. J Neurophysiol. **96**: 3485-91.

Silver RA. (2010) Neuronal arithmetic. Nat Rev Neurosci. **11**: 474-89.

Silver RA, Colquhoun D, Cull-Candy SG, Edmonds B. (1996) Deactivation and desensitization of non-NMDA receptors in patches and the time course of EPSCs in rat cerebellar granule cells. J Physiol. **493**: 167-73.

Silver RA, Traynelis SF, Cull-Candy SG. (1992) Rapid-time-course miniature and evoked excitatory currents at cerebellar synapses in situ. Nature. **355**: 163-6.

Simat M, Parpan F, Fritschy JM. (2007) Heterogeneity of glycinergic and gabaergic interneurons in the granule cell layer of mouse cerebellum. J Comp Neurol. **500**: 71-83.

Simpson JI, Hulscher HC, Sabel-Goedknegt E, Ruigrok TJ. (2005) Between in and out: linking morphology and physiology of cerebellar cortical interneurons. Prog Brain Res. **148**: 329-40.

Sims RE, Hartell NA. (2005) Differences in transmission properties and susceptibility to long-term depression reveal functional specialization of ascending axon and parallel fiber synapses to Purkinje cells. J Neurosci. **25**: 3246-57.

Sims RE, Hartell NA. (2006) Differential susceptibility to synaptic plasticity reveals a functional specialization of ascending axon and parallel fiber synapses to cerebellar Purkinje cells. J Neurosci. **26**: 5153-9.

Singer W, Gray CM. (1995) Visual feature integration and the temporal correlation hypothesis. Annu Rev Neurosci. **18**: 555-86.

Smythies J. (1997) The functional neuroanatomy of awareness: with a focus on the role of various anatomical systems in the control of intermodal attention. Conscious Cogn. **6**: 455-81.

Sola E, Prestori F, Rossi P, Taglietti V, D'Angelo E. (2004) Increased neurotransmitter release during long-term potentiation at mossy fibre-granule cell synapses in rat cerebellum. J Physiol. **557**: 843-61.

Solinas S, Nieus T, D'Angelo E. (2010) A realistic large-scale model of the cerebellum granular layer predicts circuit spatio-temporal filtering properties. Front Cell Neurosci. **4**: 12.

Sotelo C, Llinás R. (1972) Specialized membrane junctions between neurons in the vertebrate cerebellar cortex. J Cell Biol. **53**: 271-89.

Soteropoulos DS, Baker SN. (2006) Cortico-cerebellar coherence during a precision grip task in the monkey. J Neurophysiol. **95**: 1194-206.

Spencer RM, Ivry RB. (2009) Sequence learning is preserved in individuals with cerebellar degeneration when the movements are directly cued. J Cogn Neurosci. **21**: 1302-10.

Stell BM, Brickley SG, Tang CY, Farrant M, Mody I. (2003) Neuroactive steroids reduce neuronal excitability by selectively enhancing tonic inhibition mediated by

delta subunit-containing GABAA receptors. Proc Natl Acad Sci U S A. **100**: 14439-44.

Stopfer M, Bhagavan S, Smith BH, Laurent G. (1997) Impaired odour discrimination on desynchronization of odour-encoding neural assemblies. Nature. **390**: 70-4.

Strick PL, Dum RP, Fiez JA. (2009) Cerebellum and nonmotor function. Annu Rev Neurosci. **32**: 413-34.

Sultan F, Bower JM. (1998) Quantitative Golgi study of the rat cerebellar molecular layer interneurons using principal component analysis. J Comp Neurol. **393**: 353-73.

Szapiro G, Barbour B. (2007) Multiple climbing fibers signal to molecular layer interneurons exclusively via glutamate spillover. Nat Neurosci. **10**: 735-42.

Tadayonnejad R, Anderson D, Molineux ML, Mehaffey WH, Jayasuriya K, Turner RW. (2010) Rebound discharge in deep cerebellar nuclear neurons in vitro. Cerebellum. **9**: 352-74.

Tahon K, Volny-Luraghi A, De Schutter E. (2005) Temporal characteristics of tactile stimuli influence the response profile of cerebellar Golgi cells. Neurosci Lett. **390**: 156-61.

Tang AH, Karson MA, Nagode DA, McIntosh JM, Uebele VN, Renger JJ, Klugmann M, Milner TA, Alger BE. (2011) Nerve terminal nicotinic acetylcholine receptors initiate quantal GABA release from perisomatic interneurons by activating axonal T-type (Cav3) Ca^{2+} channels and Ca^{2+} release from stores. J Neurosci. **31**: 13546-61.

Tempia F, Miniaci MC, Anchisi D, Strata P. (1998) Postsynaptic current mediated by metabotropic glutamate receptors in cerebellar Purkinje cells. J Neurophysiol. **80**: 520-8.

Tia S, Wang JF, Kotchabhakdi N, Vicini S. (1996) Developmental changes of inhibitory synaptic currents in cerebellar granule neurons: role of GABA(A) receptor alpha 6 subunit. J Neurosci. **16**: 3630-40.

Turner JR, Kellar KJ. (2005) Nicotinic cholinergic receptors in the rat cerebellum: multiple heteromeric subtypes. J Neurosci. **25**: 9258-65.

Uusisaari M, De Schutter E. (2011) The mysterious microcircuitry of the cerebellar nuclei. J Physiol. **589**: 3441-57.

Van Der Giessen RS, Koekkoek SK, van Dorp S, De Gruijl JR, Cupido A, Khosrovani S, Dortland B, Wellershaus K, Degen J, Deuchars J, Fuchs EC, Monyer H, Willecke K, De Jeu MT, De Zeeuw CI. (2008) Role of olivary electrical coupling in cerebellar motor learning. Neuron. **58**: 599-612.

Van Der Giessen RS, Maxeiner S, French PJ, Willecke K, De Zeeuw CI. (2006) Spatiotemporal distribution of Connexin45 in the olivocerebellar system. J Comp Neurol. **495**: 173-84.

van Kan PL, Gibson AR, Houk JC. (1993) Movement-related inputs to intermediate cerebellum of the monkey. J Neurophysiol. **69**: 74-94.

Varela JA, Sen K, Gibson J, Fost J, Abbott LF, Nelson SB. (1997) A quantitative description of short-term plasticity at excitatory synapses in layer 2/3 of rat primary visual cortex. J Neurosci. **17**: 7926-40.

Verret L, Léger L, Fort P, Luppi PH. (2005) Cholinergic and noncholinergic brainstem neurons expressing Fos after paradoxical (REM) sleep deprivation and recovery. Eur J Neurosci. **21**: 2488-504.

Vervaeke K, Lorincz A, Gleeson P, Farinella M, Nusser Z, Silver RA. (2010) Rapid desynchronization of an electrically coupled interneuron network with sparse excitatory synaptic input. Neuron. **67**: 435-51.

Volgushev M, Kudryashov I, Chistiakova M, Mukovski M, Niesmann J, Eysel UT. (2004) Probability of transmitter release at neocortical synapses at different temperatures. J Neurophysiol. **92**: 212-20.

Vos BP, Maex R, Volny-Luraghi A, De Schutter E. (1999a) Parallel fibers synchronize spontaneous activity in cerebellar Golgi cells. J Neurosci. **19**: RC6.

Vos BP, Volny-Luraghi A, De Schutter E. (1999b) Cerebellar Golgi cells in the rat: receptive fields and timing of responses to facial stimulation. Eur J Neurosci. **11**: 2621-34.

Walker MP, Stickgold R, Alsop D, Gaab N, Schlaug G. (2005) Sleep-dependent motor memory plasticity in the human brain. Neuroscience. **133**: 911-7.

Wall MJ. (2002) Furosemide reveals heterogeneous GABA(A) receptor expression at adult rat Golgi cell to granule cell synapses. Neuropharmacology. **43**: 737-49.

Wall MJ. (2003) Endogenous nitric oxide modulates GABAergic transmission to granule cells in adult rat cerebellum. Eur J Neurosci. **18**: 869-78.

Wall MJ. (2005) Alterations in GABAA receptor occupancy occur during the postnatal development of rat Purkinje cell but not granule cell synapses. Neuropharmacology. **49**: 596-609.

Wall MJ, Usowicz MM. (1997) Development of action potential-dependent and independent spontaneous GABAA receptor-mediated currents in granule cells of postnatal rat cerebellum. Eur J Neurosci. **9**: 533-48.

Wang HY, D'Andrea MR, Nagele RG. (2002) Cerebellar diffuse amyloid plaques are derived from dendritic Abeta42 accumulations in Purkinje cells. Neurobiol Aging. **23**: 213-23.

Wang X, Gorini C, Sharp D, Bateman R, Mendelowitz D. (2011) Anaesthetics differentially modulate the trigeminocardiac reflex excitatory synaptic pathway in the brainstem. J Physiol. **589**: 5431-42.

Watanabe D, Nakanishi S. (2003) mGluR2 postsynaptically senses granule cell inputs at Golgi cell synapses. Neuron. **39**: 821-9.

Watt AJ, Cuntz H, Mori M, Nusser Z, Sjöström PJ, Häusser M. (2009) Traveling waves in developing cerebellar cortex mediated by asymmetrical Purkinje cell connectivity. Nat Neurosci. **12**: 463-73.

Welsh JP, Yamaguchi H, Zeng XH, Kojo M, Nakada Y, Takagi A, Sugimori M, Llinás RR. (2005) Normal motor learning during pharmacological prevention of Purkinje cell long-term depression. Proc Natl Acad Sci U S A. **102**: 17166-71.

Wu HS, Sugihara I, Shinoda Y. (1999) Projection patterns of single mossy fibers originating from the lateral reticular nucleus in the rat cerebellar cortex and nuclei. J Comp Neurol. **411**: 97-118.

Xu W, Edgley SA. (2008) Climbing fibre-dependent changes in Golgi cell responses to peripheral stimulation. J Physiol. **586**: 4951-9.

Xu-Friedman MA, Regehr WG. (2003) Ultrastructural contributions to desensitization at cerebellar mossy fiber to granule cell synapses. J Neurosci. **23**: 2182-92.

Yamamoto K, Kobayashi Y, Takemura A, Kawano K, Kawato M. (2002) Computational studies on acquisition and adaptation of ocular following responses based on cerebellar synaptic plasticity. J Neurophysiol. **87**: 1554-71.

Yokoi A, Hirashima M, Nozaki D. (2011) Gain field encoding of the kinematics of both arms in the internal model enables flexible bimanual action. J Neurosci. **31**: 17058-68.

Yuan Y, Atchison WD. (2003) Methylmercury differentially affects GABA(A) receptor-mediated spontaneous IPSCs in Purkinje and granule cells of rat cerebellar slices. J Physiol. **550**: 191-204.

Yeo CH, Hesslow G. (1998) Cerebellum and conditioned reflexes. Trends Cogn Sci. **2**: 322-30.